
# Using Seismic Mixtures to Extract Tilts and Recover Estimates of Ground Displacements

Ramaswamy Thiyagu

Research Thesis

January 2011

School of Computing, Information Technology and Engineering
University of East London
London, UK

## Abstract:

One of the goals of seismology is to understand the behaviour of the earth's movements during the occurrence of an earthquake. This research focuses on the recovery of better estimation of the true ground displacements as the tilt components are inherent in recorded acceleration time histories. The raw acceleration time histories recorded in seismograms of the near field earthquake are contaminated by the effects of tilt time histories. The effects of tilt time histories cause non–zero baseline errors in seismic records thereby providing offset in the ground velocity although the final velocity never ends to zero and ground displacement diverges from the constant value. To perform baseline corrections it is therefore necessary to remove the tilt and noise components.

Tilt separation was undertaken using a model designated the Tilt Separation – Independent Component Analysis (TS-ICA) model, and an enhanced version of the Extended Generalised Beta Distribution (EGBD) model. Several source distributions such as Normal, Gaussian, Non-Gaussian, Sub and Super Gaussian and skewed distribution with zero kurtosis has been modelled using EGBD and separated using EGBD-ICA. In order to refine the EGBD-ICA model, a randomised mixing matrix was introduced in the existing EGBD-ICA model using MATLAB. With the introduction of the mixing matrix, the consistency of the source separation has improved and particularly tilt separation was convincing for both artificial tilt separation from the Hector Mine earthquake data and real-time tilt separation from the real-time acceleration time histories. The tilt separation and de-noising by the TS-ICA model has given better estimates of ground displacement than the tilt contaminated ground displacement.

The estimated tilt angle can provide further scope for seismic scientists and civil engineers to improve their understanding of the tilt behaviour during an earthquake and can add another dimension to their research by making it possible to improve the stability of the building structures in the seismically active regions and areas which are potentially prone to earthquake.

## Acknowledgement

I would like to thank the seismology expert Mr Andrew A Chanerley, for all the help, support, his wealth of ideas and guidance throughout my research studies. I am also extremely grateful for the freedom to develop my own ideas and his support to let me pursue them.

I would also like to thank Professor Roy Perryman, who has provided valuable comments to my thesis, and for taking the time to read through my work and provide recommendations for improvements.

I also thank Dr Wada Honsy for his relentless help and encouragement throughout the course of my research.

My sincere gratitude to Dr Robert Pillet (French Seismologist) for sharing his experimental SCV data files of the Taiwan earthquake and also Professor Sinan Akkar and Mr Ozkan Kale (Earthquake Engineering Research Centre, Ankara, Turkey) who have provided the raw data from all the stations of the Koceali earthquake.

The department of Servicio Sismologico Universidad de Chile helped me by providing the Chile earthquake data for my research purpose. I thank Dr David M Boore who gave me good directions and great links to obtain the variety of earthquake data from different parts of the world.

I would like to particularly thank Professor Luis B Almedia, Instituto Superior Técnico, Lisbon, Portugal, who gave me valuable ideas on linear and nonlinear source separation.

Of course, I would never have got this far without the support of my family, particularly the encouragement from my wife and daughter. I owe them a special debt for putting up with my ups and downs over the last four years.

I would like to dedicate this thesis to my parents, for supporting me through the period of my research and always encouraging me with their great support.

# TABLE OF CONTENTS

## List of Figures

## List of Tables

## Nomenclature

Acceleration in the direction

Angle of the pendulum rotation

Beta distributions

Centered vector

Corrected ground acceleration

Correlation matrix

Covariance matrix

Earthquake Magnitude

Estimated sample moments

Expectation of functions

Fraction of critical damping of the transducer

Inverse matrix

Lambda distributions

Length of pendulum arm

Kurtosis – fourth order statistics

Mean of source signal

Mixing matrix

Natural frequency of the accelerometer

New corrected ground acceleration

Observed vector

Raw ground acceleration

Recorded response of the instruments

Rotation of the ground surface about the axis (tilt)

Tilt angle

Skewness – third order statistics

Transpose of matrix

Variance of source signal

Whitened vector

## List of Abbreviations

CLT – central limit theorem

EW – east west directions

EGBD – enhanced generalised beta distributions

EGLD – extended generalised lambda distribution

EVD – Eigen value decomposition

GBD – generalised beta distributions

GPS – global positioning system

ICA – independent component analysis

MISEP - Mutual Information-Based SEParation

NDF – normal distribution function

NFA – non factory analysis

NS – north south directions

NW – north west directions

PCA – principle component analysis

PDF – probability density function

SW – south west directions

V – vertical direction

# Chapter 1

# Introduction

## 1.1 Aims of the thesis

The aim of this thesis is to investigate a model which will identify instrument tilts and/or rotational trends within seismic time histories in the case of magnitudes . The work will also apply the model to seismic data to evaluate their usefulness in separating tilt trends inherent in seismic data. This is undertaken by estimating the tilt acceleration within the main acceleration time histories in order to provide a better estimate of ground velocity and displacement.

## 1.2 Motivation

During an earthquake, accelerographs record the acceleration of ground movements against time. These accelerographs are the best representation and measure of the damage potential of structures. The purpose of the accelerograph is to record strong shaking predominantly when located close to the earthquake source.

Baseline correction is a term used to determine the error incurred in the processing of accelerograms (Akkar and Boore, 2009). This method corrects the recorded signal for non – zero final velocity value and any long-period drift in the velocity zero level that may arise from instrument noise or from the digitisation of analog accelerograms. In order to perform baseline corrections it is necessary to remove any distortion due to noise and acceleration jumps due to instrument tilts.

As shown in figure 1.1 the final velocity does not end to zero, which is due to tilt and noise in the accelerogram recording. Therefore it is necessary to perform baseline correction so that tilt time histories and noise can be removed (Chanerley and Alexander, 2009).

Tilt and noise contamination makes double integration of the accelerometer data difficult. The question therefore is how much of the seismogram is due to tilt and the answer is related to the long period Rayleigh waves and free oscillations which occur (Rodgers, 1968). Horizontal sensors are used to measure acceleration time histories which are sensitive to the second derivative of displacement and to tilt. Double integration of the horizontal axes equations will produce the total sum of displacement. Assuming that tilt is proportional to velocity (Bouchon and Aki, 1982; Trifunac, 1972; Trifunac and Todorovska, 2001), double integration will give results proportional to the integral of displacement. This appears to look like long period noise, as shown in figure 1.1. Near field source ground acceleration data are contaminated by instrument response to small rotational motion, and causes the tilt effects in the recording of raw data.

A novel approach to removing the tilt component which is investigated and described in this thesis uses independent component analysis (ICA) to extract the time series of the acceleration tilt which is inherent in the acceleration. The proposed contribution to new knowledge in this research programme is to determine the ground displacement by extracting the tilt time histories, thus de-noising the signal.

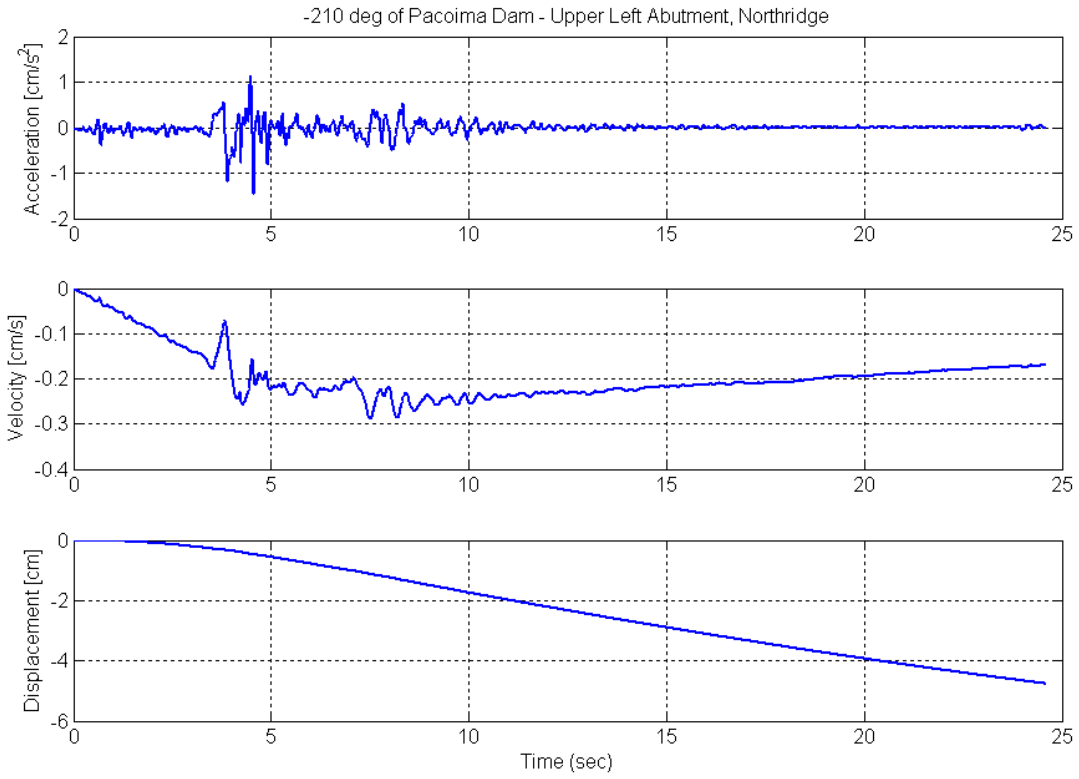


Figure 1.1: The horizontal component of uncorrected records; of Pacoima Dam - Upper Left Abutment, Northridge. MATLAB source code to plot Pacoima Dam ground acceleration, velocity and displacement time histories is attached in Appendix B, Page 199

## 1.3 Expected Outcomes

The outcome of this research includes an understanding of the effects of tilt in the strong ground motion in the near field earthquake. The work will also involve identifying and estimating the tilt acceleration in the original ground acceleration from the seismogram records and to separate and de-noise the tilt time histories from the ground acceleration, in order to achieve an estimate of the true ground velocity and permanent displacement time history. The estimates of true ground acceleration, velocity and displacement can then be applied to the design of buildings and bridges.

## 1.4 Outline of the thesis

The introductory chapter 1 briefly reviews the literature regarding the problems due to instrument tilt, linear motion, angular acceleration, and cross axis excitations that provide background information in understanding the subsequent chapters.

Chapter 2 will provide review of the literature and developments in the area of analysis of seismic mixtures to recover estimates of the ground velocity and displacement, including problems related to the tilts, baseline error and background noise in the recordings of ground acceleration data.

In chapter 3, a novel method of seismic data analysis techniques are examined and discussed, which is identified as Tilt-Separation Independent Component Analysis (TS-ICA) and is an enhancement to ICA, which was developed to recover estimates of ground displacement and tilt angle separation from the acceleration records. Advantage is taken of the well characterised Enhanced Generalised Beta Distribution to test the applicability of TS-ICA method.

In chapter 4, a novel approach is presented to analyse the tilt problem and to provide an alternative method to resolve the tilt data.

In chapters 5 and 6, the tilt angle time histories are analysed which is extended for earthquakes of greater magnitude earthquake data. Chapter 5 analyses the operational behaviour of lesser magnitude ( ) earthquake data. Chapter 6 provides the results from the earthquakes CHI-CHI 1999, Taiwan earthquake data , CHILE 2010, earthquake data , Kocaeli 1999, TURKEY earthquake data and Christchurch 2011, New Zealand earthquake data .

The chapters 6 and 7 are based on enhancements to the Independent Component Analysis procedures used to separate and de-noise the tilt time histories that are described in chapter 3.

Chapter 8 presents the results and analysis, with further more discussion regarding the tilt evaluation.

Chapter 9 summarises the conclusions of the thesis and provides directions in which the work presented in the thesis can be extended.

## 1.5 Background

### 1.5.1 Seismology

Large portions of the world's population live in regions of seismic hazard and are at risk from earthquakes of varying severity and varying frequency of occurrence. Earthquakes cause a significant loss of life and damage to property every year. Many seismic construction designs and technologies have been developed over the years in an attempt to mitigate against the effects of earthquakes on buildings, bridges, and other structures and the contents.

During an earthquake, most of the strain energy is converted into heat with only a few percent converted to seismic waves. But this is still enough to generate the powerful tremors to cause buildings to collapse.

The digitisation process of analog seismogram essentially transforms the record into a series of coordinates for modelling and analysis but unfortunately this process introduces small errors (long-period noise) into the recording, which are mainly due to the imperfection of the tracking the digitisation process. The recording may also be contaminated with noise from the distortion of the recording medium. The effects of noise on these recordings are seen during the integration of the acceleration time history. These can include a non-zero value of final velocity and a final displacement that is unreasonably large.

### 1.5.2 Some background

Noise enters into the recording from a number of sources including:

- Transducer drift
- Recording medium lateral drift
- Speed variation
- Trace density variations
- The digitisation process

Instrumental errors:

- Transducer distortions of amplitude and phase
- Instruments are limited to 3 degrees of freedom: instruments are not designed for 6 degrees of freedom. Nevertheless instruments record some of the tilt/rotations experienced during an earthquake, which contribute to the baseline error.
- With the older analog instruments the transverse movement of the recording paper/film causes variations of up to several millimetres as well as non-uniform time marks.
- Instrument drift: over long periods, temperature and humidity effects will cause a drift in the original component specifications of the instrument. Such changes will affect the data recorded unless the instrument is recalibrated.
- Instrument slip

Digitisation errors: these are errors in strong motion records due to the digitisation of analog signals.

- Digitisation rate: a large number of digitised points are required to obtain a good representation of the continuous accelerogram. Its accuracy is reduced due to the low number of digitised points.
- Resolution: inadequacy of the digitising equipment; cost is a factor.
- Low-Pass filtering: some instruments are designed with filtering techniques which are the effects of mechanical digitisation (this approximates to a continuous function by a sequence of discrete points)

- Baseline shifts in the axes of translations and/or rotational motion can be considered as random long period errors.

The horizontal pendulums are sensitive to the acceleration effects of:

- Linear motion
- Tilt
- Angular acceleration: all transducers (vertical and horizontal components) are affected by angular acceleration.
- Cross axis excitations.

Very small tilts in the accelerogram can produce baseline shifts. These very small tilts produce large displacement affects, which makes it difficult to obtain reasonable estimates of permanent ground displacements.

### 1.5.3 Baseline correction

In triangulation networks the scalar distance between two benchmarks determines the scale of networks. In GPS, the same term means the vector difference in position between two benchmarks. In INSAR (Pritchard, 2006) it means the vector separation or scalar distance between two orbital trajectories (Aki and Lee, 2003).

Difficulties in determining the baseline position:

- A threshold is set above which the instrument will commence recording, therefore some of the initial ground motion may not be recorded. The same applies at the end portion of the time history. This contributes to the baseline error.
- The final velocity should end at zero, but in most cases it is not zero due to the background noise and the offsets due to tilts.
- It is difficult to determine the final displacement because of baseline shifts (DC level).

In order to obtain true ground velocity and displacement from the seismic records of ground motion from an earthquake, it is necessary to remove the tilt and noise contamination from the acceleration of the ground motion. Currently acceleration based design of structures is the normal practice, however displacement based design of structures can be effective providing good estimates of displacements are available.

# Chapter 2

## Review of Literature

### 2.1 Past studies

**Bradner, H. and Reichle, M. (1973). Some methods for determining acceleration and tilt by use of pendulums and accelerometers, Bull. Seism. Soc. Vol. 63, pp. 1-7.**

Seismic records of ground motion in earthquakes ordinarily cannot separate horizontal accelerations from angular tilts, because tilts in a gravity field effectively introduce only a horizontal component which is indistinguishable from horizontal acceleration.

Bradner and Reichile, (1973) have considered the use of pendulums in measuring the horizontal component of ground motion. From the recorded ground motion in earthquakes it is not easy to separate the horizontal accelerations from the angular tilt because the coefficient of horizontal acceleration and the horizontal components of gravity caused by tilt are approximately identical.

**Bouchon, M. and Aki, K. (1982). Strain, Tilt, and Rotation associated with strong ground motion in the vicinity of earthquake faults, Bull. Seism. Soc. Vol. 72, pp. 1717-1738**

Several authors have attributed some of the structural damage and failure caused by earthquakes to second order differential ground motions. (Bouchon and Aki, 1982). Hart, *et al.* (1975) describes a large part of the torsional response of high-rise buildings observed during the San Fernando (1978) earthquake and the Miyagi-Ken-Oki (1978) earthquake to the rotational component of ground motion. In the paper by Bouchon and Aki, (1982) they present the simulations of the time history of tilt, strain, and rotation generated near earthquake faults buried in layered media for strike-slip faults and thrust fault models as shown in figure 2.1.2.

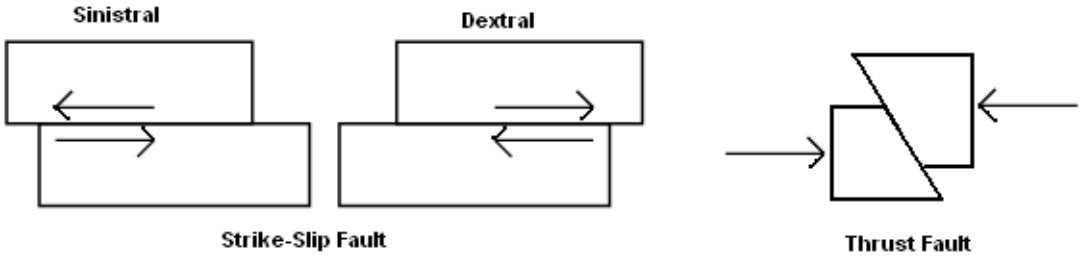


Figure 2.1.2: Strike-slip faults and thrust fault

“The computation of the corresponding time histories of tilt, strain and rotation is a straight forward matter because the wave field in the discrete wave number method is expressed as a simple sum of plane waves.”

“The first earthquake source that was considered was a 30 km long vertical strike-slip fault buried 1.5 km below the surface and extending down to a depth of 10 km. The tilt time histories for the earthquake sources were considered, the large value was obtained and normalised to a slip of 1 m on the fault, which were for the strike-slip and for the dip-slip. Like the longitudinal strain, the tilt produced by strike-slip earthquake decays very rapidly away from the source while in the case of a thrust or a normal fault, it is efficiently radiated in the form of , and Rayleigh waves.”

“High frequencies are associated with high phase velocities ( ) while low frequencies travel with lower phase velocities ( ). This indicates different modes of propagation and results in a distortion of the spectrum. The shallowest part of the fault is where strain and tilt are the largest although the longitudinal strain and horizontal velocity waveforms are still quite similar. Their relative amplitude yields a phase velocity of 2.4 km/s, at sites the fault plane and around the epicentre the velocity waveforms differ significantly from the strain and tilt histories, except for the disturbance generated at the upper tip of the fault.”

Bouchon and Aki, (1982) conclude that strain and tilt are closely related to ground velocity. This provides a basis for estimating the shear, rotational, and rocking motion from the

velocity records. Measurements of velocity, acceleration, strain and tilt (and/or rotation) at the same location depends on the direction of propagation of the waves and their phase velocities.

**Trifunac, M. D. and Todorovska, M.I. (2001). A note on the useable dynamic range of accelerographs recording translation, Soil Dyn. Earthq.Eng, no. 21, pp. 275-286.**

With the increase in the dynamic range of accelerograph recordings, output gain increases from 65 to 135 dB (decibel), this provides new possibilities in the calculation of permanent displacement of the ground and of structures in the near field provided all six components of strong motion (three translation and three rotation) have been recorded and the records are corrected for transducer rotation, misalignment and cross-axis sensitivity.

Trifunac and Lee, (1973) adopted a more conservative approach and assumed that permanent ground displacement cannot be calculated from digitised analog records of translation only. They worked with the simplified equation because the digitisation noise in analog records is large:

(2.1)

where,

is recorded amplitude
is ground displacement
is natural frequency of accelerometer
is fraction of critical damping in the recording transducer
is magnification factor

There are many factors contributing to the noise in digitised and processed data. These factors depend on the type of the transducer and its mechanical and electrical properties, properties of the recording system and the methods of data processing.

Even for the most accurate digitisation of analog records, the digitisation noise is larger than the largest contribution from the spectra of ( ) in the pendulum equation. Therefore, for linear wave motion in the far-field, the contribution to 'translation' records coming from tilting of accelerographs through the angle ( ) can be neglected.

For a 12 bit PDR-1 recorder, however, the effect of tilting can become comparable to or larger than the digitisation noise and cannot be neglected. Recording only translational acceleration with 18 and 19 bit recorders without recording rotation is costly and not considered necessary. This can allow the recording of smaller earthquakes and aftershocks, but cannot contribute to accurate calculations of permanent displacement of the ground and of structures in the near field.

Trifunac (2001) emphasised that recording rotation is essential for the complete specification of the response of the horizontal acceleration transducers and cannot be neglected for digital recorders with a resolution of greater than 12 bits. Moreover, only in the linearised form of the differential equation of the transducer recording, the vertical acceleration is not affected by strong motion tilting. All transducers (vertical and horizontal) however, are affected by angular acceleration but the effect is relatively small in the vertical transducer either because the arm of the pendulum is small or zero depending on the details of the transducer design.

The permanent ground displacement cannot be computed without knowledge of the rotational components of strong motion, especially in the near field of moderate and strong earthquakes where the response of the ground and structure may be non-linear. On the other hand, simultaneous recording of all six components (three translations and three rotations) of motion will enable computation of permanent displacement in structures, soils and in the near field of ground near shallow earthquake faults.

**Boore D. M. (2001). Effect of baseline corrections on displacements and response spectra for several recordings of the 1999 Chi-Chi, Taiwan, earthquake. Bull. Seism. Soc. Am., vol. 91, no. 5, pp. 1199-1211.**

Displacements derived from many of the accelerogram recordings of the Chi-Chi (1999), Taiwan, earthquake show drifts when only a simple baseline derived from the pre-event portion of the record is removed. The appearance of the velocity and displacement records suggests that changes in the DC level or zero level of the acceleration are responsible for these drifts. The source of the shifts in the DC level is difficult to determine, but in at least one case it is almost certainly due to tilting of the ground (Boore, 2001).

A wide range of final displacement was obtained for different choices of baseline correction and the results suggest that the response spectra for oscillation periods of less than about 20 seconds are usually unaffected by the baseline correction. The digital accelerations network installed and maintained by the Central Weather Bureau in Taiwan produced a rich set of records from the Chi-Chi (1999), Taiwan earthquake of magnitude with GPS measurements (Central Geological Survey, 1999) shown in figure 2.1.3. This earthquake produced the most complete set of strong-motion recordings ever obtained.

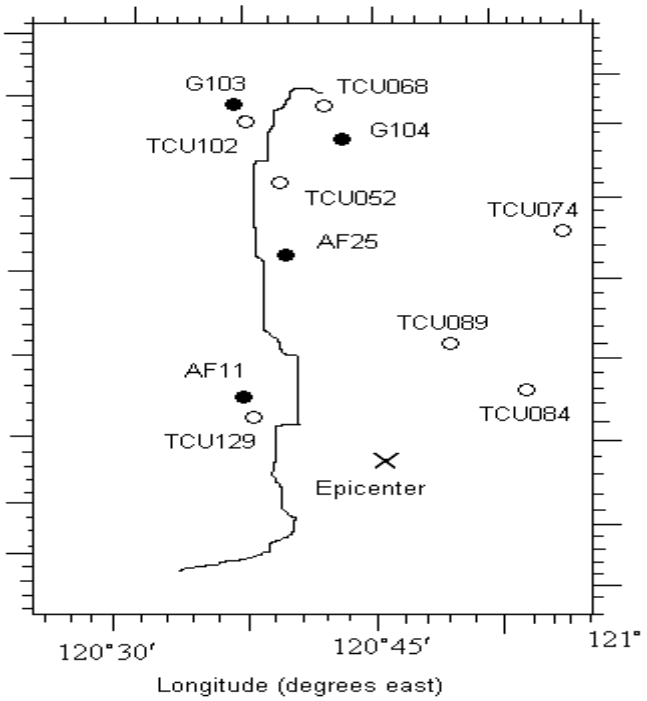


Figure 2.1.3: Map showing surface expression of fault (zigzag line), strong-motion station (open circles) and GPS stations (filled circles). The co-ordinates of the GPS stations are approximate; they were scaled from the figure from the Central Geological Survey, Taiwan (1999) (Ref: Figure 1. p 1200 (Boore, 2001)).

A zeroth-order correction has been applied to all records by removing the mean determined from a segment of the pre-event part of the original record from the whole original acceleration record.

**2.2 The Need for the Baseline Corrections**

Modern digital instruments have the potential to allow the recovery of the complete ground displacement data from accelerometer records taken close to large earthquakes. The only correction applied to the recorded information of TCU068 EW of Chi–Chi (1999) earthquake was the removal of the pre-event mean from the whole records. The velocities and displacement are obtained by the method of integration of the accelerations. The displacements reach essentially constant residual values, and the velocities oscillate around zero after the end of the strong shaking. The almost linear trend in velocity is a direct

indication that the baseline of the acceleration for at least the last half of the TCU068 EW record is not the same as that from the pre-event portion of the record.

The difference in acceleration baseline levels from zero level does not need to be large to produce the observed slope in the velocity and the correspondingly large final displacement. A small shift in the acceleration baseline from the zero level will have a large effect on the final displacement. Figure 2.1.4 shows the shift in the baseline due to tilt.

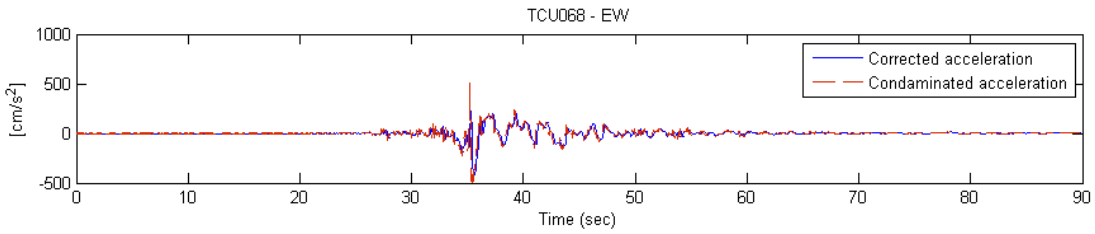


Figure 2.1.4: Baseline shift, the dotted line is tilt contaminated acceleration

A number of causes of the baseline offsets have been proposed, including tilting (either dynamic or permanent), the response of the transducer to strong shaking, or analog-to-digital quantisation error. Small tilts in the instruments can produce baseline shifts. A tilt of produces a shift in the baseline for horizontal components as shown in the following equation:

(2.2)

and for the vertical component, the equation becomes:

(2.3)

The shift in baseline from zero level caused by this very small tilt will produce a large displacement offset after a long duration, thus it will be difficult to obtain estimates of permanent ground displacement by double integration of the horizontal component

accelerations. The effect of tilt on vertical components should be much smaller and therefore easier to integrate.
In conclusion, baseline corrections are needed for almost all of the digitally recorded accelerograms are obtained from the earthquake source.

**Boore D. M., Stephens, C. D. and Joyner, W. B. (2001). Comments on baseline correction of digital strong-motion data: Examples from the 1999 Hector Mine, California, earthquake. Bull. Seism. Soc. Am. pp 123-138.**

The residual displacements for large earthquakes can sometimes be determined from the recordings of modern digital instruments. High-dynamic-range, broadband digital recording of ground accelerations from the earthquake has the potential to yield ground displacement giving the residual static deformation following an earthquake (Boore, *et al.* 2001). This paper discusses records of interest in separating the complexities (repeated fault ruptures) of fault rupture for engineers designing large structures with very long period response. These digital records are often plagued by baseline offsets even for small accelerations, and these baseline offsets can produce unrealistic ground displacements because of the unknown origin. Boore, *et al.* (2001) suggests a correction technique by studying the character of the velocity obtained which can be derived from the acceleration traces by a single integration. There are many sources which cause the offsets, for example shaking of the sensor, static build-up in the analog-to-digital converter, or tilting of the ground, and there is no universal correction scheme that can be applied to correct these offsets. So engineers and earthquake modellers are looking for appropriate methods that are accurate representations of the true ground motion.

One physical constraint of the ground motion is that the final ground velocity should be zero and the best way to determine whether there are baseline problems in the recorded acceleration is by looking at the velocity determined by integrating the acceleration. The drift away from zero clearly indicates a baseline problem, and this problem produces a growing displacement that is clearly unrealistic as the drift in velocity appears to be a straight line. This uncertainty about the details of baseline offsets is the reason that such offsets are difficult to correct.

These problems indicate the difficulty in understanding the true source of the offsets. There are a variety of potential sources, including mechanical/electrical hysteresis of the sensor, problems with the analog-to-digital converter, and ground tilt and rotation, due to elastic deformation or to inelastic deformation from slumping or cracking of the earth beneath the recording site. The drift in the velocity and displacement may be because of the random errors in the accelerogram resulting from single and double integration of the random noise. For older records this noise enters into the recording from a number of sources including transducer drift, recording medium lateral drift and speed variation, trace density variations, and the digitization process (Iwan, *et al.* 1985). The formula for the standard deviation of the final displacement is much smaller than the observed final displacement obtained by integrating the zeroth-order-corrected accelerations, and the double integration of random noise is not the cause of the observed drifts in velocity and displacement. The baseline problem for a particular transducer is attributed to hysteresis occurring because the acceleration going beyond . The peak acceleration for those recording is much less than (Bradner and Reichle, 1973).

**Boore D. M. (2003). Analog-to-digital conversion as a source of drifts in displacements derived from digital recordings of ground acceleration, Bull. Seism. Soc. Am., vol. 93, pp. 2017-2024.**

Displacements obtained from the double integration of digitally recorded ground accelerations cause drift in the actual accelerations and the drifts are much larger than those excepted for the true ground motion. These drifts might be due to many things like dynamic elastic ground tilt, inelastic ground deformation, hysteresis in the instruments, and cross feed due to misalignment of nominally orthogonal sensors (Boore, 2003).

**Graizer, V. M. (2006b). Equation of pendulum motion including rotations and its implications to the strong-ground motion, in *Earthquake Source Asymmetry, Structural Media and Rotation Effects* R.Teisseyre, M.Takeo, and E.Majewski (Editors), Springer-Verlag, New York, pp. 471-485.**

The most questionable perception brought from classical seismology into strong-motion (records) is the assumption of simple linear input motion of the ground, with the rotational (tilt) component being negligible, which leads to two consequences:

1. Primitive knowledge of theoretical or indirect assessments on the rotational components (Bouchon and Aki, 1982).
2. The output of the instruments was approximated as translational acceleration (by integrating this signal Graizer (2006b) assumed that this resulted in translation velocity and displacement).

In the real near field of an earthquake, the rotational components may not be negligible, because translation acceleration is the sum of acceleration and tilt.

In the real near field of an earthquake it is therefore necessary to measure all six components of the motion, three linear and three rotational motions.

It is important to consider rotational motion because of the new trends in technology and data processing. The seismological researchers apply various techniques of acceleration data processing including permanent ground displacement calculations although this should be done only if certain conditions apply.

The differential equations of a horizontal pendulum oscillating in a horizontal plane are:

(2.4)

(2.5)

where,

is the recorded response of the instruments,

is the angle of the pendulum rotation,

is the length of pendulum arm,

is the natural frequency,

is the fraction of critical damping of the transducer,

is acceleration due to gravity,

is the ground acceleration in direction,

is a rotation of the ground surface about the axis.

The equations 2.4 and 2.5 for the two horizontal directions L (longitudinal) and T (transverse) describe the pendulum response to low amplitude motions, when .

Sensitivity of the vertical pendulum to tilts is different for small tilts, and may be negligible, refer to equation 2.2 and 2.3 (Graizer, 2006b). Thus, horizontal pendulum equations 2.4 and 2.5 are sensitive to the acceleration of linear motion, tilt, angular acceleration, and cross-axis excitations. In the past, cross-axis excitation and angular acceleration were not taken into account by Golitsyn, (1912) and Aki and Richards, (1980) respectively.

According to Graizer (2006b) it is important to study the sensitivity of a pendulum to the second, third and fourth terms on the right hand side (R.H.S) of equations 2.4 and 2.5. These terms are considered to be small enough to be neglected in teleseismic studies. However, Graizer (1989) considers that the possible impact of different terms on the R.H.S of equations 2.4 and 2.5, based on numerical simulations performed for a number of typical strong-motion instruments could significantly influence the output of the horizontal pendulum. The terms caused by tilting are always present for the horizontal pendulum, and cannot be neglected.

Simplifying only the horizontal pendulum equations 2.4 and 2.5, for small oscillations, the vertical seismometer is almost insensitive to tilts. Neglecting the cross-axis sensitivity terms the differential equations of the horizontal pendulums simplify to:

(2.6)

(2.7)

Thus, for a typically strong-motion triaxial instrument the two horizontal sensors are responding to a combination of inputs corresponding to horizontal acceleration and tilt, but the vertical sensor is mainly responding to the vertical acceleration. The horizontal sensor is sensitive to the second derivative of displacement and to tilt. By double integrating the equations 2.6 and 2.7 thus will produce the sum of displacement and tilt. Assuming that tilt is proportional to velocity (Trifunac and Todorovska, 2001), double integrating will provide results proportional to the integral of displacement, and the result can look like long-period noise.

The artificial tilt generation test was performed at the Hector Station during the Hector Mine earthquake (N-S component, HEC-N) and it was assumed that this is an ideal ground motion with the corresponding ideal acceleration, and is shown in figure 2.1.5.

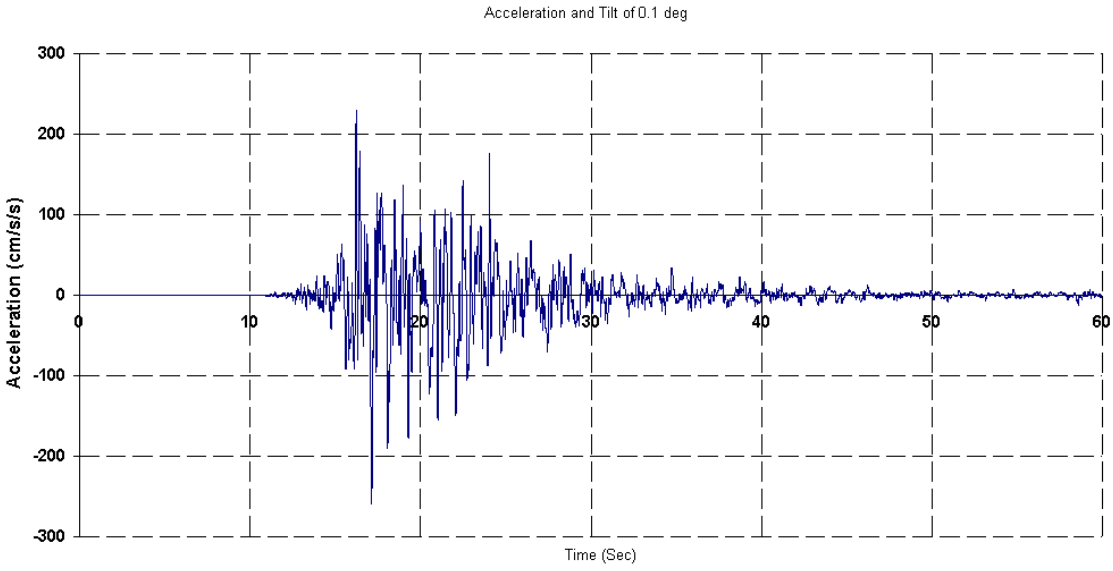


Figure 2.1.5: Tested Acceleration signal (ref: fig-4 page 202 Graizer, 2006b)

The tilt record was generated based on the assumption that the tilt spectrum is proportional to the ground velocity curve and was normalised to the maximum amplitude corresponding to

the tilt of . In this case the maximum amplitude of tilt motion was less than of the peak translation acceleration, and the result is shown in figure 2.1.6.

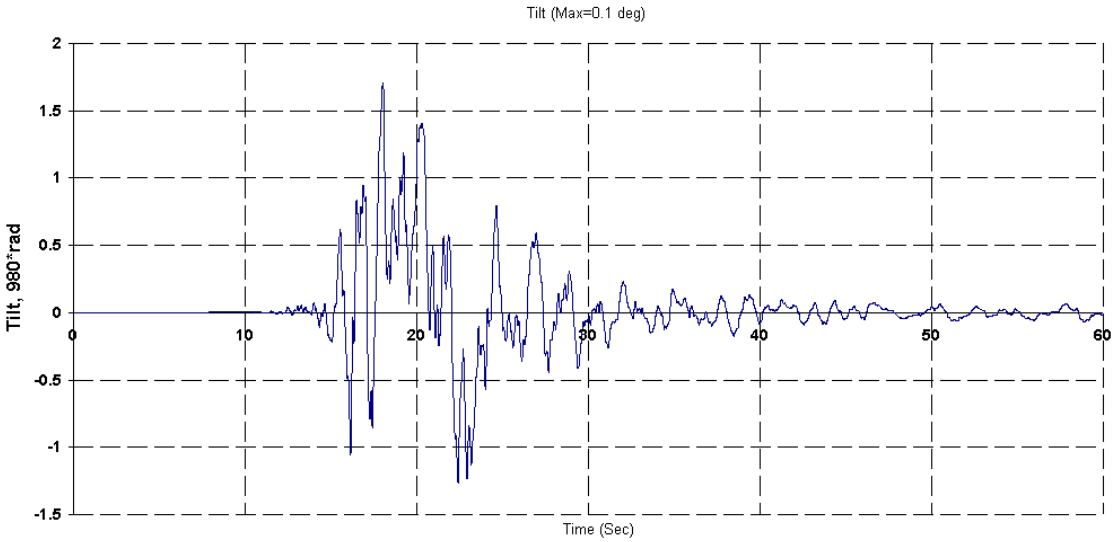


Figure 2.1.6: Tilt with maximum amplitude of (ref: fig-4 p 202 Graizer, 2006b)

Figure 2.1.7 shows three curve of true displacement, contaminated displacement and baseline corrected displacement. The dashed line shows the true or ideal displacement, the dotted line shows the displacement obtained by double integration of true acceleration contaminated by tilt, and the full line shows displacement calculated using Graizer's, (1979) algorithm for base line correction.

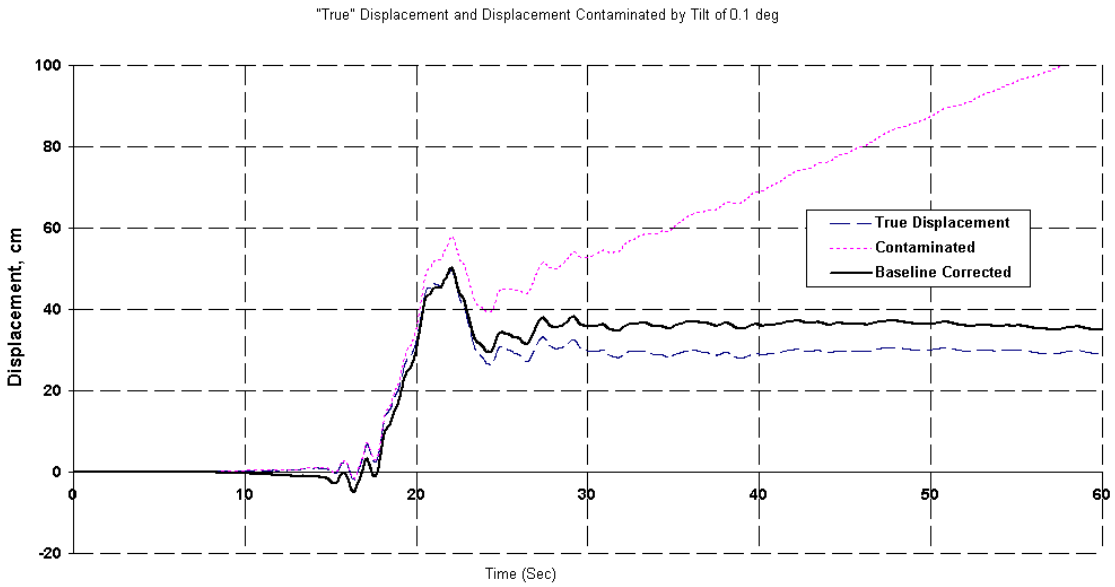


Figure 2.1.7: True displacement calculated from the test acceleration (blue, dashed line) signals and displacement calculated from the record contaminated by tilt (purple, dotted line), and displacement obtained from using Graizer's algorithm for baseline correction). (ref: fig.4. page 202 Graizer, 2006b).

In conclusion, numerical experiments demonstrate that ignoring the tilt effects in strong motion studies can introduce long-period errors in calculating residual displacements. In contrast to horizontal sensors, vertical sensors are less sensitive to tilt. Digital filters can eliminate the long-period components partially introduced by tilt but they can also eliminate the low frequency of the strong motion.

**Cochard, A., Igel, H., Schuberth, B., Suryanto, W., Velikoseltsev, A., Schreiber, U., Wassermann, J., Scherbaum, F., and Vollmer, D. (2006). Rotational Motions in Seismology: Theory, Observation, Simulation. BMBF-Geotechnologien.**

The rotational component of earthquake-induced ground motion has basically been ignored in past decades, compared to the substantial research in observing, processing and inverting translational ground motion, even though there are theoretical considerations suggesting that the observation of such motions may indeed be useful and provide additional information (Cochard, *et al.* 2006). This paper focuses on studies of the vertical rotational components

(twist, spin, or rotation around the vertical axis) and reviews the recent results on the fundamental concepts that are necessary to understand current broadband observations.

The rotational ground motion of teleseismic (pertaining to earthquakes at distances greater than 1,000 km from the measurements site) events illustrate the accuracy with which observed horizontal phase velocities match with theoretical predications, even though the precise waveforms are quite different due to inaccuracies in crustal models or rupture properties. This may have implications for sparse networks or situations where extremely few or even single-station observations are taken. To fully characterise the motion of a deformed body at a given point in the context of infinitesimal deformation, one needs three components of translation, six components of strain, and three components of rotations. Rotation motions induced by seismic waves have been essentially ignored for a long time, first because rotational effects were thought to be small (Bouchon and Aki 1982), and second because sensitive measuring devices were not available. “However as an approximation, rotations are proportional to displacement divided by the phase velocity” (Cochard, *et al.* 2006). When the wave velocity becomes smaller, rotations become comparatively larger. Thus, it is not unlikely that, near seismic sources, where rotations and strain can become relatively large even in normal media, rotations and strains become really large and can be responsible for the substantial damages. There is also growing seismological evidence that rotational amplitudes have been underestimated (Castellani and Zembaty, 1996).

In an attempt to measure rotational motions with high sensitivity, during the past years ring laser gyroscopes were developed, primarily to observe variations in the earth’s absolute rotation rate with high precision (Stedman, *et al*. 1995; Stedman, 1997). These observations gave evidence that optical sensors provide sufficient accuracy to record seismic rotations. However, the recordings were not fully consistent in terms of phase and amplitude with translational motions and also limited consistency being obtained only for a narrow frequency band. The previous attempt to observe ground motion with other devices like solid state rotational velocity sensors were limited to large signals close to earthquake sources and simulated results (Nigbor, 1994). Aki and Richards (2002) mention that “as of this writing seismology still awaits a suitable instrument for making measurements”. Although in recent

years the subsequent development of ring laser technology indicates that a significant part of the gap has been filled, as demonstrated by Schreiber, *et al*. (2003b) and Igel, *et al*. (2007).

Rotations can also be determined with array measurements, but with important limitations like the instruments should be as close as possible for the finite difference approximations to the true gradients. The uncertainty in the gradients will be larger if the instruments are closer together and finally, the assumption made by the researchers (Cochard, *et al.* 2006) that linearity of the displacement will be greatly affected by side effects at the station.

The recording of even smaller, potentially non-damaging, rotational motions is expected to be very useful. First, translation recordings are polluted by rotations. There is a purely geometrical effect when the reference axis of the seismometer is rotated, introducing a cosine factor, which will be negligible for very small deformations. However, this could become significant in the case of very strong ground motion and the inertial contributions are also very important. It is also well known that surface tilt (horizontal rotations) induce a translation signal (Aki and Richards, 2002).

In conclusion, at the earth's surface, horizontal rotation corresponds to tilt. As a consequence, waves generate horizontal rotation at the surface whereas they are ir-rotational in the mass. There is an additional contribution to horizontal rotation due to converted waves at the surface. 'It is still an open question what technology is best suitable for the various components of rotation' (Cochard, *et al.* 2006)

**Graizer V. M. (2006a). Tilts in Strong Ground Motion. Bull. Seism. Soc. Am., vol. 96, no. 6, pp. 2090-2102.**

Most instruments used in seismological activities to record ground motion are pendulum seismographs designed to measure translational motion. In most cases it is assumed that seismic instruments are only sensitive to the translational motion, and this paper by Graizer (2006a) focuses on the equation of pendulum motion, including the inputs of rotations and tilts.

Graizer (2006a) concludes that the rotational component can be neglected during seismological investigation which gave birth to the two independent branches of research.

1. Seismometry (the measurement of ground displacement, velocity, and acceleration)
2. Inclinometry (the measurement of tilt)

Sometimes instruments of the same pendulum type as used in seismometery were used to measure tilt. Graizer (2006a) concentrates on strong motion seismology and also brings attention to the classical seismologists with the development of super long period seismology, although these long periods ground motions may be contaminated, in some cases, by pendulum response to rotation. Cochard, *et al.* (2006) made successful measurements of rotation performed at telesesmic distances using ring laser gyroscopes but this technology gives uncertainty in the gradients which will be larger if the instruments are closer together. Graizer (2006a) focuses on the normal response of a typical pendulum to the complex input motion consisting of translation and rotation.

Equation of Pendulum:

The differential equations of small oscillations of horizontal pendulum motion:

(2.8)

where,

is the recorded response of the instruments; ,

is the angle of the pendulum rotation,

is the length of pendulum arm,

is the natural frequency,

is the fraction of critical damping of the transducer,

is acceleration in the direction,

is a rotation of the ground surface about the axis

The sensitivity of the vertical pendulum to tilts is different for a small tilt as it is proportional to:

(2.9)

The equations of the vertical pendulum then can be written:

(2.10)

Where,

is the cross axis excitations

The second item on the R.H.S. of equation (2.10) is the tilt sensitivity , which becomes small for angle , and for angles then , and consequently can be neglected.

Therefore neglecting gives:

(2.11)

Where,

is the cross axis excitations

Thus, a horizontal pendulum is sensitive to the acceleration of linear motion, tilt, angular acceleration, and cross-axis excitations (equation 2.8), and a vertical pendulum is sensitive to the acceleration of linear motion, angular acceleration, and cross-axis excitations equation (2.11). The difference in tilt sensitivity of vertical and horizontal pendulums is well known to the instrument designers, but is usually ignored in data processing and analysis.

The vertical accelerometer is almost not sensitive to tilts and neglecting the cross-axis sensitivity term because of the short pendulum arm for small oscillations of the pendulum,

this simplifies the differential equations of the horizontal and vertical pendulums respectively to be:

(2.12)

and,

(2.13)

From equation 2.12, the second term on R.H.S. of the equation shows the tilt sensitivity , whereas equation 2.13 for vertical sensor is mainly responding to the vertical acceleration.

“To what extent is tilt responsible for the differences between horizontal and vertical components in long periods during a real earthquake?” (Graizer, 2006a).

**Akkar, S. and Boore, D. M. (2009). On Baseline Corrections and uncertainty in Response Spectra for Baseline Variations Commomly Encountered in Digital Accelerograph Records. Bulletin of the Seismological of America, vol.99, No.3, pp. 1671-1690.**

Most digital accelerograph recordings are plagued by long period drifts, these drifts are best seen in the velocity and displacement time series obtained from the integration of the acceleration time series. The initial velocity of the acceleration should start with zero and the final velocity drifts often result in velocity values that are non-zero near the end of the record. This is due to noise in the acceleration signal which can lead to inaccurate estimates of peak ground displacement and the long period spectral response. The source of the long period noise seems in many cases may be due to variations in the acceleration baseline. These variations could be the result of the true ground motion, tilting and rotation, local permanent ground deformation, instrumental effects, or analog-to-digital conversion.

There is a need for ground motion estimations over longer periods, and recent ground motion predication equations (GMPEs) have extended their spectral estimations to periods well

above those previously obtained (Akkar and Bommer, 2007; Boore and Bommer, 2008). GMPE requires the specification of ground motions over long periods to estimate the peak nonlinear oscillator displacements. The main obstacle in obtaining long-period ground motion data is the noise in the acceleration records, due to this distortion to the signal it can lead to apparent errors in long period motions and the source of the noise can be due to dynamic rotation and tilting produced by wave propagation (Boore, 2003). A small noise component confined to narrow duration segments of the time series, not necessarily distributed in a stationary manner throughout the record, can cause drift in the displacement. This noise is embedded in records from both analog and digital accelerographs. From figure 2.1.8c the noise is easy to see on the displacement time series, where it most often takes the form of wavering.

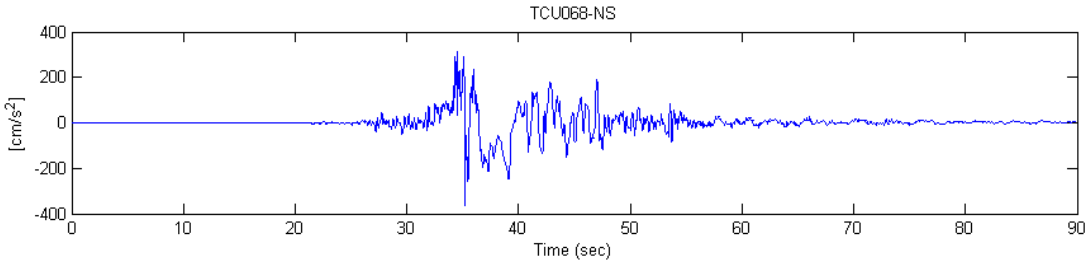


Figure 2.1.8a: Recorded accelerograms from 1999, Chi-Chi Earthquake, TCU068 Station NS component

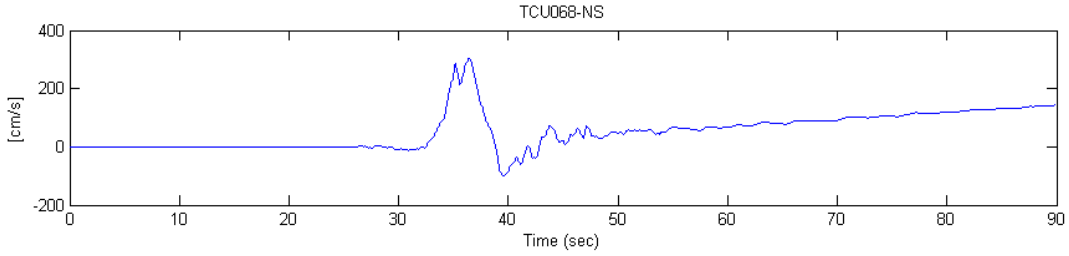


Figure 2.1.8b: Noise in the velocity, so the final velocity is nonzero near end of the record

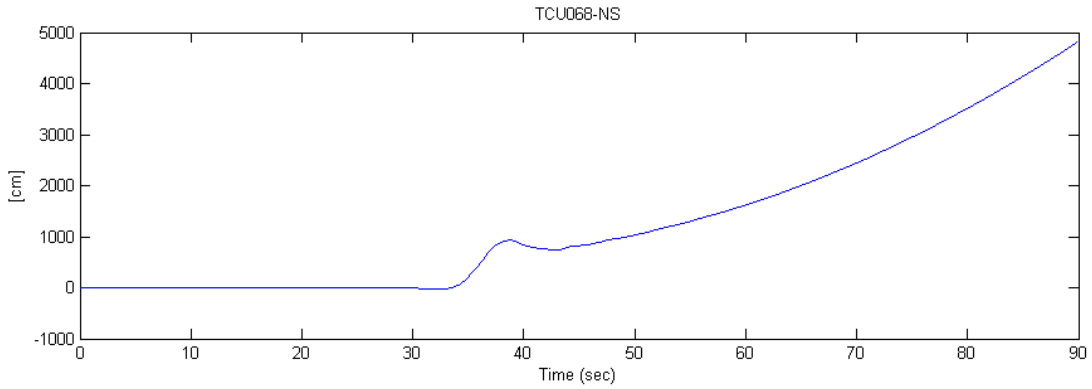


Figure 2.1.8c: Displacement drift after double integrating the acceleration time series

In digital records, the noise is generally easier to describe since it appears as a drift in displacement (and may be contaminated by tilt), corresponding to one or several linear trends in velocity. A small variation in the acceleration baseline often occurs near instantaneous shifts in the baseline level because the velocity does not lead to zero at the end of the record, which is shown in the figure 2.1.8b. The contaminated ground velocity obtained by single integration from the ground acceleration of TCU068 Chi-Chi (1999) earthquake is shown in figure 2.1.8a.

In conclusion, Akkar and Boore, (2009) have contributed the Monte Carlo Based (MCB) baseline correction procedure which can be used to provide some level of confidence in spectral displacements at periods longer than normally considered in routine processing. Iwan's, *et al.* (1985) method has modified the work of Akkar and Boore, (2009) to describe a robust way of determining spectral displacement. The method MCB can be used to assess the relative reliability of different recordings (there are 16 different station recording used in this paper). The observation that the long period noise in digital accelerography recordings is often in the form of a linear trend in the velocity time series after the strong shaking has stopped. If the long-period noise is due to variations in the acceleration baseline, no baseline variations could have occurred after the beginning of the linear trend due to the linearity of this trend in velocity. These observations put constraints on the time interval in which baseline variations could have occurred, but the MCB method is subject to these constraints for four models (Model-1 to Model-4) of the base line variations in order to find a suite of

baseline corrected acceleration time series. Finally, differences of the mean values from the various noise models would imply that the values are not accurate.

## 2.2 Conclusion

In conclusion, from the studies of previous research it is reported that instrument tilting causes baseline shifts in velocity and acceleration. The tilt angle is contaminated with ground acceleration data and it is often difficult to find the true ground displacement. The main aim of this research is therefore to investigate the tilt angle and separate the tilt and/or tilt plus noise from the ground acceleration time histories.

# Chapter 3

**Enhancement of Generalised Beta Distributions**

This chapter describes the methods used in the TS-ICA algorithm to process and analysis raw seismic data signals from the accelerogram recordings. In the first section 3.1 discusses the reasons relating to the choice of Independent Component Analysis and discuss how the TS-ICA algorithm is used to correct the offsets in the final displacement and separation of tilt time histories. Section 3.2 describes the numerical simulations for processing and analysing the seismic data, the MATLAB 7.x statistical tool is used to develop the code of the TS-ICA algorithm to quantitatively estimate and measure the tilt angles. Section 3.3 describes the real time seismic data recording configuration used in this research. Three different sources including (density of negative kurtosis), (density of positive kurtosis) and Gaussian distributions with a mean of zero and a variance of one (density of zero kurtosis) are mixed with random noise and separated using the proposed TS-ICA model. The de-mixed signal results are discussed in sections 3.4.1, 3.4.2 and 3.4.3. Also the TS-ICA procedure for estimation of tilt components from raw seismic data recordings is discussed in section 3.4.4. Finally section 3.5 considers the hypothesis for the tilt problem which often affects the estimate of the true ground velocity and displacement.

## 3.1 Introduction

The general model of separation is shown in Figure 3.1. It shows that the only information available to for the separation system is the observation mixed signal set. In this model, no assumption is made about the number or type of input signals and the selection of the mixing matrix, which may be quite different from the observed signals.

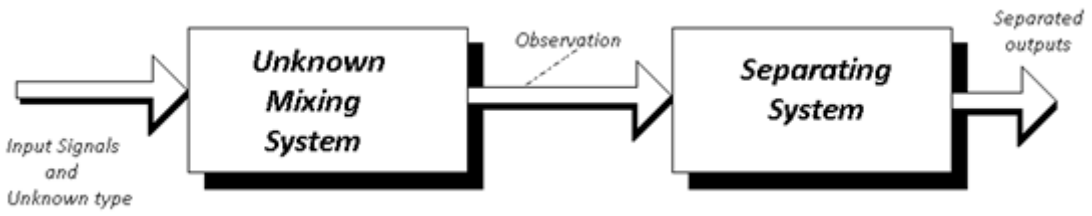


Figure 3.1: General separation model

### 3.1.1 Enhanced GBD Model

In the source separation model, the linear instantaneous model of independent sources is the most useful model in separating the tilt component. The separation within this algorithm is called the independent component analysis (ICA), where the independent components are the separated signals. The assumptions made about the source signals are as follows:

1. The source signals are all statistically mutually independent from one another.
2. Each source signal has a zero mean value and a stationary probability distribution.
3. Source signals include sub-Gaussian, super-Gaussian, and skewed distributions with zero kurtosis.
4. Apply enhanced Generalised Beta Distributions (EGBD) to correct the input signal and extract the tilt component. This can be achieved by the selection of appropriate values and from the EGBD method.
5. The number of linearly independent output signals is greater than the number of source signals.

### 3.1.2 Independent Component Analysis

Independent component analysis (ICA) is a method for finding underlying factors or components from multidimensional statistical data. An ICA method looks for components that are both statistically independent and non-Gaussian. Here the basic concepts, applications, and estimation principles of ICA are introduced.

Considering the classical ICA model, given an observation set of random variables

(3.1)

where is the time or sample index. Assuming that the random variables are linear mixtures of statistically independent components then:

(3.2)

Hence (3.3)

where is the unknown mixing matrix and is the mixing matrix in equation 3.2. ICA analysis now consists of estimating both the mixing matrix and the statistically independent component , from the observations of . The sources are mutually independent random variables and is the unknown invertible mixing matrix. The only observation is the random vector , and both and are estimated from this observation based on general assumptions.

The starting point for ICA is the assumption that the components $s_i$ are statistically and that the independent components must have distributions. For simplicity, assume that the unknown mixing matrix is square. After estimating the matrix which computes its inverse and obtains the independent components from:

(3.4)

### 3.1.3 Principles of ICA

One might try to de-correlate the mixture signals to obtain the sources. However, this process does not have a unique solution and will not give the independent components. From the figure 3.2 two sources are represented as the joint amplitude density.

By knowing the value of does not help in guessing the value of which implies are independent components.

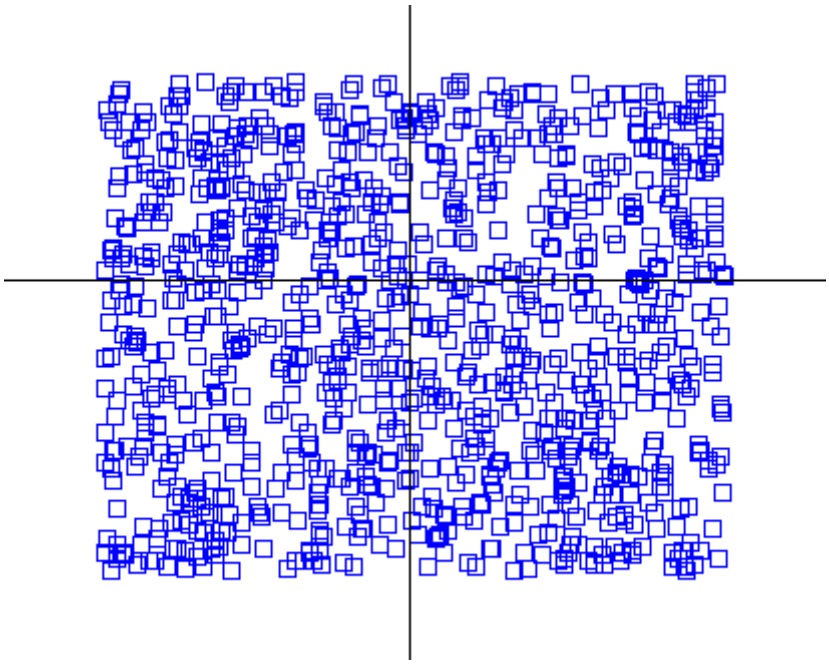

Figure 3.2: Independent components (horizontal axis) and (vertical axis) with uniform distributions. MATLAB source code to plot the independent components and with uniform distribution is attached in Appendix B, page 200

### 3.1.4 Non-Gaussian Independent Components

According to Hyvarinen *et al*, (2000), the central limit theorem which is explained in the next chapter 4, section 4.1 is the sum of non-Gaussian random variables which are closer to a Gaussian distribution than the original signals. ICA has several practical applications like noise removal from signals and feature extraction for signals.

For the linear combination of the observed mixture of variables with the linear combination of the independent components, then its non-Gaussian distribution will attain a local maximum whenever it equals any one of the independent components because if it were a mixture of two or more components, it would be closer to a Gaussian distribution due to the central limit theorem which is shown as an example in figure 3.3.

Seismic signals are non-linear, and the resulting mixture of the various tilts and cross-axis coupling may not be regarded as a simple linear superposition of the signals which makes the

process much more complicated (Almedia, 2006). However, some simplifications can be made if the form of the non-linearity is known. This situation arises most of the time if the system uses a reference signal.

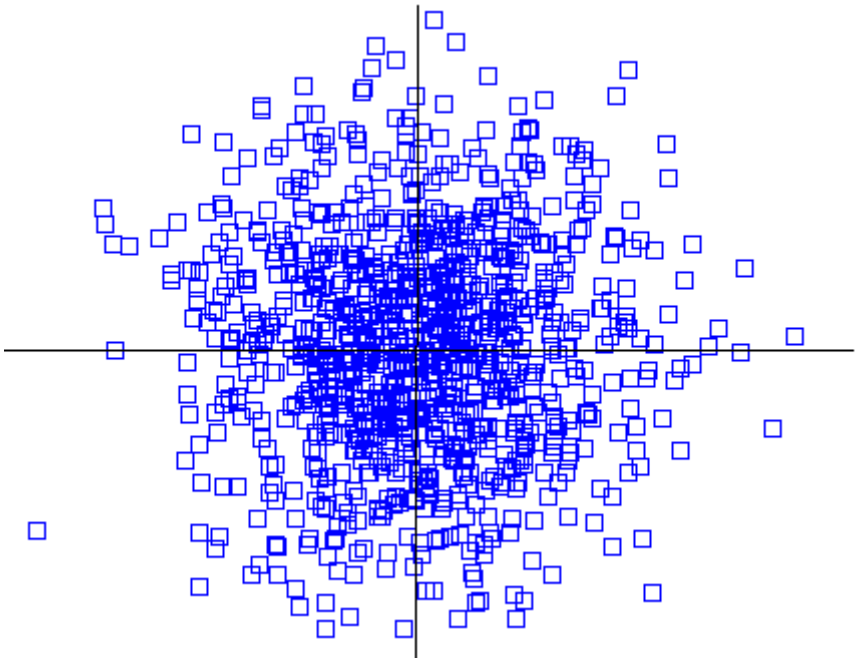

Figure 3.3: Sample of uncorrelated but not independent mixtures (horizontal axis) and (vertical axis). MATLAB source code to plot the sample of uncorrelated but not independent mixtures and is attached in Appendix B, page 200

Figure 3.4 shows the densities of the distributions given by the blue curve. For comparison, the Gaussian density is given by the green curve. Both the densities are normalised to unit variance.

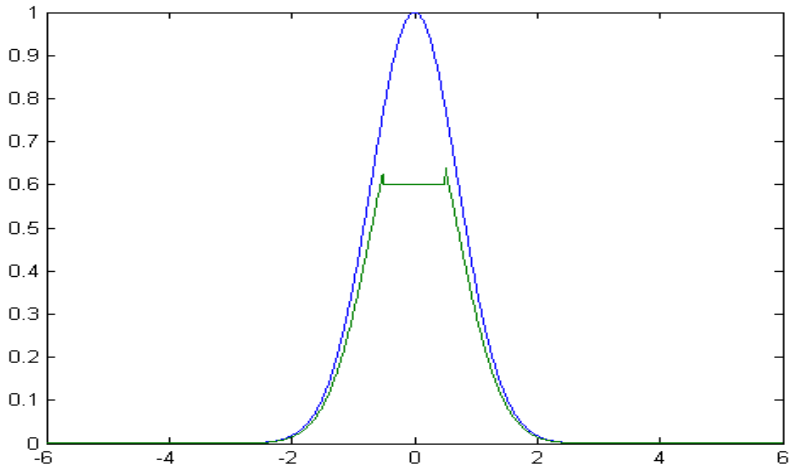


Figure 3.4: The marginal density of one of the uncorrelated dependent mixtures , where the green curve is the Gaussian density. MATLAB source code to plot the marginal density of one of the uncorrelated dependent mixtures is attached in Appendix B, page 201

### 3.1.5 Expectations and moments

A great advantage of expectations is that they can be estimated directly from the data without knowing the . Expectations have useful properties such as: linearity, linear transformability, and transformation invariance. Expectation of functions consisting of the product of components of is called moments.

The first moment of is its mean vector is given by:

(3.4.1)

The second moment of consist of correlations between pairs of components. The correlation between and is given by:

(3.4.2)

The correlation matrix of represents all its correlations conveniently.

(3.4.3)

is symmetric, positive semi-definite (not necessarily symmetric) with nonnegative Eigen values, and has mutually orthogonal Eigen vectors.

Central moments are defined like standard moments, but the means of the random quantities are subtracted first. The central moment corresponding to the correlation between and is their covariance and is given by:

(3.4.4)

The covariance matrix of ,

(3.4.5)

Correlations and covariance measure the dependence between the random variables using their second-order statistics.

### 3.1.6 Mixing of Independent Sources

Each source signal has a zero mean and a stationary probability distribution. A sequence of zeros (signal mean) of the same length are substituted for every source signal such that the indices do not overlap. This is done in order to visualise the separation result. If the final separation is successful, the same constant sequences should again be visible. The source signals are linearly mixed together using the mixing matrix and higher order ($3^{rd}$ and $4^{th}$) statistics are usually employed for separation, this is explained in chapter 4, section 4.2. If the signals or data are non-Gaussian, their higher order statistics contain a lot of extra useful information. ICA requires higher order statistics implicitly in computations via non-linearity. In experimentation higher order statistics are used to fit distributions to a set of data.

The first four sample moments such as mean, variance, skewness, kurtosis and classification of densities are shown as follows and figure 3.6 shows plots of classification densities:

- The first moment is the mean of .
- The second moment is the average power of
- The second central moment is the variance of
- The third central moment is called the skewness:
- The fourth moments or which is used less frequently

The fourth order statistic kurtosis is defined by:

(3.5)

Alternatively, the normalised kurtosis can be used:

(3.6)

for whitened data , so both kurtosis are reduced by

(3.7)

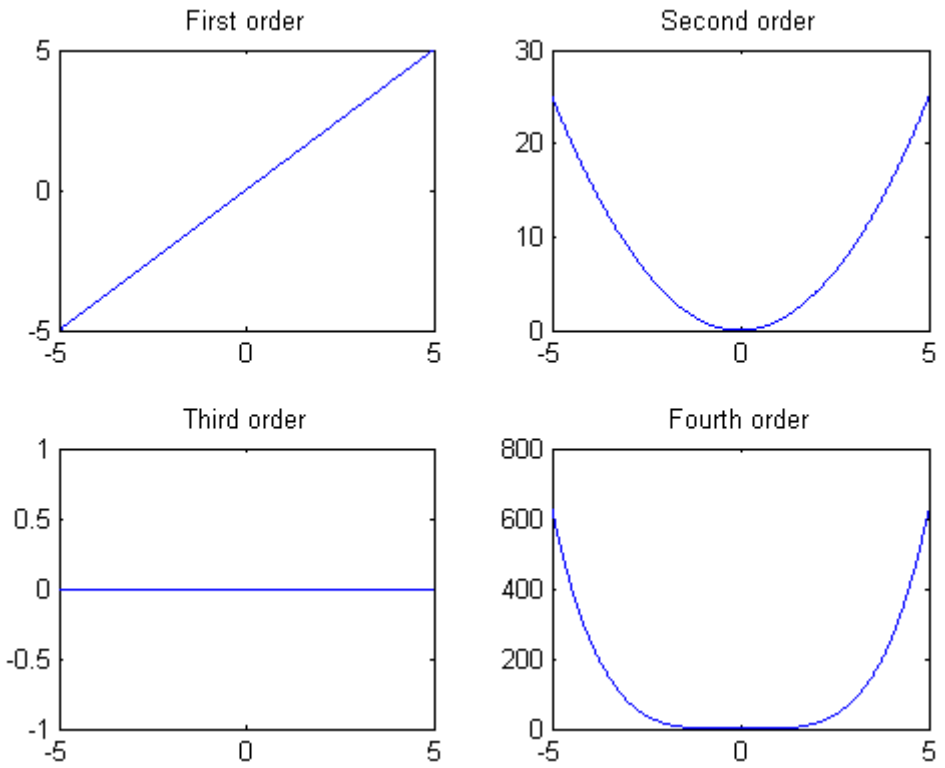


Figure 3.6: The function with increasing power of . MATLAB source code to plot the function with increasing power of is attached in Appendix B, page 202

The first four parameters generalised from Tukey's (1960) lambda distributions, the generalised lambda distributions referred to as and generalised beta distributions referred to as are easily described by the inverse distribution function given in equation 3.8:

(3.8)

Karian et al., (1996) provided a complete analysis of the and values that are associated with valid distributions. The estimation of parameters using the method of moments and the first four sample moments are calculated from the data set. For a given data set, the first two sample moments are defined by

(3.9)

(3.10)

while the sample and of skewness and kurtosis respectively, are defined by

(3.11)

(3.12)

### 3.1.7 Generalised Beta Distributions

Definition: The random variable is said to have a generalised beta distribution , if and , the probability density function of is

(3.13)

on the interval and zero outside this interval where is the constant.

The relationship of the moments of random variable with the parameter can be solved numerically (Eriksson *et al*, 2000) derived from the non-linear equations and the relation .

The following algorithm gives an overview to fit a data set with the GBD:

- Compute the sample moments by the equations (3.9) through to (3.12).
- Calculate and values by solving the equation (5.7) and equation (5.8) respectively.
- Apply score function to calculate the non-linearity of the source distribution.
- The de-mixing matrix is calculated using the TS-ICA algorithm.
- Calculate the results and estimate the output signal.

## 3.2 Numerical simulation setup

The Intel Core-2 computing system was used as the computational environment for implementing all algorithms. MATLAB R2008b was used in programming the TS-ICA algorithm in a standard high-level programming language.

### 3.2.1 MATLAB source code for TS-ICA algorithm

The following MATLAB code has been written specifically for this application.

1. Normalise the seismic ground acceleration source signal
2. Calculate the randomise mixing matrix and multiply with source signal
3. Compute the orthogonal matrix using to create orthogonal space for separating vector
4. Perform pre-processing: Centring and Whitening to the source signal
5. Compute the contrast function for new transformation
6. Initially calculate Beta1, Beta2, Beta3, Beta4 values by using Alpha1, Alpha2, Alpha3, Alpha4 values
    - where and values are calculated using equation 5.7 and 5.8 in chapter – 5.
7. Novel Enhanced Generalised Beta Distributions method
    - Use score function and its derivative to compute the non-linearity of the source distributions for the initial Beta1, Beta2, Beta3, Beta4 values
    - Vary the separating vector from the knowledge of non-linearity
    - Observe the non-linearity for Gaussian deviation
    - Change in is reflected in the contrast function (step–5)
    - In turn, change in varies
    - Now new values are obtained for the source distributions
    - Calculate the score function for the new values

- Observe non-linearity and vary until the single non – zero value is obtained in .
- At convergence values where successfully optimised using EGBD method

8. Perform symmetric orthogonalisation to restore orthogonality.
9. With the de-mixing matrix , the individual components tilt and noise are separated from the ground acceleration source signal.
10. Tilt plus noise = Raw seismic data – corrected source ( )
11. New corrected source = Raw seismic data – (Tilt plus noise)
12. This can be verified either way.

### 3.3 Seismic data used

In this research four major earthquakes are used:

- CHI-CHI earthquake Taiwan, September 21st 1999, $M_W = 7.6$
- KOCAELI earthquake Turkey, August 17th 1999, $M_W = 7.4$
- MAULE earthquake Chile, February 27th 2010, $M_W = 8.8$
- CHRISTCHURCH earthquake New Zealand, February 22th 2011, $M_W = 6.3$

Data of the Chi-Chi earthquake TCU station was obtained from Central Weather Bureau, Geophysical Database Management System, Taiwan (CBW, 2010). The MAULE earthquake in Chile was obtained from DGF, (2002). The Kocaeli earthquake was obtained from 'Turkey National Strong Ground Motion Program Database' TKYHP (2009) and the Christchurch earthquake data was obtained from Seismological Observatory, Geophysics Division, Institute of Geological and Nuclear Sciences, GNS, (2011).

## 3.4 Demonstration of TS-ICA model separation

The TS-ICA algorithm was discussed in section 3.2.1 and it is demonstrated with some examples in this section which shows the source separation using three signals a) sub-Gaussian, b) super-Gaussian, and c) Gaussian sequence with a mean of zero and a variance of one. The results are shown with plots of the original signal, the mixing signal, and the corrected signal which was retained from the original signal. The sample size is 1000 for sub-Gaussian, 100 for super-Gaussian, and 1000 for Gaussian sequence. This analysis shows only 1000 observations which demonstrate the clarity of the signals as shown in figure 3.7.

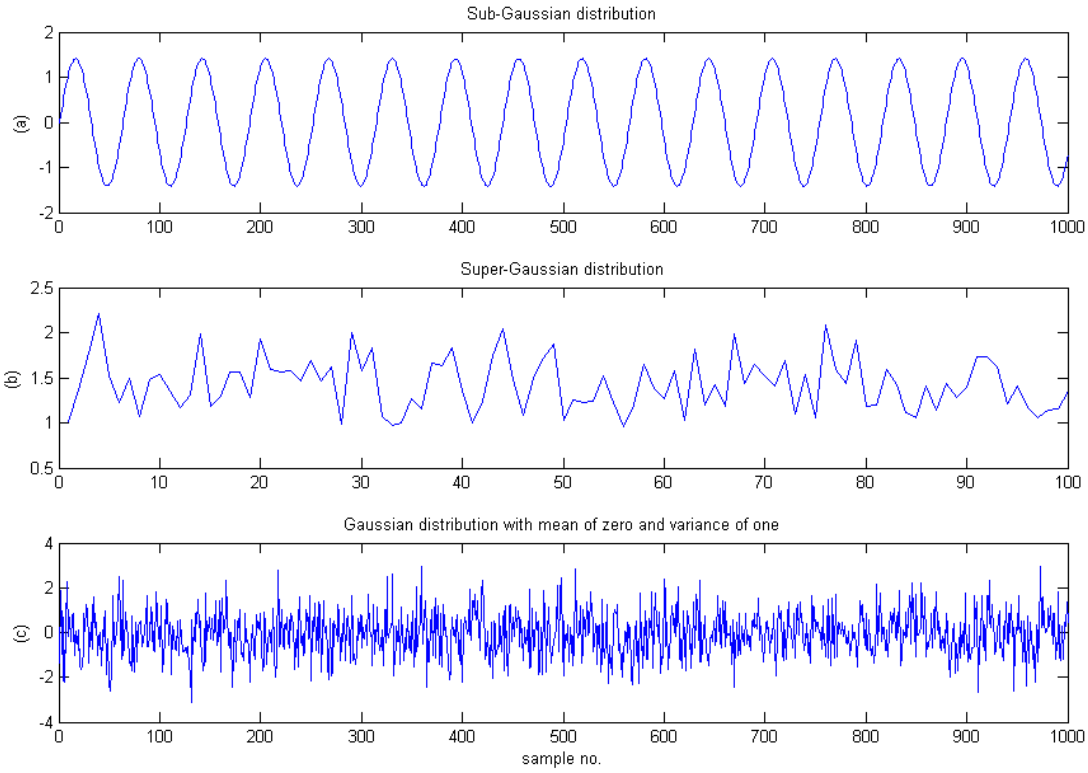


Figure 3.7: (a) Sub-Gaussian, (b) Super-Gaussian, and (c) Gaussian distributions with a mean of zero and a variance of one. MATLAB source code to plot the Sub-Gaussian, Super-Gaussian and Gaussian distributions with a mean of zero and a variance of one is attached in Appendix B, page 203

### 3.4.1 Sub-Gaussian separation

The first set of source separation shows the TS-ICA model separation of sub-Gaussian signal from the randomly mixed signal.

The novel EGBD method as discussed in section 3.2.1 step-7 in TS-ICA algorithm separates the sub-Gaussian source signal from the mixed signal as shown in figure 3.8.

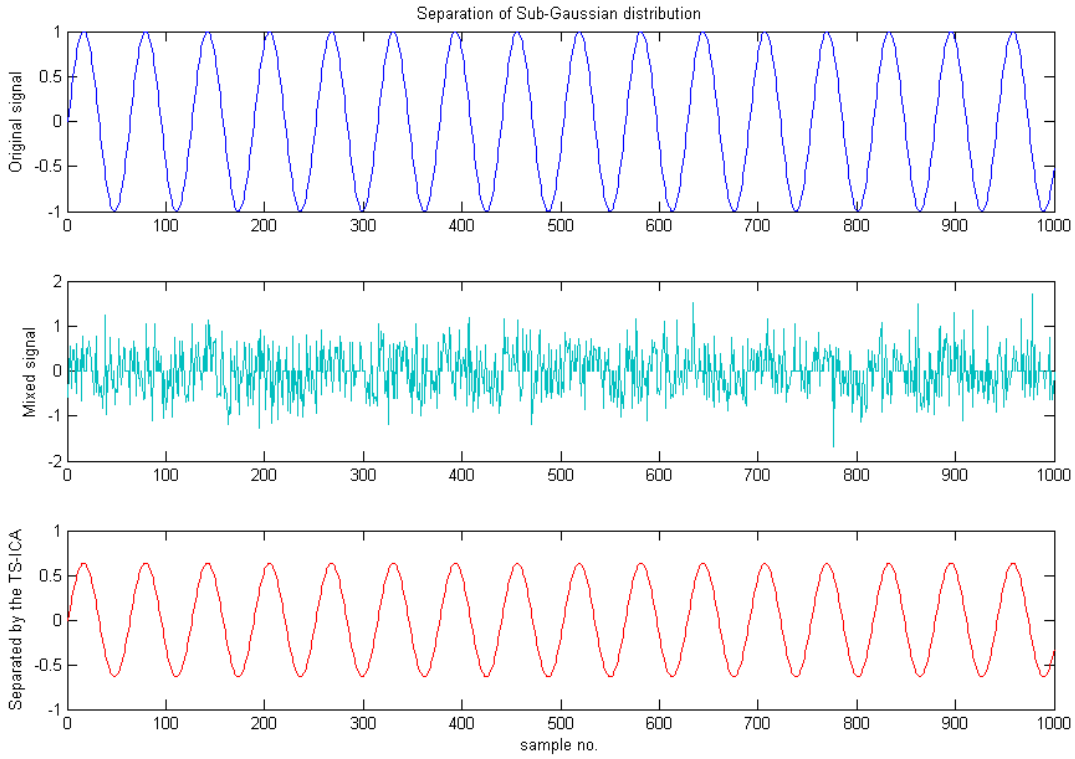


Figure 3.8: Separation of sub-Gaussian distributions from the randomly mixed signal. MATLAB source code to plot the Separation of sub-Gaussian distributions from the randomly mixed signal is attached in Appendix B, page 204

### 3.4.2 Super-Gaussian separation

The second source separation shows the TS-ICA model separation of super-Gaussian signal from the randomly mixed signal.

The novel EGBD method as discussed in section 3.2.1 step-7 in TS-ICA algorithm separates the super-Gaussian source signals as shown in figure 3.9.

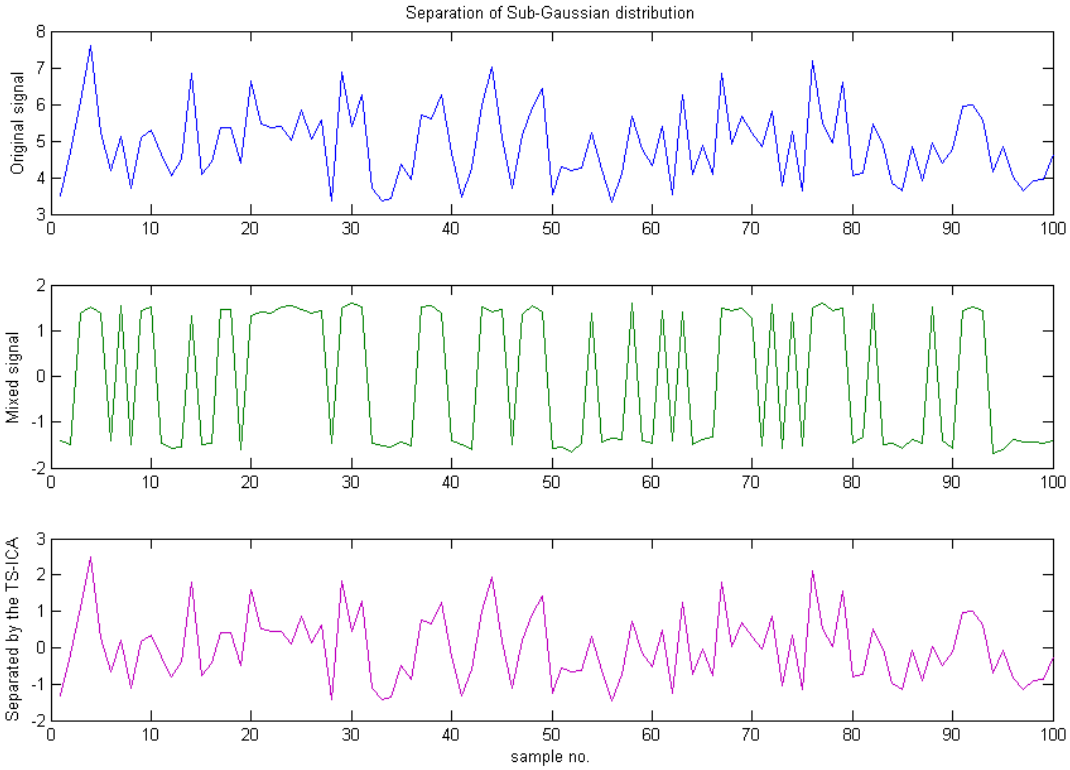


Figure 3.9: Separation of super-Gaussian distributions from the mixed signal. MATLAB source code to plot the Separation of super-Gaussian distributions from the randomly mixed noise is attached in Appendix B, page 205

### 3.4.3 Gaussian sequence with mean of zero and a variance of one

The third set of source separation shows the TS-ICA model separation of Gaussian distributions with a mean of zero and a unit variance signal from the randomly mixed signal.

The novel EGBD method as discussed in section 3.2.1 step-7 in TS-ICA algorithm separates the Gaussian distributions with a mean of zero and a variance of one source signal as shown in figure 3.10.

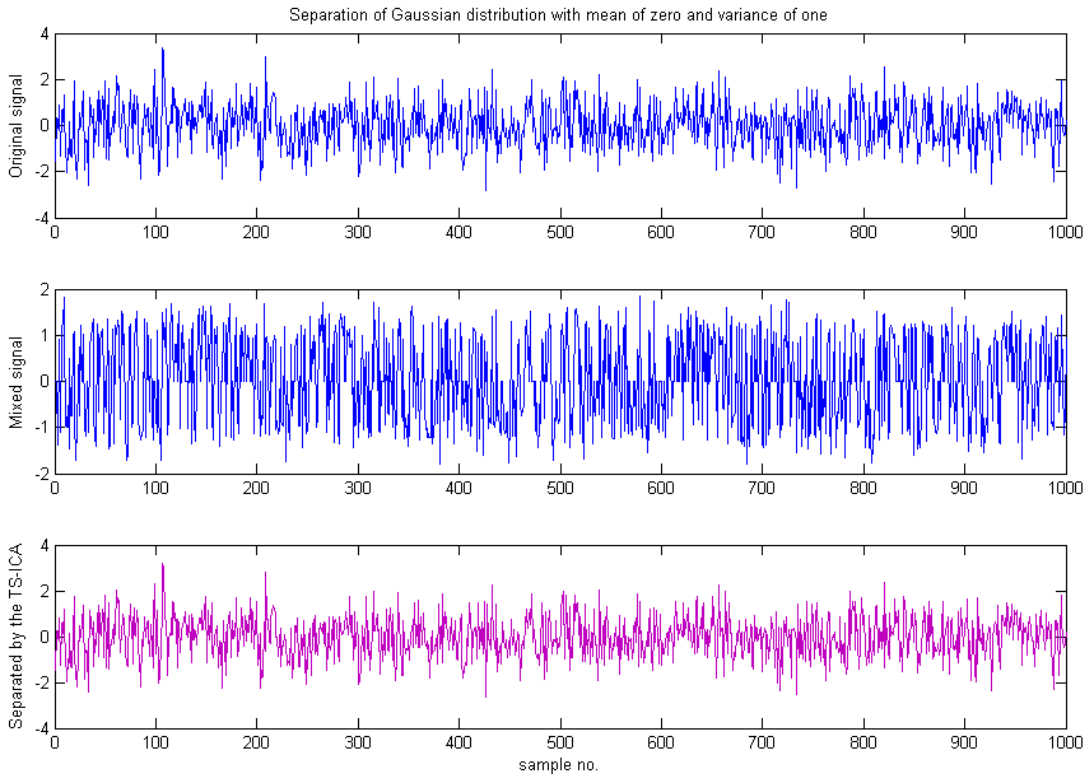


Figure 3.10: Separation of Gaussian distributions with a mean of zero and a variance of one from the mixed signal. MATLAB source code to plot the Separation of Gaussian distributions with a mean of zero and a variance of one from the mixed signal is attached in Appendix B, page 206

## 3.5 Hypothesis

In seismology, the real challenge is to find the true ground velocity and displacement from the raw recordings of ground acceleration time histories. Tilt plays a major role which contaminates the ground acceleration and it is often difficult to find the true ground velocity and displacement. The tilt acceleration can be determined from the recorded acceleration time histories and removed from the raw data, to obtain a better estimate of the true ground velocity and displacement. The TS-ICA model as discussed in section 3.2.1 recovers and

estimates the true ground velocity and displacement which was then compared to the available estimation from the published papers. The separated tilt estimation was evaluated for analysing the accuracy and reliability of the predictions by verifying the corrected source and new corrected source in step 11 and 12 in section 3.2.1.

### 3.5.1 Success criteria

To successfully obtain the tilt, this is extracted from the ground acceleration as follows:

1. The result of the TS-ICA model of ground displacement are compared to the available estimation from the published papers and the GPS measurements.
2. The tilt is separated from the predicted TS-ICA model and is verified step 11 and 12 in section 3.2.1.
3. The tilt acceleration was measured within the ground acceleration recordings to prove the reliability of the system.

## 3.6 Summary and conclusions

This chapter has introduced EGBD as an extension to the ICA model and the combination EGBD and ICA model results in TS-ICA model to separate tilt and provide useful displacement results. The mixing matrix and parameters , , , have been derived theoretically and simulations have been shown using different distribution signals. Shortcomings of the algorithm have been discussed and possible enhancements will be put forward in the next chapter 4, section 4.7.

Simulations have shown that although the separate parts of the algorithm can operate well individually, work needs to be developed to produce a complete system. Careful consideration must also be made as to the signals under consideration, since this can be affected in the final outcome of the implementations.

# Chapter 4

## Model Theories and Concepts

This chapter describes the model theories and the concept used to develop the ICA and addresses the different approaches taken to determine the tilt component. In the first section 4.1 the central limit theorem and observation of uniform distribution signals will be discussed. Section 4.2 will consider the higher order statistics, as selection of the model requires the estimation of higher order terms. Finally section 4.3 describes the other approaches using ICA.

### 4.1 Central limit theorem

Definition: “The limiting distribution of a standardised sum of independent, identically distributed summands as the number of terms increases, is a normal distribution” (Lindgren, 1976).

In adaptive systems the separation problem has two sections: firstly, the contrast must be continuously estimated and secondly, the separation criterion must be updated. It was decided that a good way to offset the effect of outliers in the data would be to design a separation method that would ignore, or at least to some degree discount, out of boundary points in the data.

Separation works in the linear ICA due to the fact that when signals are mixed they look different from unmixed signals in a quantifiable way. Theoretically, this has been approached in many ways (identified in Chapter 3, section 3.1.4), though all methods are maximising the statistical independence of the signals.

This approach is demonstrated in figure 4.1a and 4.1b by adding two signals, and the resulting distribution will be more Gaussian shaped than either of two individual signals as shown in figure 4.2.

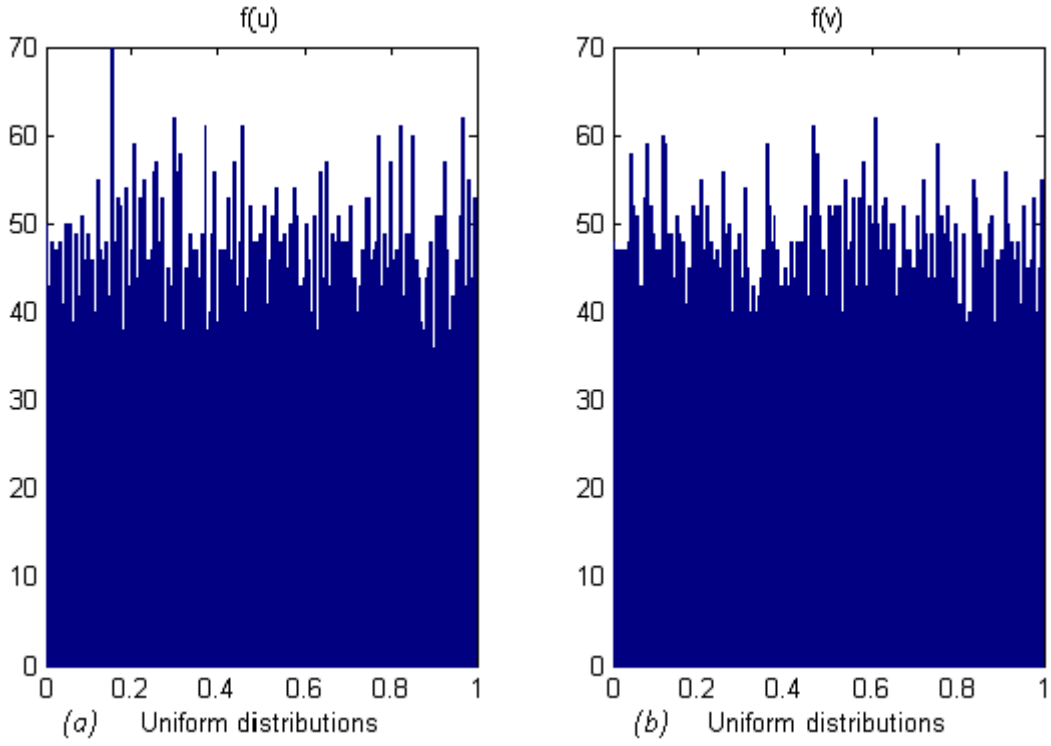


Figure 4.1: (a) and (b) histogram of signals with uniform distributions of function . MATLAB source code to plot the histogram of signals with uniform distributions of function is attached in Appendix B, page 207

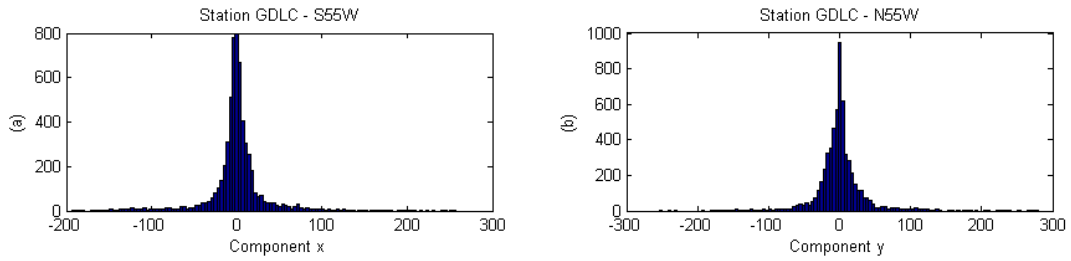


Figure 4.2: (a) and (b) histogram of signals with two different components, where is referred to GDLC – S55W component and is referred to GDLC – N55W. MATLAB source code to plot the histogram of signals with uniform distributions of two different components is attached in Appendix B, page 208

Figure 4.1a and figure 4.1b show histograms of two independent signals drawn from uniform distributions . When signal is added to signal , the resulting histogram is shown in figure 4.3. It is clear that this distribution is more Gaussian than the independent signals of uniform distribution . The shape of the added signals looks triangular, as if it were a convolution of the frequency distributions of . In fact, the addition of the two signal values produces a probability distribution equivalent to a scaled convolution of their individual probability distributions. Moreover, the limiting case when convolving an infinite number of independent signals is Gaussian. Figure 4.2a and figure 4.2b shows histograms of two independent earthquake components from the station GDLC – S35W and N55W.

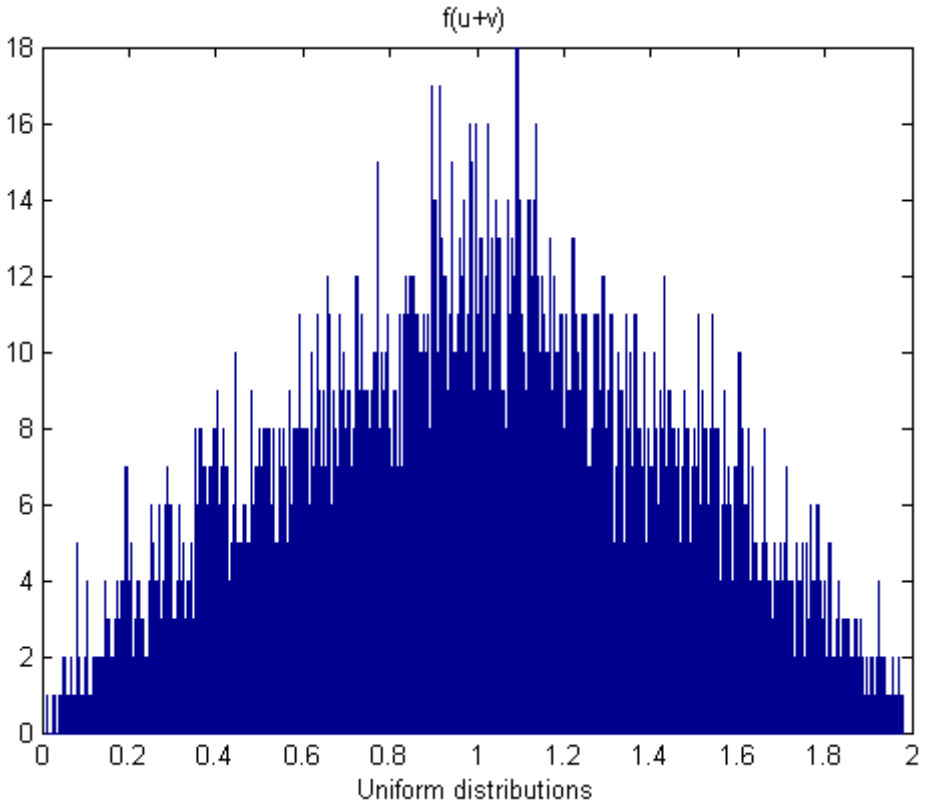


Figure 4.3: Histogram addition of two signals . MATLAB source code to plot the histogram addition of two signals is attached in Appendix B, page 209

Figure 4.4 is obtained by adding two ground acceleration signals GDLC-S35W and GDLC-N55W, the histogram results clearly shows more Gaussian in shape.

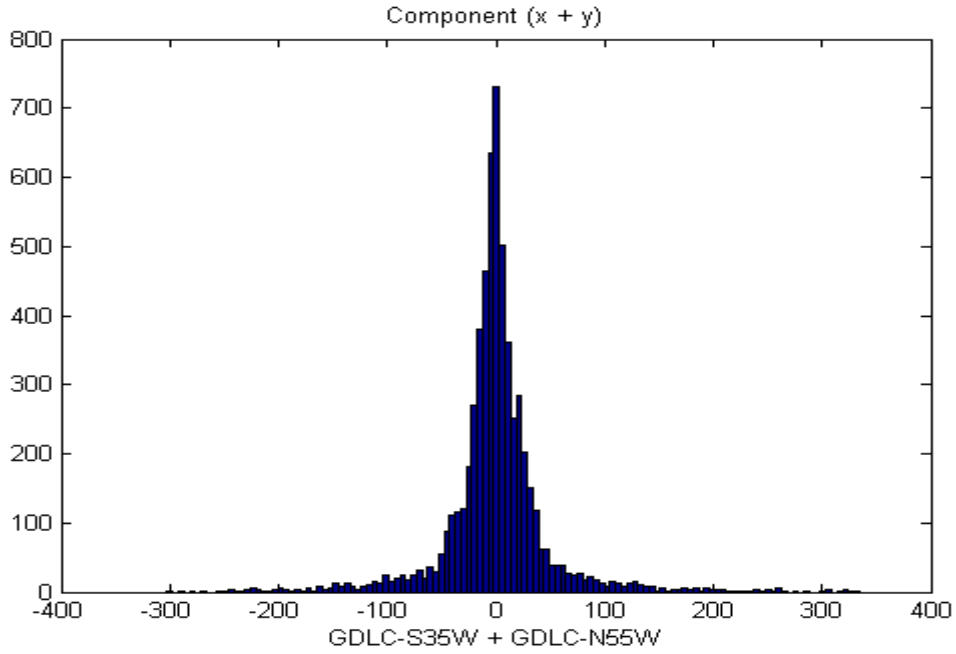


Figure 4.4: Histogram addition of two components . MATLAB source code to plot the Histogram addition of two components is attached in Appendix B, page 210

The figure 4.5 shows the histogram generated for the signal which is added to the signal . The distribution has changed in shape and is no longer a triangular shape, but has more curved appearance of a Gaussian distribution. This phenomenon is why so many processes in nature have a Gaussian distribution and these are often made up of many independent contributing factors. Figure 4.6 shows the histogram generated for the test where component , is added to the signal .

In conclusion, the separation of signals involves maximising their non-Gaussian nature. If a method can be found to measure the distance between the two distributions, then a separation criterion could be designed.

The derivation of a simple metric with which to measure distances between probability density functions has been pursued for many years. For example, the Edgeworth and Gram-Charlier expansions (approximate to a ) are two of many such attempts to parameterise density functions for this purpose. These expansions have even been used to form separation systems (Comon, 1994).

In linear signal separation, complex parameterisations of density functions are not necessarily required. The problem does not necessitate the measurement of distances between distributions for its solution but simply requires some metric of the independence of the signals to be identified.

Using these observations, a simpler numerical method TS-ICA is derived which has the property that it is resistant to a number of observations and depends only on the independence of the data.

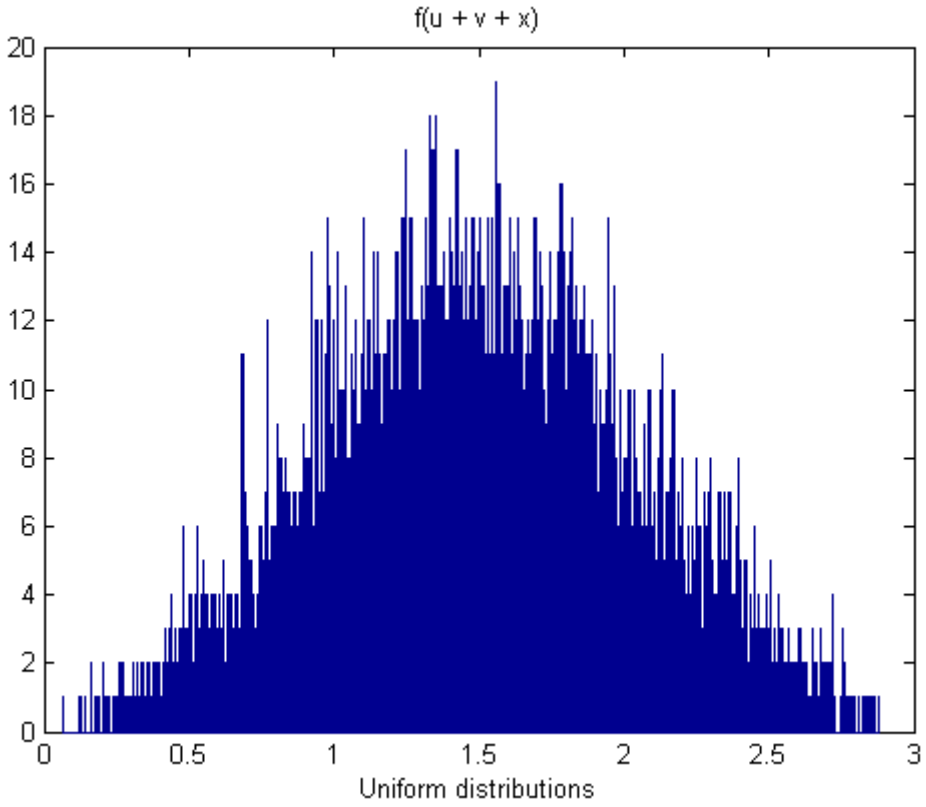


Figure 4.5: Histogram addition of three signals . MATLAB source code to plot the Histogram addition of three signals is attached in Appendix B, page 211

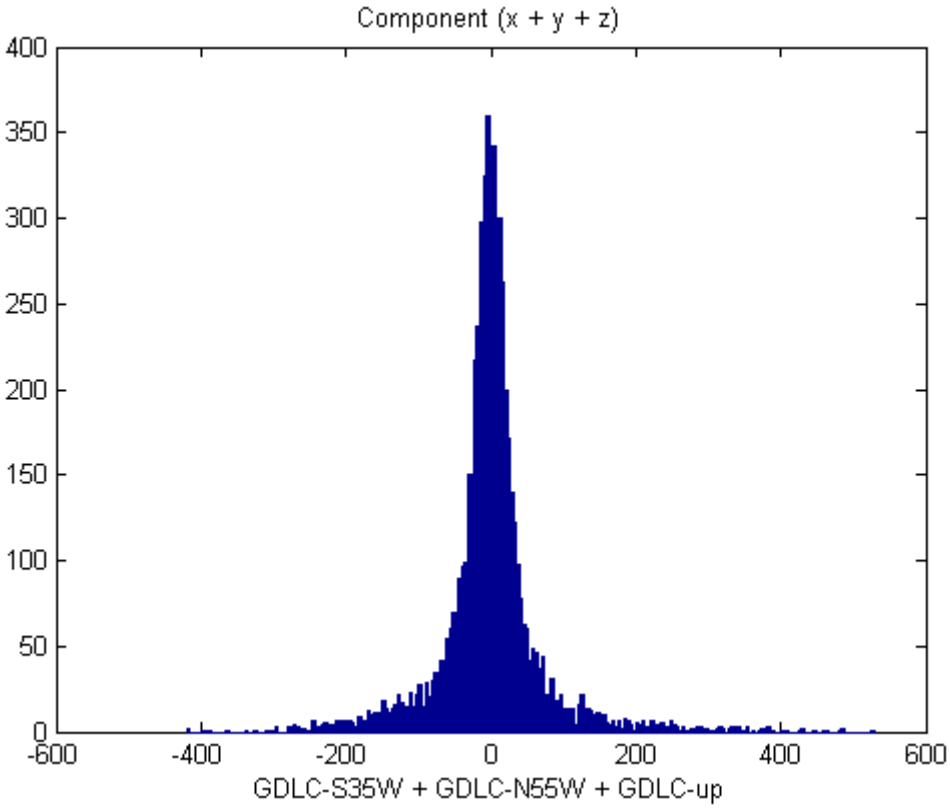


Figure 4.6: Histogram addition of components . MATLAB source code to plot the Histogram addition of components is attached in Appendix B, page 212

### 4.2 Higher order statistics

One of the problems with higher order statistics is that of being disproportionately affected by outliers in the data. Every data point would have equal weighting on the measurement of the separation function, and each datum carries equal information. In practice this is not possible because an exact knowledge of the probability distribution would have to be obtained beforehand, and the fact that this is not easily measured is what makes the separation problem significant in the first place.

Figure 4.7 shows the illustration for estimating the fourth order moment, the signal drawn from a Gaussian distribution whose elements have been raised to the power of three.

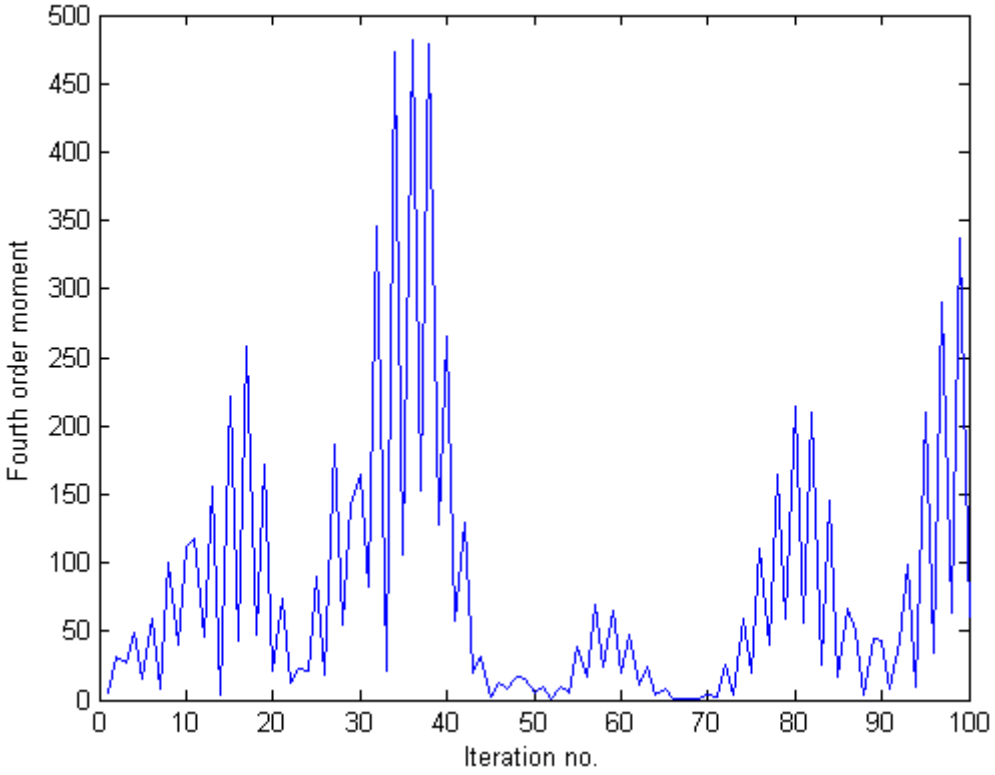


Figure 4.7: Iterative estimation of fourth order moment. MATLAB source code to plot the iterative estimation of fourth order moment is attached in Appendix B, page 213

When large data values pass through the estimator their disproportionately large fourth moments cause a large deviation from the correct value of the moment. Since the actual range of the difference in a given problem is usually much smaller than this deviation, the use of such higher order statistics in this way is problematic.

The reason for this behaviour is illustrated in figure 4.8, which shows the relative values of different orders of moment. This figure graphically illustrates the differences produced between second and fourth orders of power compared with a linear relationship, as the variable is increased. If the function being learned is a linear function of the input then it updates in a linear way. However, if it is of higher order then a large input has a much greater than linear effect on the function, which can disturb the estimate. Just how big this difference is can be seen in figure 4.8. If the input has a value of 2, the corresponding fourth order moment is 16 that is 8 times its value.

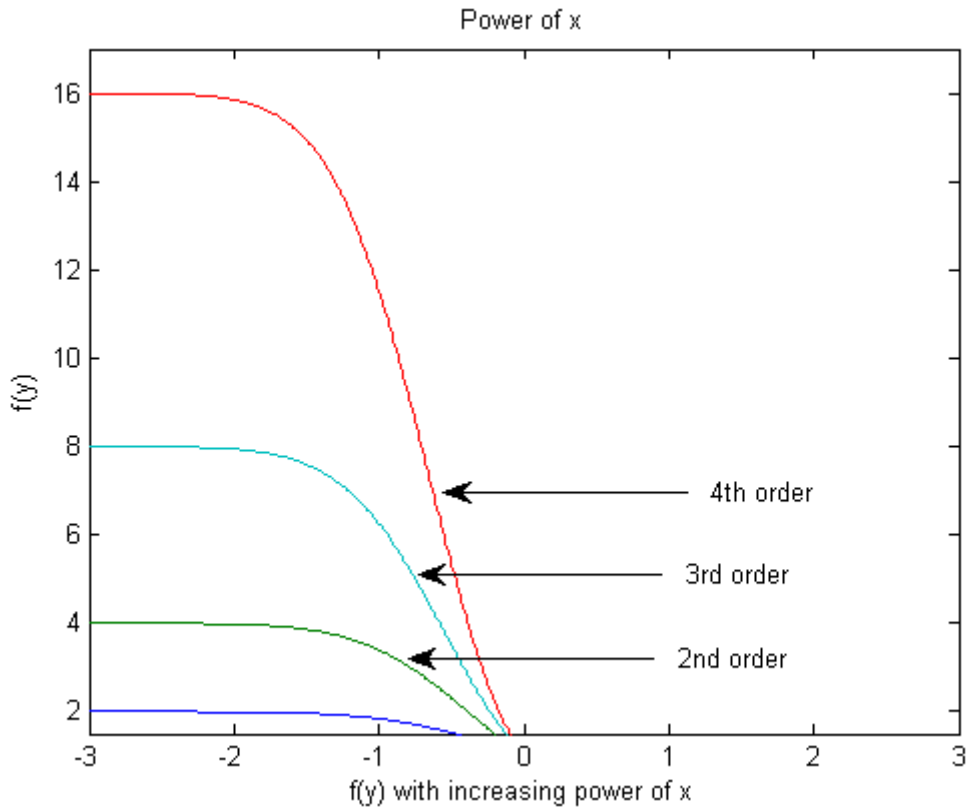


Figure 4.8: Function with increasing power of . MATLAB source code to plot the function with increasing power of is attached in Appendix B, page 214

With an increase in power of the error function also increases linearly thereby providing poor estimates so the higher order moments are used to approximately measure the deviation but not precisely. The skewness and kurtosis are used to measure the Gaussian deviation approximately to observe the non-linearity. TS-ICA is able to exploit the differences in higher order moments in the case of skewness with zero kurtosis.

### 4.3 Other approaches using ICA

For non-linear source separation, other three methods are considered, which are extensions of the ICA methods proposed by several authors, was tried to separate the tilt and also to recover the estimation of true ground displacements. These methods provide poor convergence when compared to the novel TS-ICA model.

1. Post Non-Linear method (PNL) (Taleb and Jutten, 1999)
2. Mutual Information-Based SEParation method (MISEP) (Almeida, 2002)
3. Ensemble Learning – based separation method (NFA) also called Non-Factory Analysis method (Ilin *et al*, 2004)

### 4.3.1 PNL method

The PNL method was initially proposed by Taleb and Jutten (1999), for which there are several sets of constraints imposed to solve the Post Non-Linear ICA problem in order to eliminate its ill-posedness, making the solution essentially unique. Such constraints are interesting in practical situations for the PNL method and were subject to an extensive study by Achard and Jutten, (2005) which included:

- The mixing matrix should be an invertible matrix and has at least two non-zero elements per row and per column
- The functions are invertible and differential
- The of each source is zero in one point at least

Although these constraints are applicable in finding the true displacement results which are close to optimisation, the output signal also diverges. The displacement signals are normalised in order to compare the results, as shown in the figure 4.9.

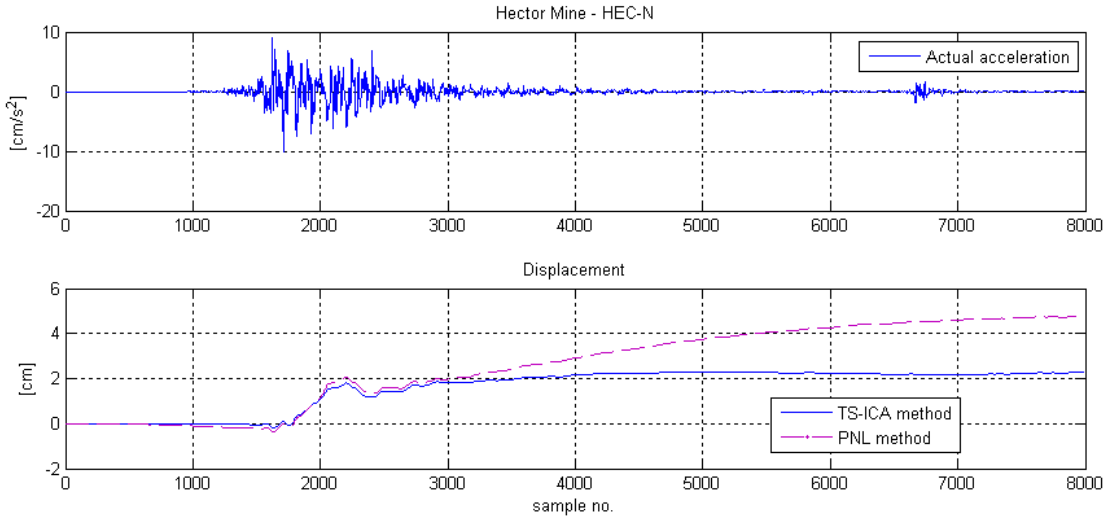


Figure 4.9: Comparison of the TS-ICA model provided displacement results with PNL method. MATLAB source code to plot the comparison of the TS-ICA model provided displacement results with PNL method is attached in Appendix B, page 215

### 4.3.2 MISEP method

The MISEP method is an extension of the INFOMAX linear ICA method for the nonlinear separation framework, and was proposed by Almeida, (2000)

- This method uses maximum entropy for the estimation of
- It computes the gradient with the network weights using the gradient based optimisation method
- It computes the gradient through back propagation to determine the desired results

This method is appropriate for the large number of elements equal to non-zero, whereas the ground acceleration contains a lot of elements with zero values. This constraint often occurs when calculating the gradient of a weight which will be an increasing error and will not produce optimised results.

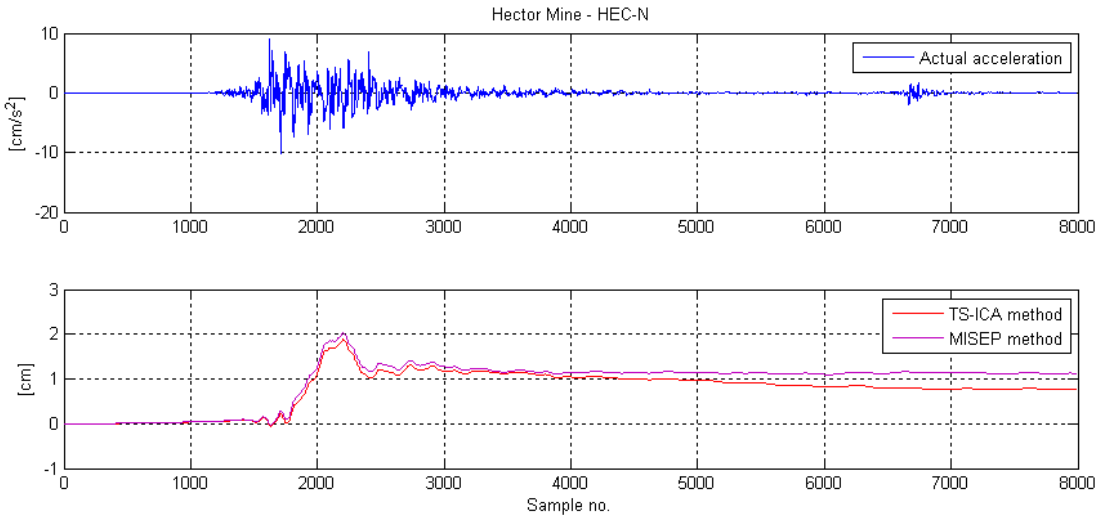


Figure 4.10: Comparison of the TS-ICA model provided displacement results with MISEP method

The normalised displacement results are shown in figure 4.10. This method generates results close to optimisation but does not give good results for earthquake data of higher magnitude ( ), and results diverge as compared to the TS-ICA model.

The complete source code for the MISEP method is available at [http://www.lx.it.pt/~lbalmeida/ica/mitoolbox.html/MIToolbox.zip].

### 4.3.3 Ensemble Learning method

This method provides good results for the input data with a minimum sample length. However for the large data set a high speed computer is required to process the data otherwise it takes a long time to solve. Also a large number of iterations must be considered, otherwise the output signal does not converge which can be seen in the figure 4.11.

The procedures for the method are:

- Non-linear ICA using Ensemble Learning and noise assumed to be independent and Gaussian with a zero mean

- The central aspect of this method is the representation that corresponds to an encoding with minimal length.
- Apply the minimal length to find the source with the optimal solution.
- Approximation of the cost function is based on quadratic or linear behaviour of the non-linearities

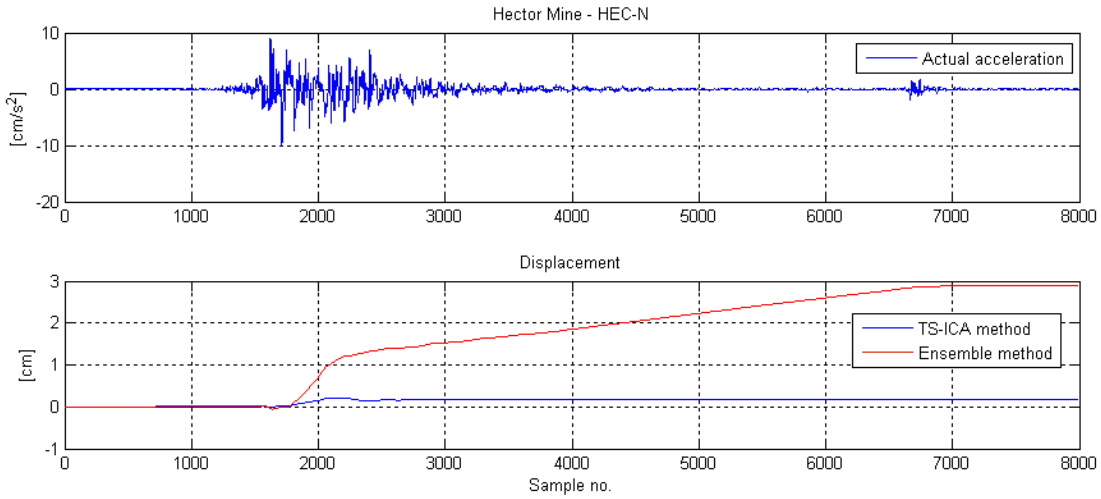


Figure 4.11: Comparison of the TS-ICA model provided displacement results with Ensemble Learning method.

Figure 4.11 shows a comparison of results from the two methods. The Ensemble method results diverges the output signals and is not close to optimisation for a small number of iteration.

The complete source code for the Ensemble Learning method is available at [http://research.ics.tkk.fi/bayes/software/ nlfa-2.0.tar.gz].

## 4.4 Summary

The model, theories and concepts used to develop the ICA model are discussed. It includes the Central Limit Theorem (CLT) which states that the sum of individual independent components lead to a Gaussian distribution. Hence, the principle of separation of individual components is obtained by maximizing the non-Gaussian distribution. Therefore, CLT is used to estimate the separating vector. The higher order statistics are required for TS-ICA. Fourth order statistics such as kurtosis is the measure of non-Gaussian distribution. Other nonlinear methods such as PNL, MISEP and Ensemble Learning, are used to obtain the estimation of ground displacement and these methods results in poor convergence when compared to the TS-ICA model.

# Chapter 5

## Tilt Separation Independent Component Analysis Model

In this chapter, a novel method of addressing the linear instantaneous (characteristics of the source signal are not changed) mixture of the seismic signals is developed in order to remove the tilt component and recover the estimation of the true ground velocity and displacement. The enhanced GBD iterative numerical algorithm is also introduced in TS-ICA model was discussed in section 3.2.1. This approach was derived by Karian *et al*, 1996 in order to address concerns over the effects of outliers of the fourth- and higher- order contrast algorithms for the adaptive system. In this chapter source separation have been made using TS-ICA model with the Hector Mine data source when mixed with an artificial tilt of .

### 5.1 Introduction

In the real near field of an earthquake, the rotational components (two horizontal components) may not be negligible as compared to the vertical components. The integration of the translational accelerations, is actually the sum of linear acceleration, tilt and noise, results in velocity contaminated with tilt plus noise.

In this research it is proposed to extract the tilt component and to recover an estimate of the true ground velocity and displacement using strong motion data.

### 5.2 Strong motion data used

The Hector Mine earthquake data (Grazier, 2005) mixed with synthetic tilt from the shake table with a linearly increasing tilt around the transverse axis of to radians was input and provided a permanent tilt offset. This procedure was used to test the experimental data to remove the tilt angle and estimate the true displacement.

## 5.3 Numerical simulation setup

The TS-ICA model was demonstrated in section 3.4 with an example of two sources of random sub-Gaussian and super-Gaussian distributions in section 3.4. Both signals were mixed with random noise and using the TS-ICA model was used to separate the source signals from the noise component provided good separation as shown in chapter 3 figures 3.8 and 3.9. In the next part the real time Hector Mine earthquake acceleration data (Grazier, 2005) was used. Synthetic tilt data was mixed with the real time strong motion data. The tilt component was separated using the model TS-ICA which is discussed in section 5.5. Further real time earthquake data will be used in chapter 6 to separate the tilt acceleration in order to estimate the true ground velocity and displacement.

### 5.3.1 TS-ICA model procedure

A summary of the TS-ICA model algorithm is described in the following steps:

- Select the component with tilt contaminated signal (vertical or NS or EW components)
- Source signal has zero mean and a stationary probability distribution
- Estimate the mixing matrix
- Pre-process the signal for centring and whitening data
- Calculate the sample moments
- Estimate the parameters initially using GBD
- Apply novel EGBD method to the source signal
- Calculate non-linearities (score function) for the signal
- Vary the contract function until the convergence
- At convergence EGBD optimises the beta values
- Compute corrected source
- Tilt plus noise = Raw seismic data – corrected source
- New corrected source = Raw seismic data – (tilt plus noise)
- This can be verified either way

### 5.3.2 Examples used

Two channel examples are considered here. The signals in these examples were chosen to approximate the kind of separation that may be encountered in real situations. The probability distributions of two signals' in the shorter version (with less data) are shown in figure 5.1.

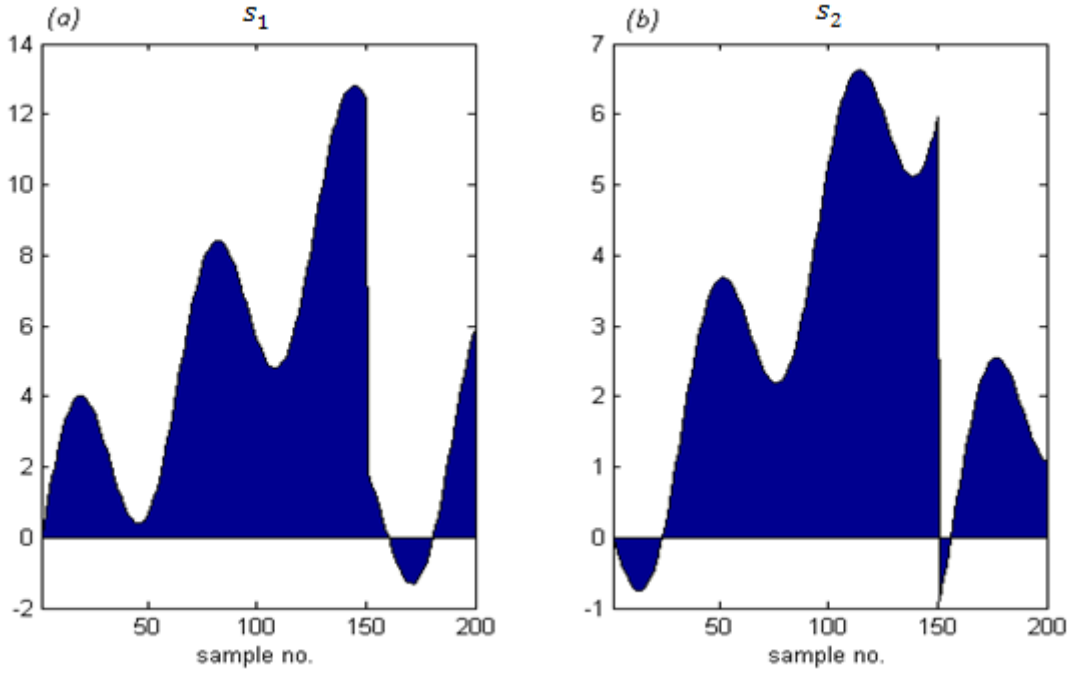


Figure 5.1: Probability distributions of two signals and . MATLAB source code to plot the probability distributions of two signals and is attached in Appendix B, page 218

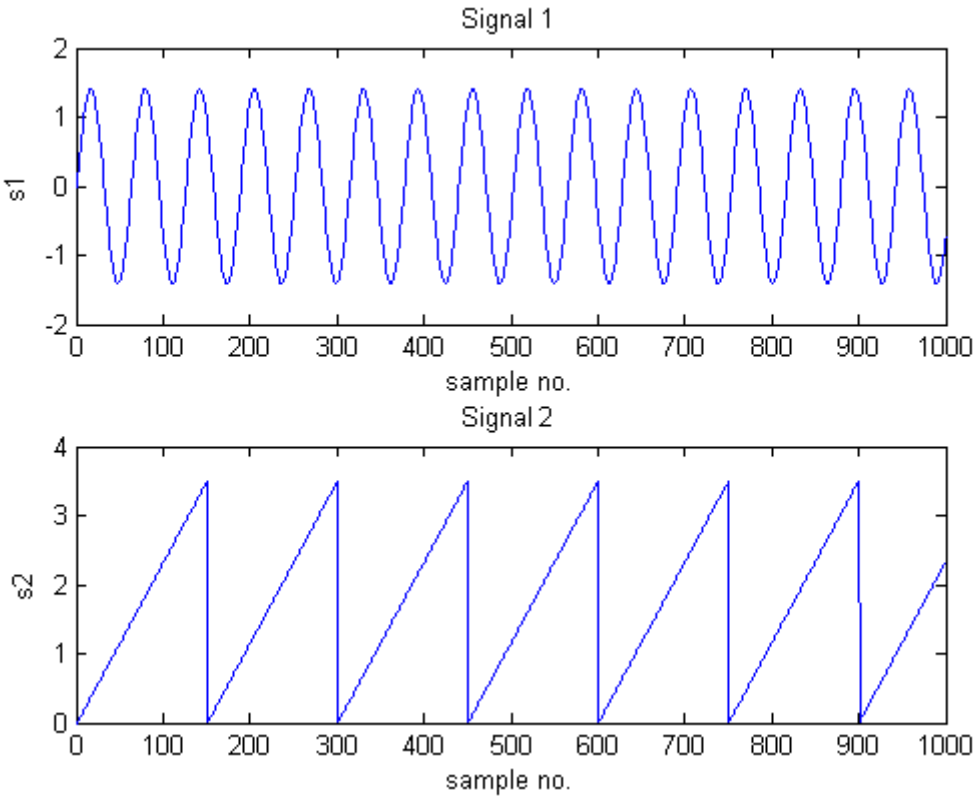


Figure 5.2: Two signals Signal 1 = sine wave and Signal 2 = triangular wave.

Figure 5.2 shows the plots of two signals the sine wave and the triangular wave with 1000 samples of the two sources. The sine wave and triangular wave each had a different period to ensure independence. Figure 5.3 shows a plot of two signals which are and applied to the mixing matrix which have been linearly transformed to identify the original distributions. The signals are then required for pre-processing to achieve the separation efficiently.

The mixing matrix , used was: ,

The mixed signals were formed by:

(5.1)

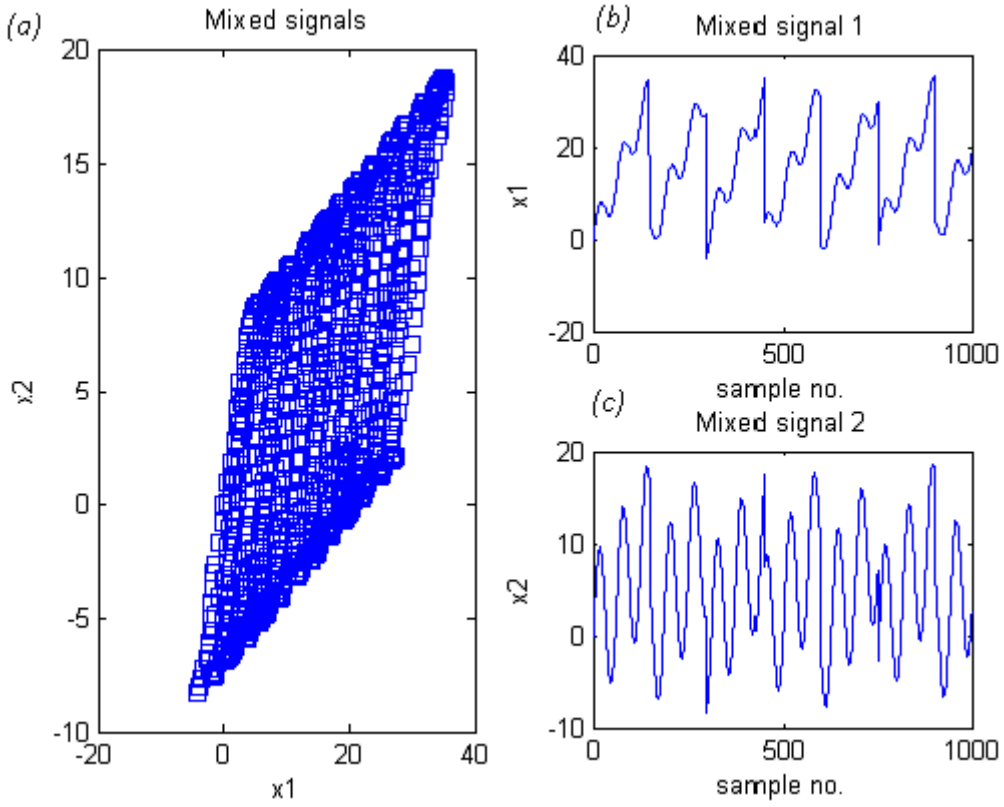


Figure 5.3: (a) Two signals and are linearly transformed; (b) mixed signal 1 ; (c) mixed signal 2 . MATLAB source code to plot two signals and are linearly transformed, mixed signal 1 and mixed signal 2 is attached in Appendix B, page 219

### 5.3.3 Pre-processing the data

#### 5.3.3.1 Introduction

Several techniques are used in the separation process which helps achieve solutions more efficiently although some algorithms fail to separate at all without some pre-processing. These techniques are not separation methods in themselves, but are used frequently in separation methods.

Pre-processing involves signal whitening, where this is a de-correlation method that converts the covariance matrix of a set of samples into the identity matrix . This effectively creates

new random variables that are uncorrelated and have the same variances as the original random variables.

An additional reason to introduce whitening is that some higher-order separation methods rely on the fact that the separation matrix is orthogonal for their operation, and whitening the data fulfils that condition. Further details regarding this process are discussed in section 5.3.3.4.

#### 5.3.3.2 Data processing

To estimate for , the mixed signals need to be centred by subtracting the mean :

(5.2)

After centring the data as shown in figure 5.4, the data should now be whitened,

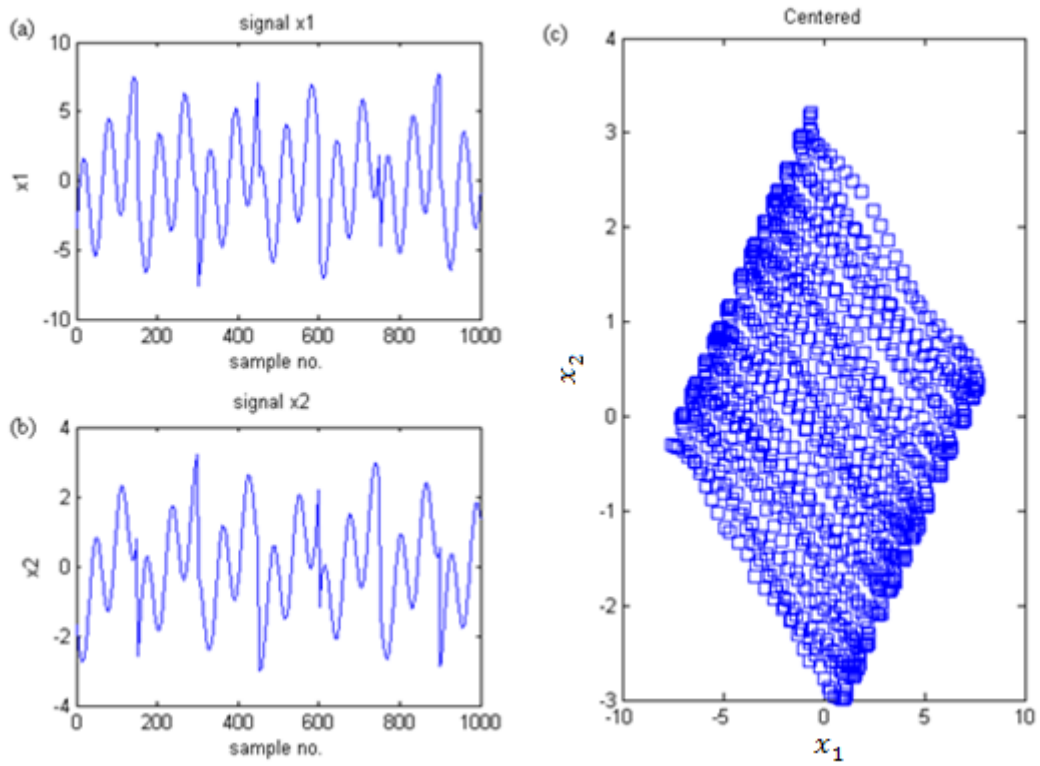


Figure 5.4: (a) signal plot; (b) signal plot; (c) joint distribution of centred signals and . MATLAB source code to plot signal , signal and joint distribution of centred signals and is attached in Appendix B, page 220

### 5.3.3.3 De-correlation of data

De-correlation is equivalent to orthogonalisation in the classic matrix computation. In Principal Component Analysis (PCA) there are techniques to whiten data using the de-correlation condition. That is, when the signals are uncorrelated the expectation of their product is zero. This forces the correlation matrix to be diagonal. With the further condition that the second order statistics are normalised, "the correlation matrix then becomes the unit matrix", this property was independently proposed by Plumbley (1993).

#### 5.3.3.4 Whitening

The signals are normally considered white if their spectral densities are approximately flat over the entire bandwidth of interest. In the discrete-time domain a signal is referred to as (discrete-time) white, if it is uncorrelated with itself from one time point to the next, which is given by:

(5.3)

and

(5.4)

where is a constant, for the variance of , which is independent of frequency. Because this definition of white noise involves only second order statistics, it is sometimes termed second-order white noise since it is possible to characterise white noise by higher than second order statistics (Nikias and Mendel 1993).

When considering whiteness in the source separation field, the definition is slightly more restrictive. In this case the variance is generally constrained to unity (Comon, 1994, Karhunen *et al*. 1995, Cardoso and Laheld, 1996). This normalisation presents no problems in source separation because the signal scaling is undetermined after the mixing anyway.

Whitening is an important pre-processing strategy in ICA. The observed vector is linearly transformed into the new vector which is whitened. The components of the whitened vector are uncorrelated and have unit variance. In other words the covariance matrix equals the identity matrix.

(5.4.1)

Eigen Value Decomposition (EVD) of the covariance matrix is the method used for whitening.

(5.4.2)

where,

is the orthogonal matrix of the Eigen vector of

is the diagonal matrix of the Eigen values

Whitening is achieved by use of the equation , and whitening transforms the mixing matrix into a new mixing matrix .

(5.5)

The process of whitening resides in the fact that the new mixing matrix is orthonormal ( ), that is . Whitening therefore reduces the number of parameters to be estimated, so instead of estimating parameters of the original mixing matrix , it is necessary to estimate only the parameters of the new orthogonal mixing matrix . The orthogonal matrix contains degrees of freedom.

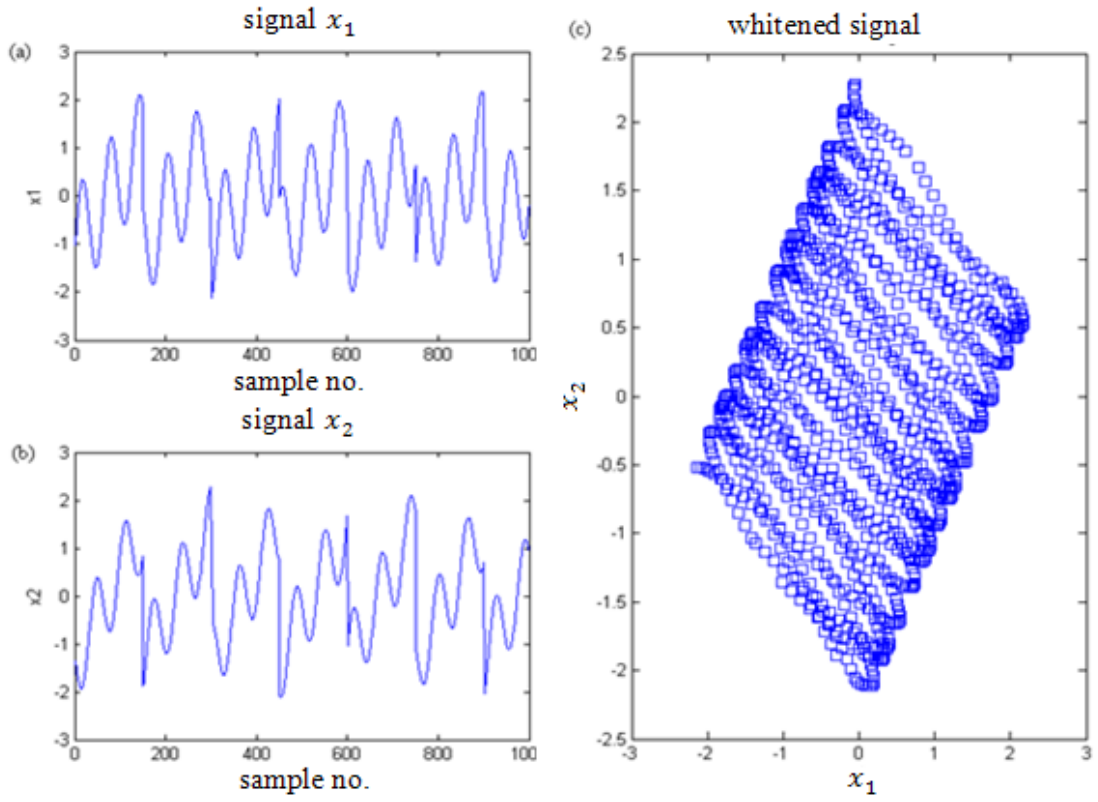


Figure 5.5: (a) signal plot (b) signal plot (c) joint distribution of whitened and centred signals and . MATLAB source code to plot signal , signal and joint distribution of whitened and centred signals and is attached in Appendix B, page 221

In a two dimensional representation the orthogonal transformation is determined by the single angle parameter . In the two dimensional representation of figure 5.5(c) the joint distribution of and which was previously square in shape, after whitening, the signal is rotated to an orthogonal angle and it then becomes the only parameter to be estimated. The size of an orthogonal matrix reduces the size of the original arbitrary mixing matrix. Therefore whitening reduces the analysis by half which reduces the complexity of the problem.

In general, the dimension of the data can be estimated by whitening. Consider the Eigen values and discard those that are small like PCA. PCA maximises the variance and de-correlates the data whereas the whitening in ICA only de-correlates the data.

For continuity, the examples of two signals and were mixed with random noise and the TS-ICA model was applied to separate the mixed random noise. Figure 5.6 indicates that source separation using TS-ICA model is possible to separate a given sub-Gaussian source from the randomly mixed noise signal.

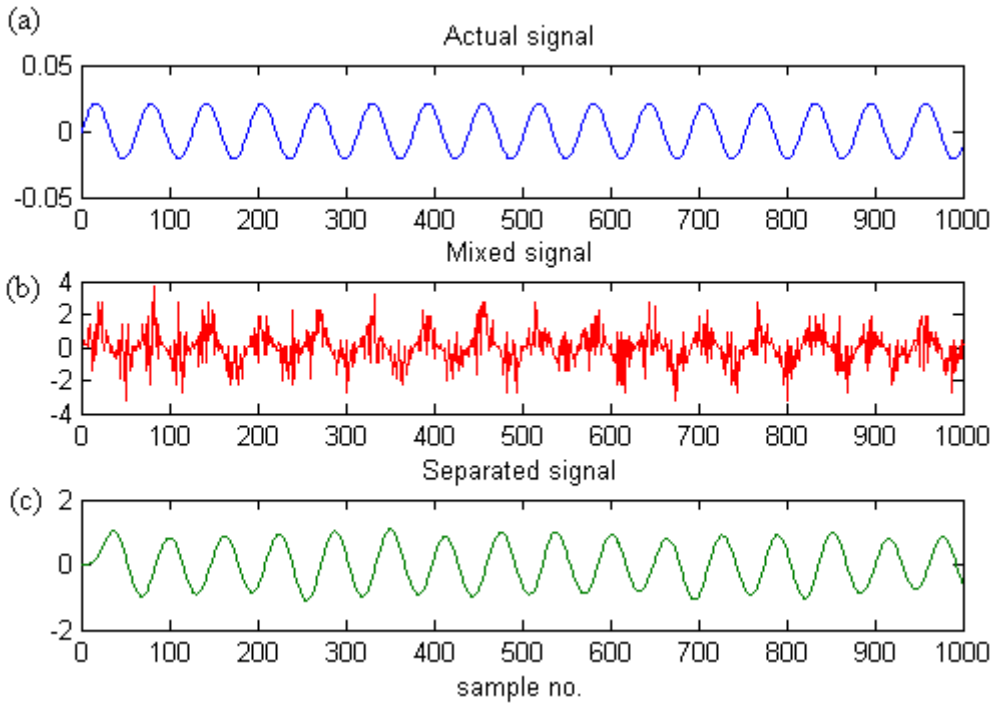


Figure 5.6: (a) Signal of sub-Gaussian source; (b) Signal mixed with random noise; (c) Separation of sub-Gaussian signal from mixed noise

After the simulation was complete, the inverse matrix was estimated and the mixed components were reconstructed.

The estimation of the mixing matrix is:

(5.6)

The values from equation (5.6) are estimated and are approximately equal to the initial mixing matrix. The mixing matrix mixed the signals initially, and its inverse provides the

original signals. Figure 5.7 indicates that source separation using TS-ICA model is possible to separate a given super-Gaussian source from the randomly mixed noise signal.

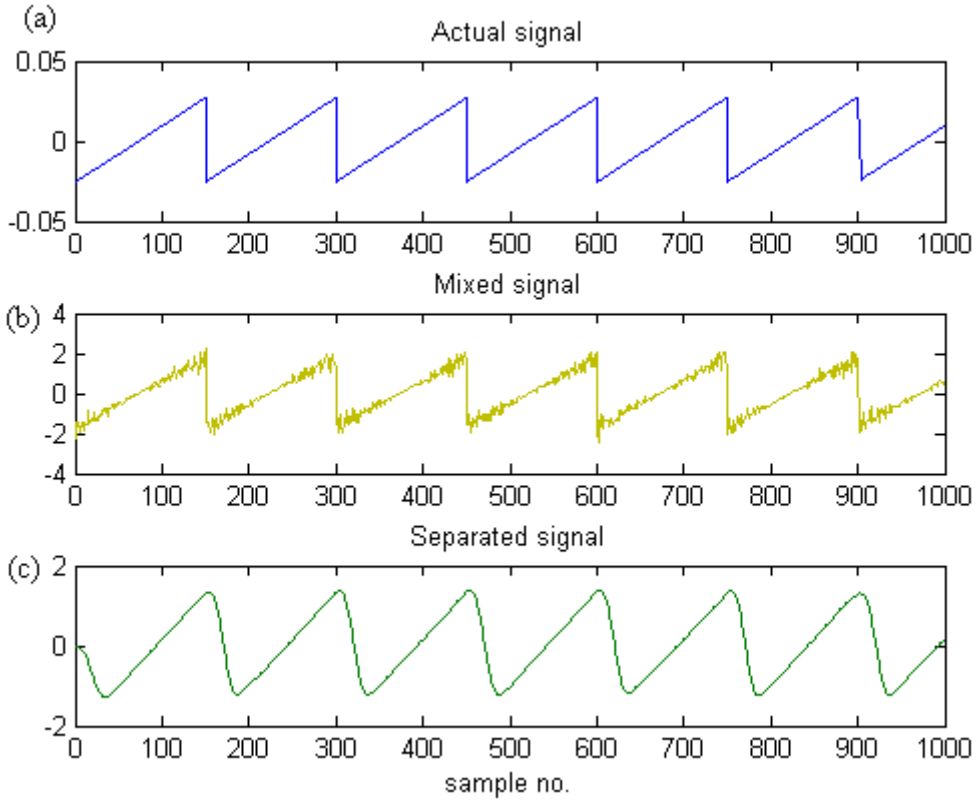


Figure 5.7: (a) Signal of super-Gaussian source; (b) Signal mixed with random noise; (c) Separation of super-Gaussian signal from mixed signal

## 5.4 Enhanced GBD

The main advantage of using EGBD is to provide a bound limit to compared to in GLD, also EGBD is consistent in this process. In EGBD there are four regions of parameter values where the distributions are justifiable, which in the density function is non-negative for all , which is shown in figure 5.8

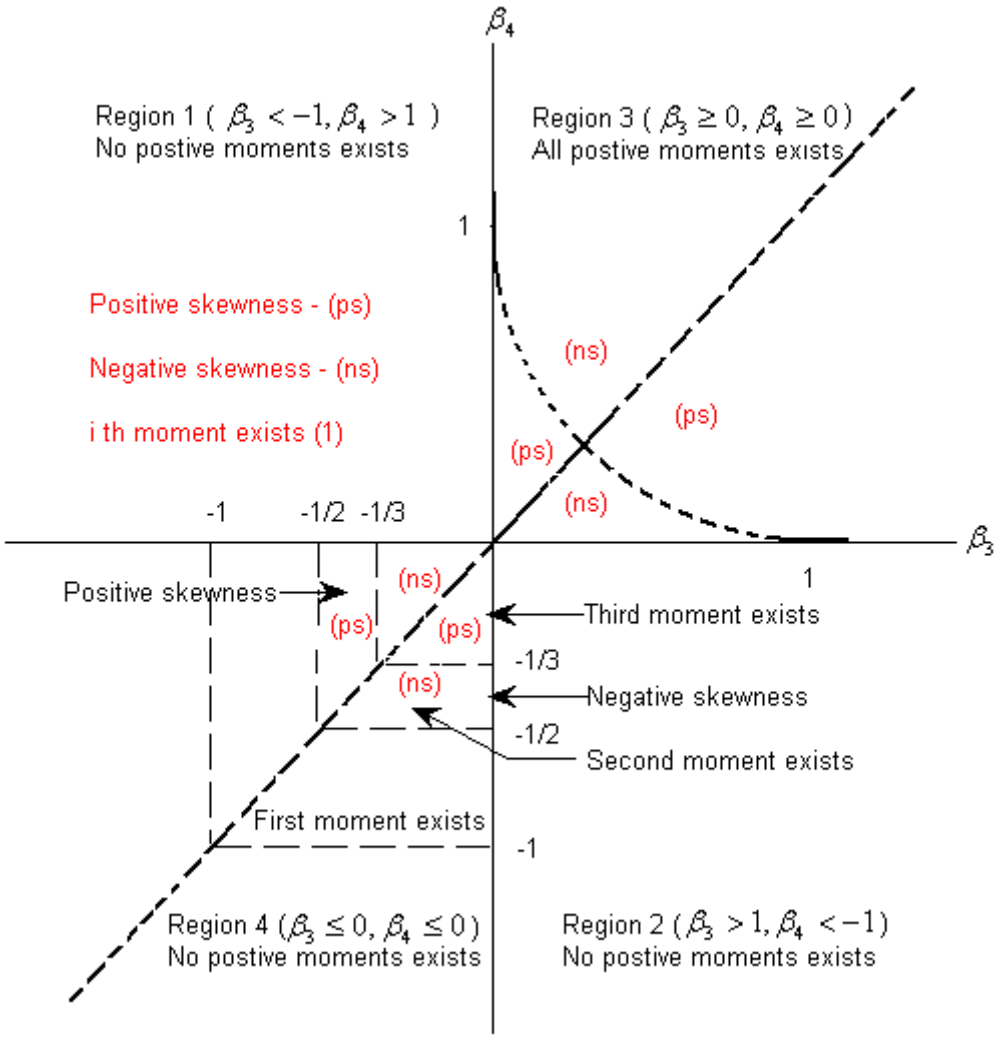


Figure 5.8: Regions 3 and Region 4 are valid EGBD regions.
Other regions is not valid for and

The author Ramberg *et al*, 1979 was interested in the centre of Region 3 and 4 since positive moments do not exist for the distributions in the Region 1 and 2. The values of lies between the Region 3 and Region 4 boundaries and the corresponding relations are given in Table 5.1 and 5.2. Using these criteria, the EGBD model is employed to calculate estimates of the and values.

| Region | The value of $\beta_2$ | The value of $\beta_3$ | The value of $\beta_4$ | Lower bound | Upper bound |
|---|---|---|---|---|---|
| 3 | $\beta_2 > 0$ | $\beta_3 > 0$ | $\beta_4 > 0$ | $\beta_1 - 1/\beta_2$ | $\beta_1 + 1/\beta_2$ |
| | $\beta_2 > 0$ | $\beta_3 = 0$ | $\beta_4 > 0$ | $\beta_1$ | $\beta_1 + 1/\beta_2$ |
| | $\beta_2 > 0$ | $\beta_3 > 0$ | $\beta_4 = 0$ | $\beta_1 - 1/\beta_2$ | $\beta_1$ |

Table 5.1: Region 3, Lower and upper bounds of the distribution

| Region | The value of $\beta_2$ | The value of $\beta_3$ | The value of $\beta_4$ | Lower bound | Upper bound |
|---|---|---|---|---|---|
| 4 | $\beta_2 < 0$ | $\beta_3 < 0$ | $\beta_4 < 0$ | $-\infty$ | $\infty$ |
| | $\beta_2 < 0$ | $\beta_3 = 0$ | $\beta_4 < 0$ | $\beta_1$ | $\infty$ |
| | $\beta_2 < 0$ | $\beta_3 < 0$ | $\beta_4 = 0$ | $-\infty$ | $\beta_1$ |

Table 5.2: Region 4, Lower and upper bounds of the distribution

The determination of values requires the calculation of the first four sample moments as given in equations 3.9, 3.10, 3.11, 3.12. The parameters of GBD are obtained by solving the equation 5.7 and 5.8.

(5.7)

and the equation for ,

(5.8)

where for .

For the parameters and these can be calculated by using

(5.9)

and

(5.10)

The conditions are, if then the parameters and are interchanged (Eriksson *et al*, 2000). With all four beta values it is now necessary to compute the score function. The score function is used to calculate the non linearities of the observation vector and the values of and are updated using the EGBD model.

The score function is derived from the inverse function which was given in the chapter 3, section 3.1.6,

(5.11)

where, and , , , and are the parameters of the distributions. Using the inverse function the score functions are calculated, which was explained in the chapter 3, section 3.1.6.

For the simple case of super-Gaussian signals to parameterise a distribution deviation from Gaussian signals is relatively simple. A probability distribution of super-Gaussian must have the same area as that of a Gaussian signals with a variance of one. Therefore, if the super-Gaussian signal has a higher kurtosis with zero for the skewed distributions than a Gaussian signal, the probability around its mean of zero has to be greater than that of a Gaussian signal. This height of the signal can then be used as a measure of the Gaussian deviation, providing the signal has a variance of one. It is this estimated parameter that has to be calculated using EGBD by the method of moments (as discussed in chapter 3, section 3.1.6) which is used in the following sample test on the uncorrected Hector Mine earthquake data mixed with the tilt component.

## 5.5 Visual interpretation of tilt separation

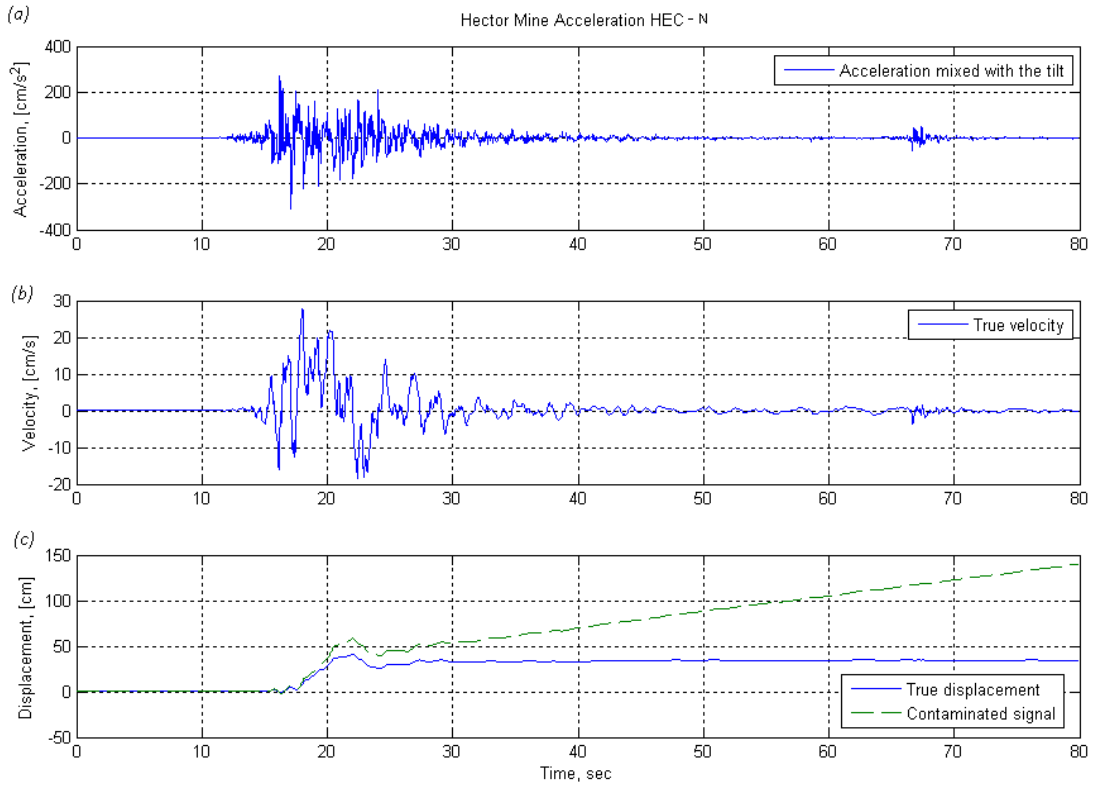


Figure 5.9: (a) the horizontal component of the uncorrected acceleration of the Hector Mine earthquake data; (b) true velocity calculated from the corrected acceleration time histories records; (c) true displacement calculated from the acceleration time histories records contaminated by tilt (dotted line), and displacement obtained using the TS-ICA algorithm for baseline correction. Refer to source code Appendix B, page 222

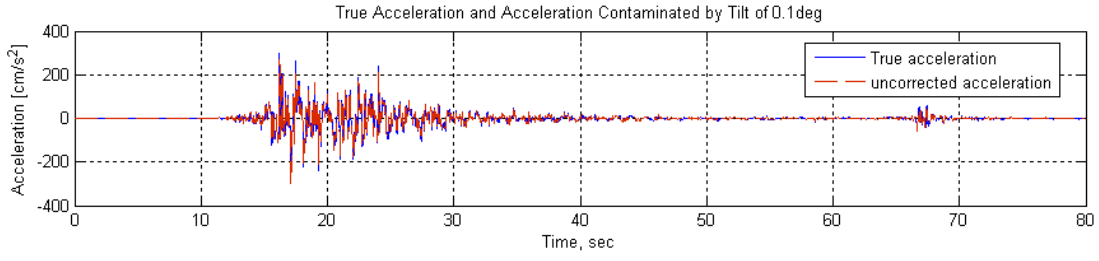


Figure 5.10: Superimposed of uncorrected acceleration time histories records with corrected acceleration time histories records of Hector Mine earthquake.

Figure 5.10 shows the superimposing of two signals corrected and uncorrected acceleration. When the corrected acceleration is integrated twice this provides a better estimation of the ground displacement without any offset. When the uncorrected acceleration is integrated twice this provides a growing displacement as shown in the figure 5.9(c). It clearly indicates that even a small deviation due to tilt and noise provides a significant drift thereby providing unrealistic ground displacement.

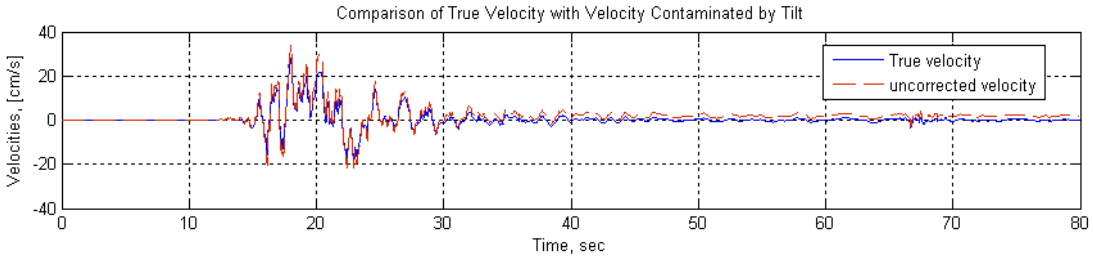


Figure 5.11: Superimposed of uncorrected velocity to corrected velocity of Hector Mine earthquake data

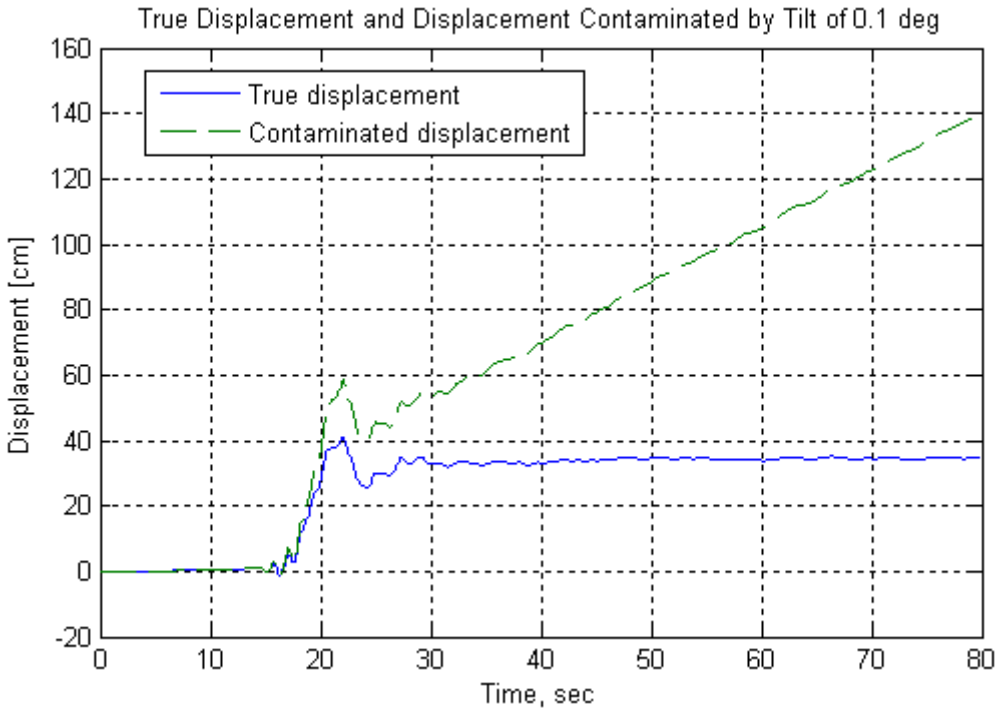


Figure 5.12: Comparison of estimated displacement of Hector Mine data, displacement calculated from the time histories records contaminated by tilt (dotted line) and estimated true displacement (dashed line) obtained using the TS-ICA algorithm for baseline correction.

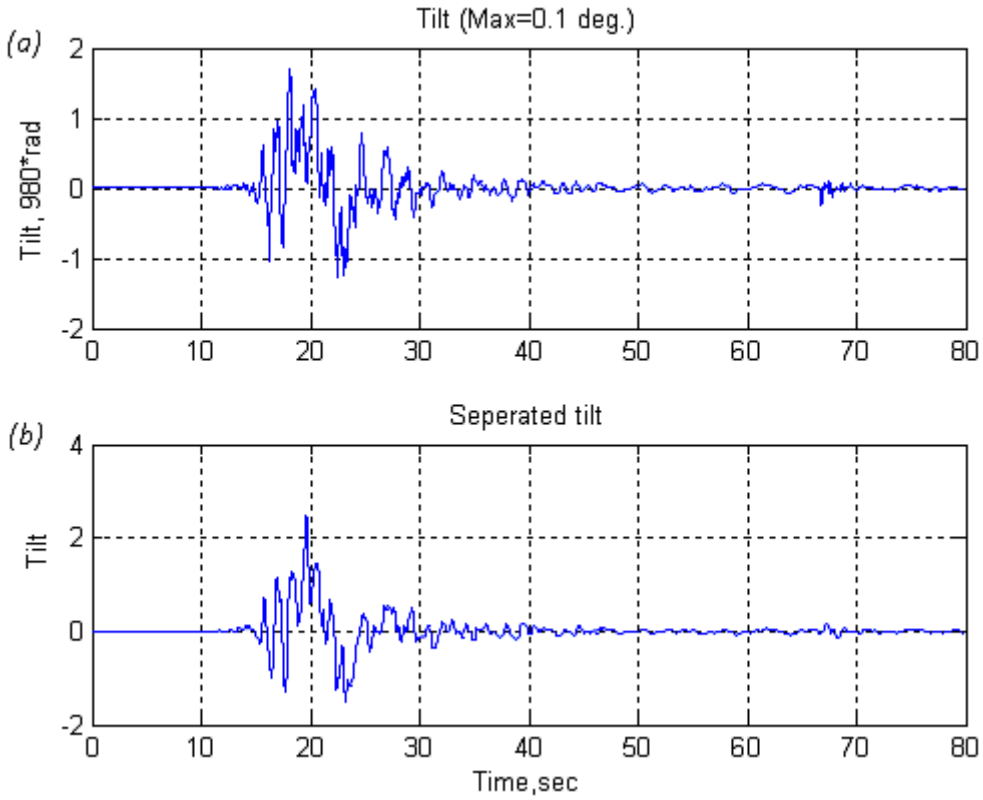


Figure 5.13: (a), Tilt with maximum amplitude of (b), separated tilt from the contaminated record of Hector mine earthquake data

Figure 5.13(a) shows the plot of artificial tilt data, and figure 5.13(b) shows separated tilt from the Hecter Mine earthquake data using TS-ICA model. It clearly indicates that the separated tilt using TS-ICA model is close in approximation to the synthetic tilt.

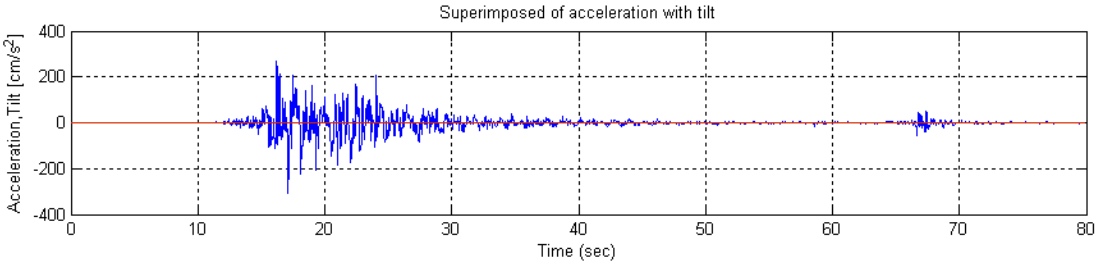


Figure 5.14: Separated tilt from the contaminated record is superimposed on the uncorrected acceleration Hector Mine earthquake data

**5.6 Two studies are presented:**

To investigate the source separation by TS-ICA model, two cases of signal separation were considered. This requires and Gaussian source signal separation from the randomly mixed noise signal and the synthetic tilt separation of the Hector Mine earthquake data. In the first case, and Gaussian signals which were mixed with noise were efficiently separated using TS-ICA, and the results were shown in figure 5.6 and 5.7 respectively.

In the second study, Hector Mine earthquake data was used with the synthetic tilt mixed with the ground acceleration data. The TS-ICA model was used for tilt separation and as a result the useful estimates of true ground acceleration, velocity and displacement were obtained and verified with the available true estimates of the Hector Mine earthquake records. The comparison of true displacement of the Hector Mine earthquake data and tilt acceleration were shown in figure 5.12 and 5.13 respectively.

Contaminated seismic data from four different earthquake's with noise combined with a tilt component for earthquakes of greater magnitude ( ) are used in the TS-ICA model in chapter 6 for the separation of these components in order to estimate the ground velocity and displacement.

## 5.7 Summary

Whitening and centring have been discussed as conditioning methods with respect to the separation problem, and methods for implementation have been suggested. Both have the aim of making the learning rate more efficient, though the natural gradient is superior as it optimises the speed of convergence.

Two set of examples were shown. The first set was randomly generated data of sub-Gaussian (figure 5.2a) and super-Gaussian (figure 5.2b) signals mixed with random noise which was separated and their corresponding mixing matrix was estimated. The second set was the real time Hector Mine earthquake data mixed with the artificial tilt which was separated and the estimated displacement is shown in figure 5.9(c).

# Chapter 6

## Application of TS-ICA model

### 6.1 Introduction

In this chapter the TS-ICA model is applied to real seismic data from four different countries (Taiwan 1999, Chile 2010, Turkey 1999, New Zealand 2011) from which a seismogram of each is tested and results are plotted. This data is provided in the four sections (6.2, 6.3, 6.4 and 6.5) for the four countries and results of components NS, EW, and V, are provided for the corrected ground acceleration, velocity, displacement and separated tilt.

### 6.2 CHI-CHI (1999) earthquake, Taiwan

#### 6.2.1 Data used

The first data set (CBW, 2010) used was from the Chi-Chi (1999) earthquake, Taiwan with a magnitude of . The header file contains the information about the type of instrument A900, station latitude – (24.277), station longitude – (120.766), record length and the sampling rate. The representation of three components are U(+) for the V-vertical component, N(+) for the NS-horizontal component, and E(+) for the EW-horizontal component (using V, NS, EW in the format for all sets of results). The first column represents the time of the recording of the , and surface wave in this order.

The raw seismic data was recorded using the TCU068 accelerometric station of the TSMIP network (Taiwan Strong Motion Instrument Programme).

```
Earthquake : UT1999/ 9/20-17:47:15.850E120.
StationCode: TCU068
LocationLongitude(°XE): 120.766
LocationLatitude (°XN):  24.277
LocationElavation(M):   276.0
InstrumentKind: A900 (T076001.263 )
StartTime: 1999/09/20-17:47:08.000
RecordLength(sec):   90.00
SampleRate(Hz): 200
AmplitudeUnit:  gal. DCoffset(corr)
AmplitudeMAX. U:  519.429~ -296.321
AmplitudeMAX. N:  312.411~ -361.937
AmplitudeMAX. E:  501.604~ -495.742
DataSequence: Time U(+); N(+); E(+)
Data: 4F10.3
    0.000    -0.060    -0.120    -0.239
    0.005     0.120    -0.060     0.179
    0.010     0.179     0.000     0.179
    0.015     0.060    -0.060    -0.120
    0.020    -0.120     0.000    -0.060
    0.025     0.060     0.000     0.060
    0.030     0.060     0.000     0.060
    0.035     0.179     0.000     0.060
    0.040    -0.120     0.000     0.060
    0.045     0.179    -0.120     0.179
    0.050     0.060     0.060    -0.120
    0.055    -0.120     0.000     0.120
    0.060     0.060     0.000     0.000
    0.065     0.179     0.060     0.120
    0.070     0.000    -0.120     0.000
    0.075     0.000     0.000     0.000
    0.080     0.060     0.060     0.000
    0.085    -0.120    -0.239     0.060
    0.090     0.000     0.000     0.060
    0.095    -0.060     0.000    -0.060
    0.100     0.120    -0.060     0.120
    0.105     0.120     0.000     0.239
    0.110    -0.060     0.000     0.120
    0.115     0.060    -0.179     0.060
    0.120     0.120     0.060    -0.060
```

Header file: Station ID - TCU068, Chi-Chi (1999) earthquake, Taiwan.

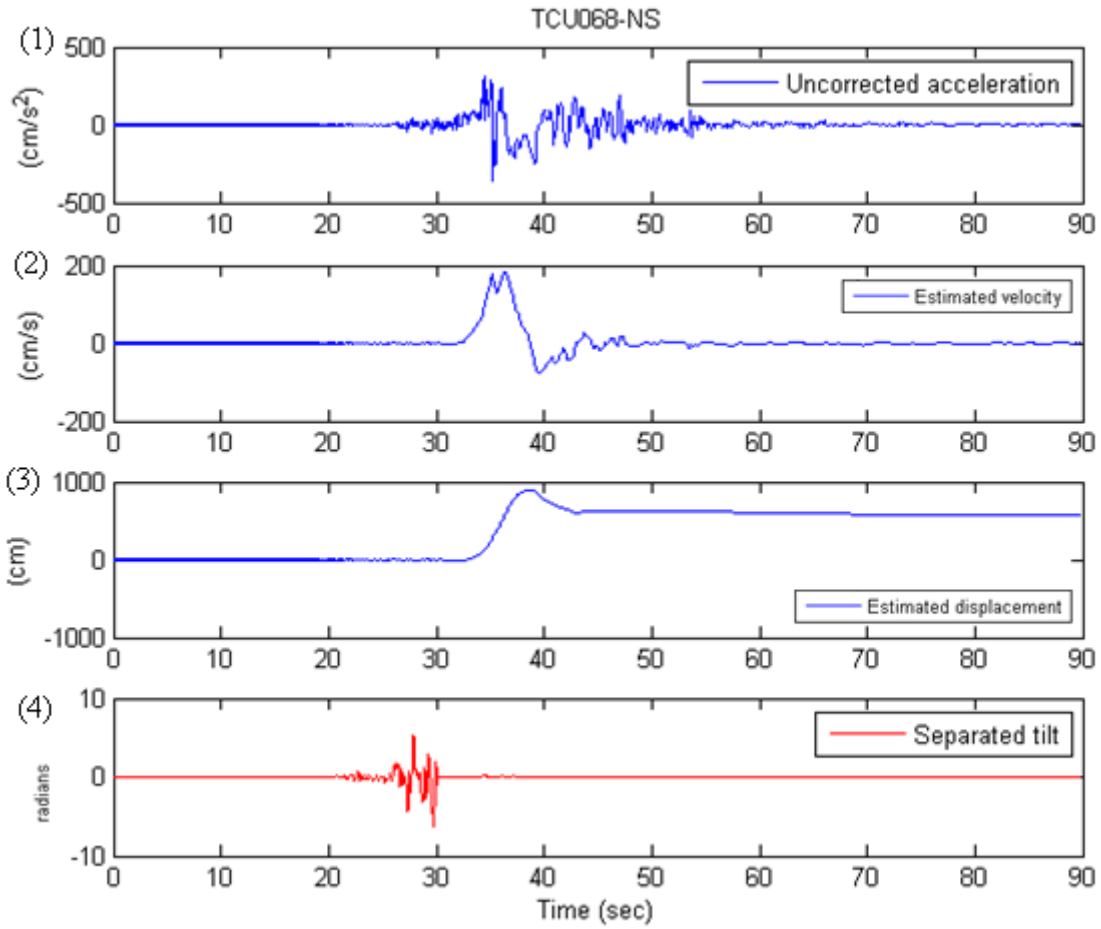


Figure 6.2.1 (a): Chi-Chi earthquake (20 September 1999, Taiwan; ); (1) plot shows the original contaminated acceleration signals in ; (2) plot shows the estimated velocity in obtained by time integration of the corrected acceleration signals; (3) plot shows the estimated displacement in obtained by the second integration of the corrected acceleration signals; (4) plot shows the separated tilt from the acceleration time histories. The estimated tilt maximum amplitude in the positive direction.

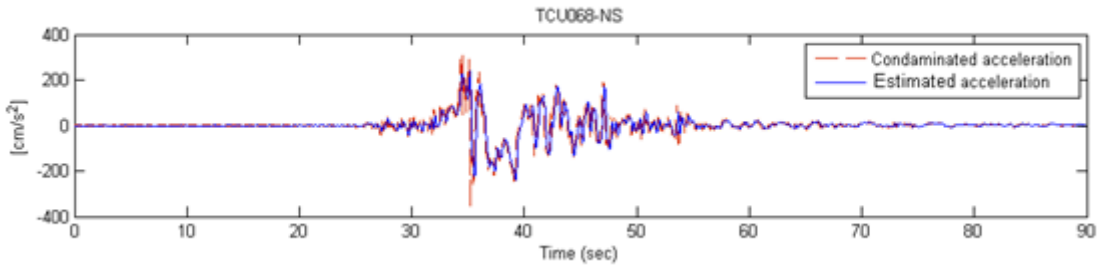


Figure 6.2.1 (b): Comparison between the actual acceleration (dotted line) with corrected acceleration (dashed line) of NS horizontal component of station-TCU068 record.

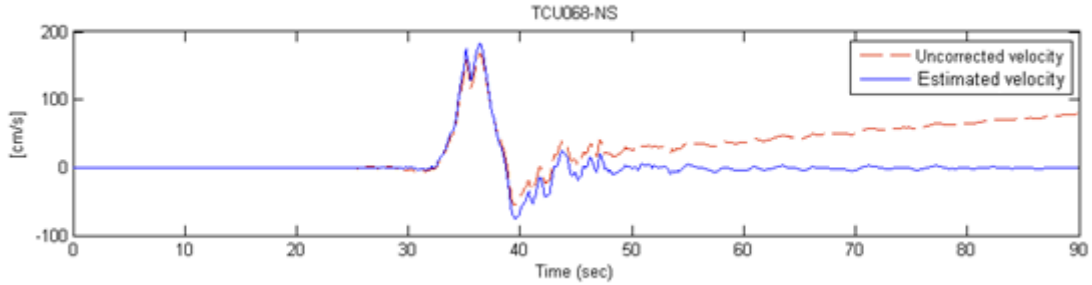


Figure 6.2.1 (c): Comparison between the uncorrected velocity (dotted line) with estimated velocity (dashed line) of NS horizontal component of station-TCU068 record

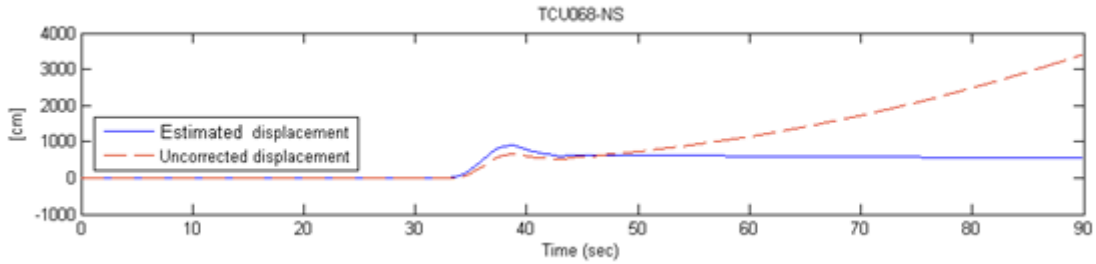


Figure 6.2.1 (d): Comparison between the uncorrected displacement (dotted line) with estimated displacement of NS horizontal component (dashed line) of station-TCU068 record

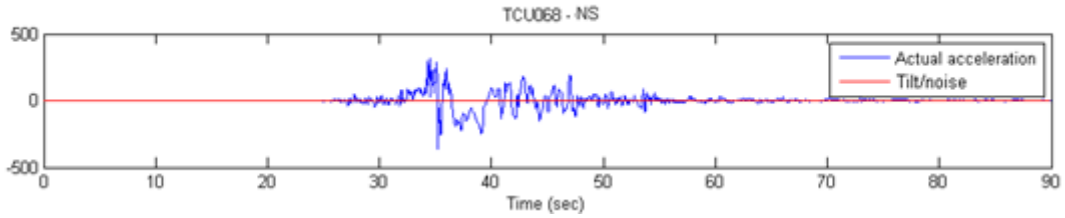


Figure 6.2.1 (e): Raw acceleration data with superimposed deduced tilt component of the horizontal NS component of station-TCU068 record

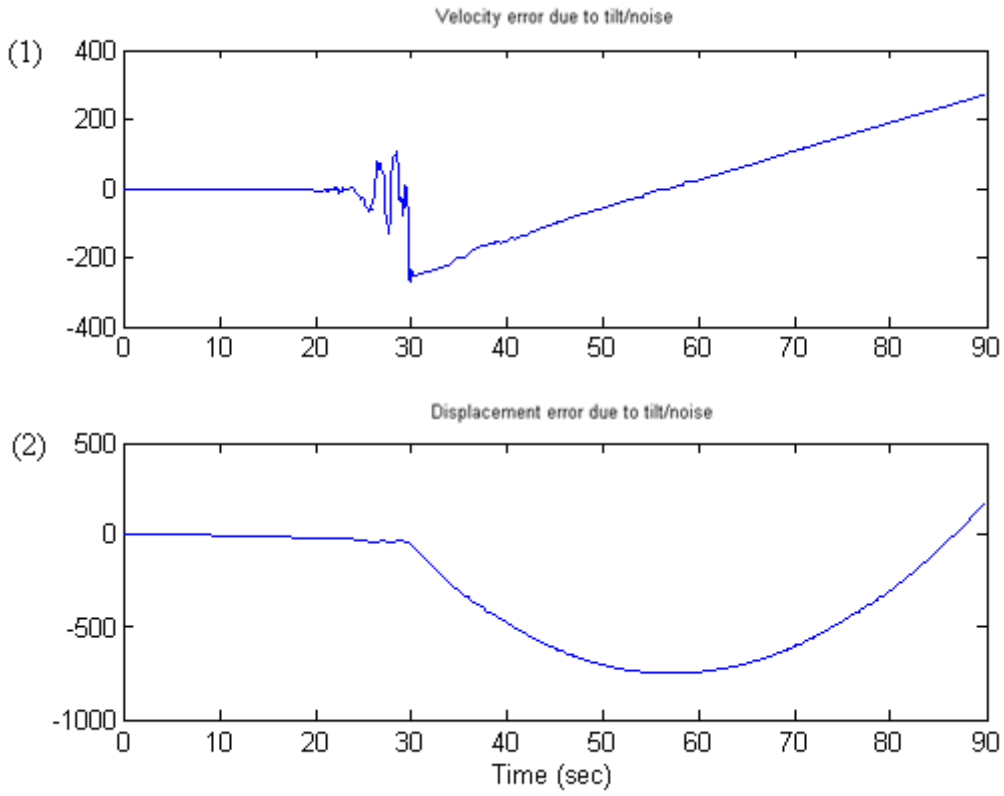


Figure 6.2.1 (f): (1) Velocity error due to tilt/noise of the NS horizontal component; (2) Displacement due to tilt/noise of the NS horizontal component

### 6.2.2 TCU068 EW horizontal component

This section shows the results of the horizontal EW component of station TCU068 of the Taiwan earthquake data, comparison of actual data with baseline corrected output of estimated velocity, estimated displacement, separated tilt, tilt velocity and displacement.

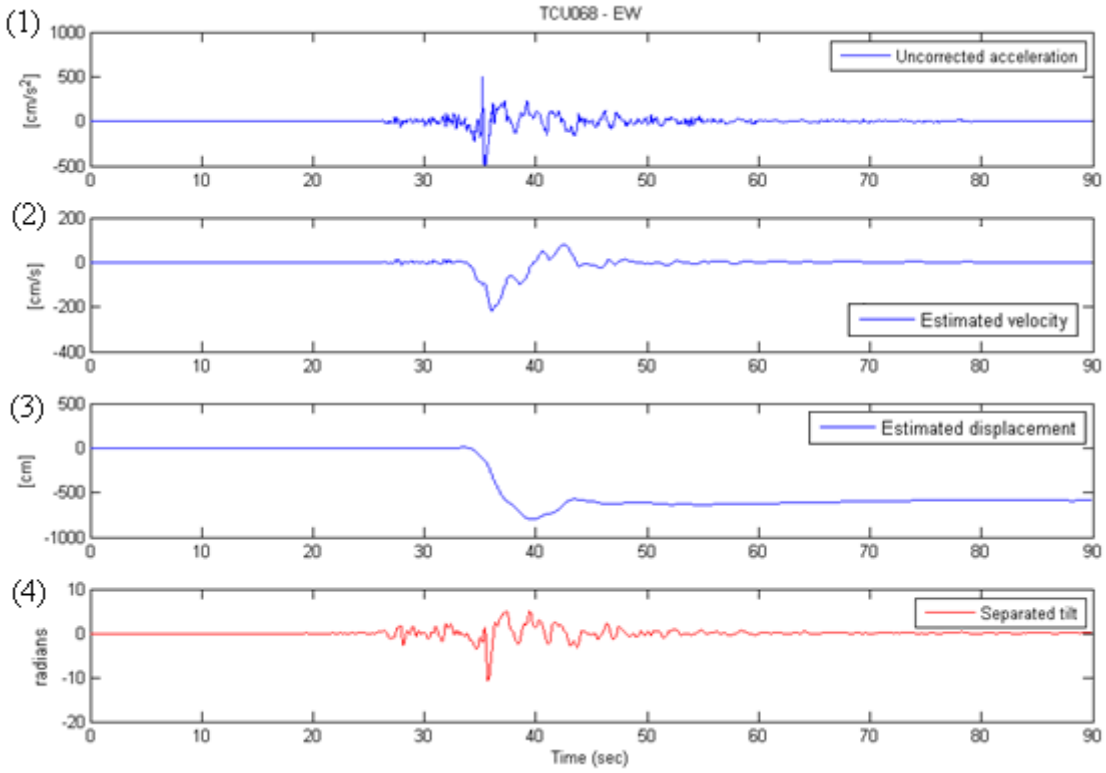


Figure 6.2.2 (a): Chi-Chi earthquake (20 September 1999, Taiwan; ); (1) plot shows the original contaminated acceleration signals in ; (2) plot shows estimated velocity in obtained by time integration of the corrected acceleration signals; (3), plot shows the estimated displacement in obtained by the second integration of the corrected acceleration signals; (4) plot shows the separated tilt from the acceleration time histories. The estimated tilt maximum amplitude in the negative direction.

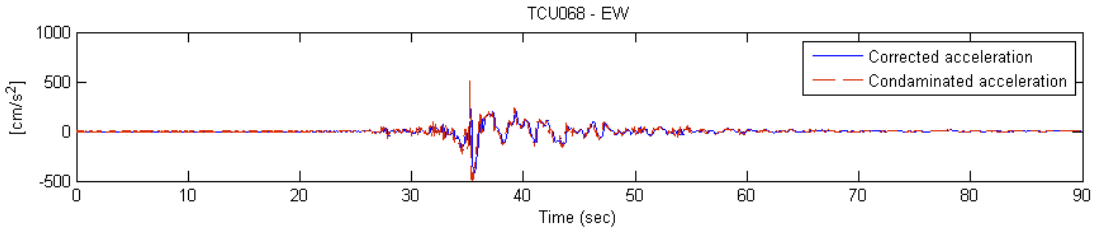


Figure 6.2.2 (b): Comparison between the actual acceleration (dotted line) with corrected acceleration (dashed line) of EW horizontal component of station-TCU068 record.

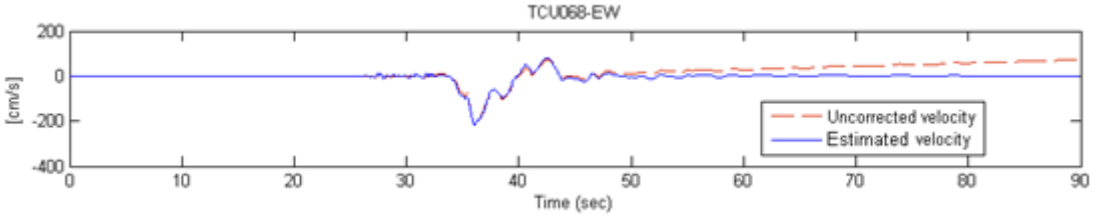


Figure 6.2.2 (c): Comparison between the uncorrected velocity (dotted line) with estimated velocity (dashed line) of EW horizontal component of station-TCU068 record

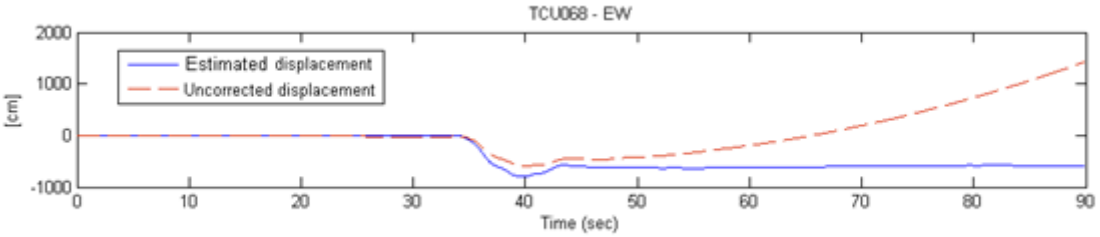


Figure 6.2.2 (d): Comparison between the uncorrected displacement (dotted line) with estimated displacement of EW horizontal component (dashed line) of station-TCU068 record.

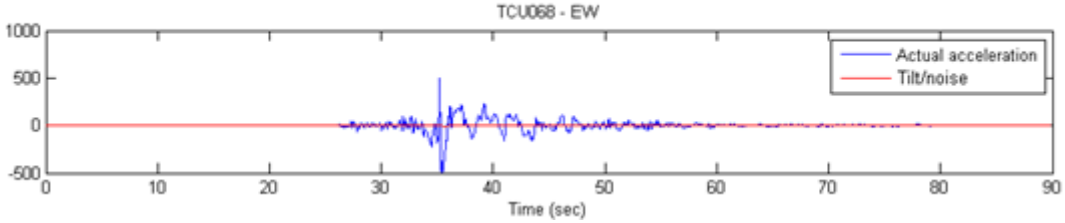


Figure 6.2.2 (e): Raw acceleration data with superimposed deduced tilt component of the horizontal EW component of station-TCU068 record.

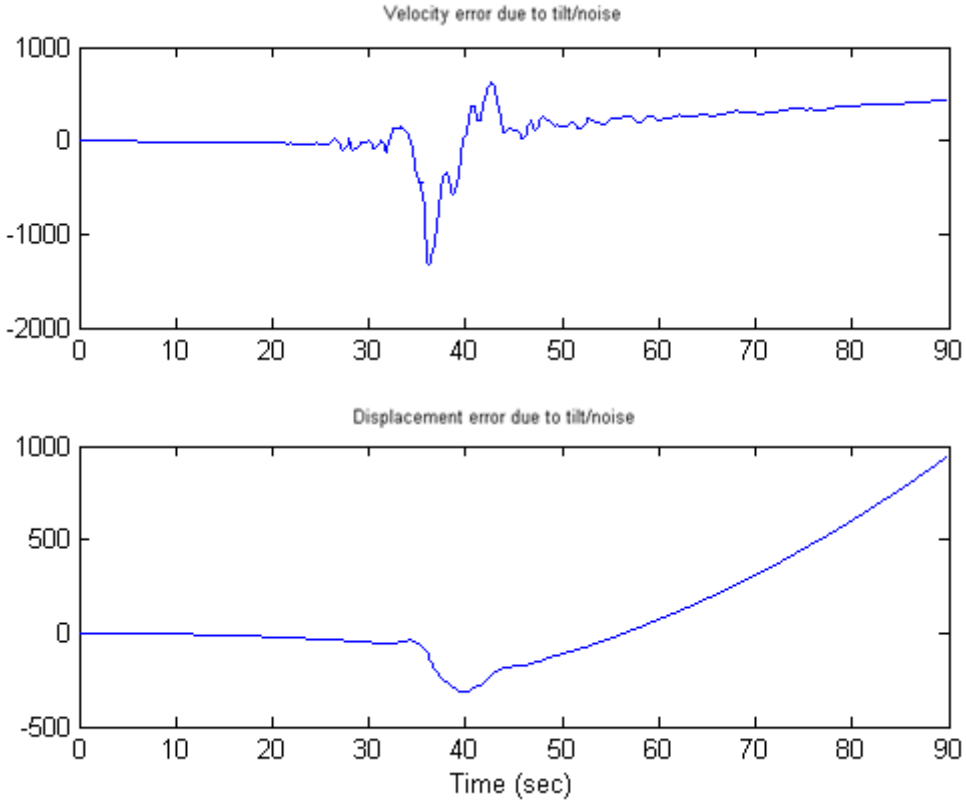


Figure 6.2.2 (f): (1) Separated tilt velocity of the EW horizontal component; (2) tilt displacement of the EW horizontal component.

### 6.2.3 TCU068 Vertical component

This section shows the results of the vertical V component of station TCU068 of the Taiwan earthquake data, comparison of actual data with baseline corrected output of estimated velocity, estimated displacement, separated tilt, tilt velocity and displacement.

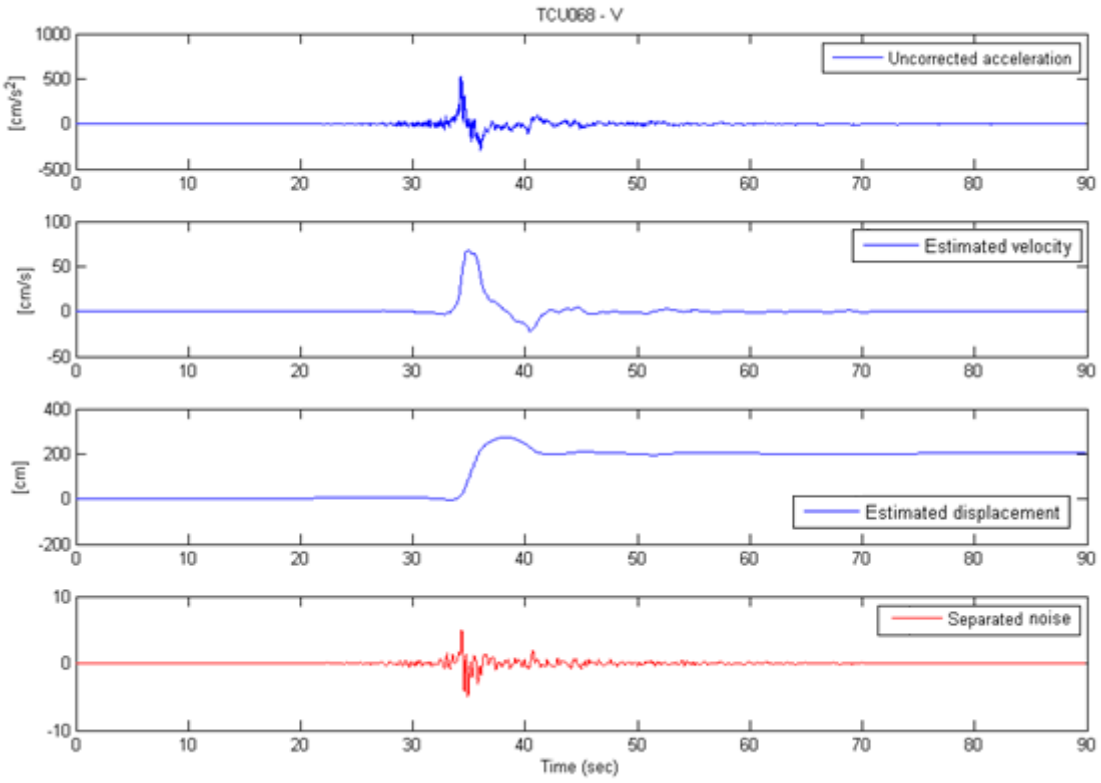


Figure 6.2.3 (a): Chi-Chi earthquake (20 September 1999, Taiwan; ); (1) plot shows the original contaminated acceleration signals in ; (2) plot shows estimated velocity in obtained by time integration of the corrected acceleration signals; (3) plot shows the estimated displacement in obtained by the second integration of the corrected acceleration signals; (4) plot shows the separated noise from the acceleration time histories.

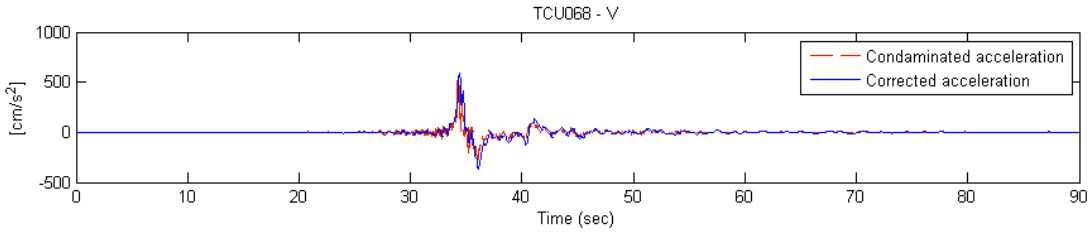


Figure 6.2.3 (b): Comparison between the actual acceleration (dotted line) with corrected acceleration (dashed line) of V vertical component of station-TCU068 record.

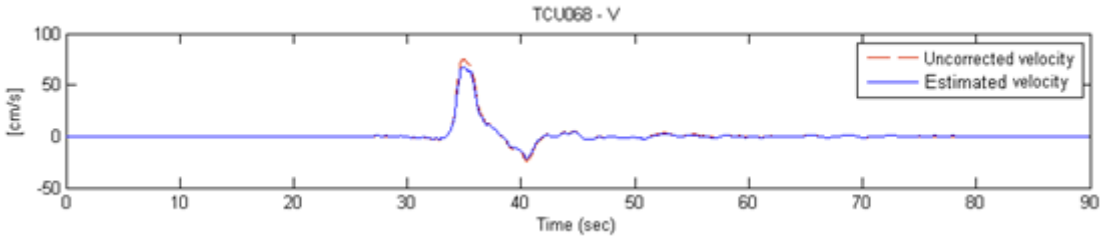


Figure 6.2.3 (c): Comparison between the uncorrected velocity (dotted line) with estimated velocity (dashed line) of V vertical component of station-TCU068 record.

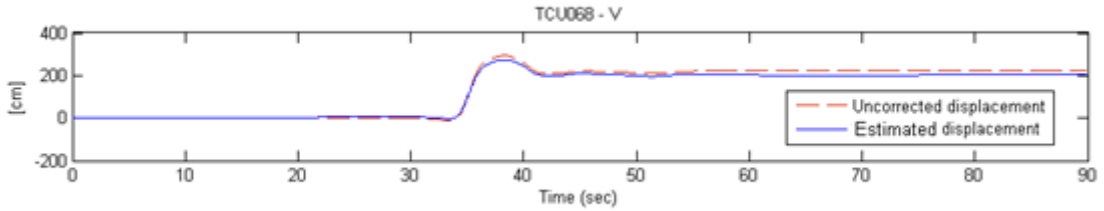


Figure 6.2.3 (d): Comparison between the uncorrected displacement (dotted line) with estimated displacement of V vertical component (dashed line) of station-TCU068 record.

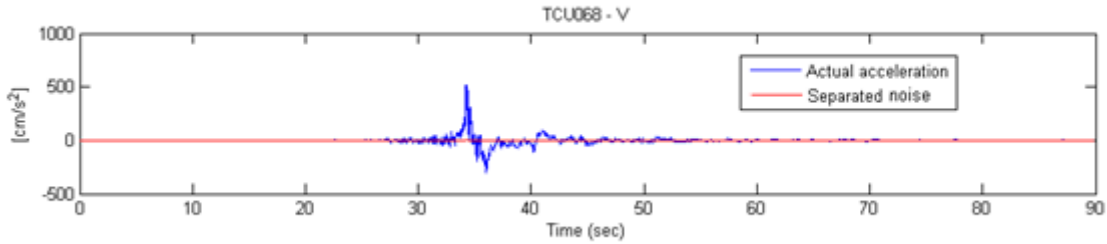


Figure 6.2.3 (e): Raw acceleration data with superimposed deduced tilt component of the V vertical component of station-TCU068 record.

## 6.3 Maule earthquake, Chile

### 6.3.1 Data used

The second data set (DGF, 2002) used was from the Maule earthquake, Chile with the magnitude of . The header file contains the information about the type of instrument SSA and station latitude – (-33.3961) and Station longitude – (-70.5369), record length and the sampling rate. The representations of three components are Z110 for the V-vertical component, N110 for the NS-horizontal component, and E110 for the EW-horizontal component.

The raw seismic data was recorded using the CLCH accelerometric station of the GDACS network (Global Disaster Alert and Coordination System) with cooperation from the United Nations of South America.

```
Localización: Departamento de Astronomía, Cerro Calan s/n - Las Condes.□□Latitud: -33.3961            Longitud:
-70.5369              Altura: 865 mts.□□Nombre                              :       CLCH (3 componentes),
IDS-24□Tipo de Sensor                 :          Acelerómetro SSA-120SLN, Terra Technology□Período Natural
      :       0.02 sec.□Frecuencia Natural          :          50 Hz □Constante Generadora del sensor  :
5Volts/2g, o sea 2.5 V/g, programado por software a 5 Volts/0.25 g o Sea 20Volts/g,valor a entrar en programa RESP□
Amortiguamiento               :       0.7 por feedback electrónico □Ganancia                  :       0 dB□Filtros
                      :       0□Constante del CAD(Rec.MediaGain):     1.048.576 Counts/Volts (0.95 uvolts/bit)□
Muestras por segundo          :       50□


                                    3110  58  2 27  6 34 29.580   450.660

 CLCHA  Z    0.00   450.66 CLCHA  N    0.00   450.66 CLCHA  E    0.00   450.66

CLCH A  Z110  58  2 27  6 34 29.580   50.00  22533                          4

    -130244    -130258    -130228    -130231    -130282    -130249    -130249
    -130271    -130230    -130251    -130267    -130256    -130292    -130294
    -130269    -130263    -130254    -130239    -130239    -130255    -130276
    -130272    -130300    -130303    -130286    -130289    -130263    -130298
    -130323    -130288    -130301    -130299    -130284    -130291    -130275
    -130260    -130286    -130298    -130277    -130278    -130281    -130263
    -130260    -130252    -130251    -130285    -130304    -130306    -130233
    -130195    -130271    -130275    -130266    -130290    -130259    -130267
    -130289    -130262    -130244    -130244    -130268    -130286    -130256
    -130246    -130276    -130262    -130212    -130277    -130246    -130258
    -130239    -130226    -130238    -130242    -130268    -130235    -130248
    -130309    -130249    -130213    -130268    -130296    -130278    -130248
    -130252    -130260    -130247    -130256    -130250    -130224    -130247
    -130274    -130277    -130287    -130278    -130270    -130283    -130268
    -130251    -130279    -130295    -130293    -130310    -130287    -130265
    -130271    -130252    -130273    -130293    -130266    -130268    -130281
    -130285    -130296    -130293    -130308    -130324    -130303    -130303
    -130319    -130321    -130266    -130296    -130319    -130277    -130301
    -130325    -130347    -130334    -130287    -130335    -130345    -130302
    -130300    -130298    -130290    -130281    -130289    -130300    -130312
    -130298    -130262    -130281    -130287    -130280    -130314    -130321
    -130315    -130332    -130322    -130307    -130301    -130274    -130281
    -130348    -130345    -130282    -130303    -130324    -130290    -130293
    -130303    -130303    -130307    -130319    -130314    -130290    -130302
    -130278    -130291    -130287    -130287    -130297    -130292    -130292
    -130286    -130299    -130309    -130284    -130288    -130303    -130282
    -130279    -130284    -130281    -130321    -130347    -130319    -130315
    -130312    -130274    -130280    -130305    -130310    -130306    -130305
    -130313    -130297    -130271    -130262    -130277    -130262    -130239
    -130251    -130241    -130248    -130247    -130214    -130230    -130248
    -130257    -130283    -130263    -130248    -130267    -130259    -130262
    -130268    -130268    -130256    -130263    -130288    -130317    -130303
    -130272    -130277    -130269    -130271    -130291    -130276    -130283
```

Header file: Station ID CLCH, Maule (2010) earthquake, Chile.

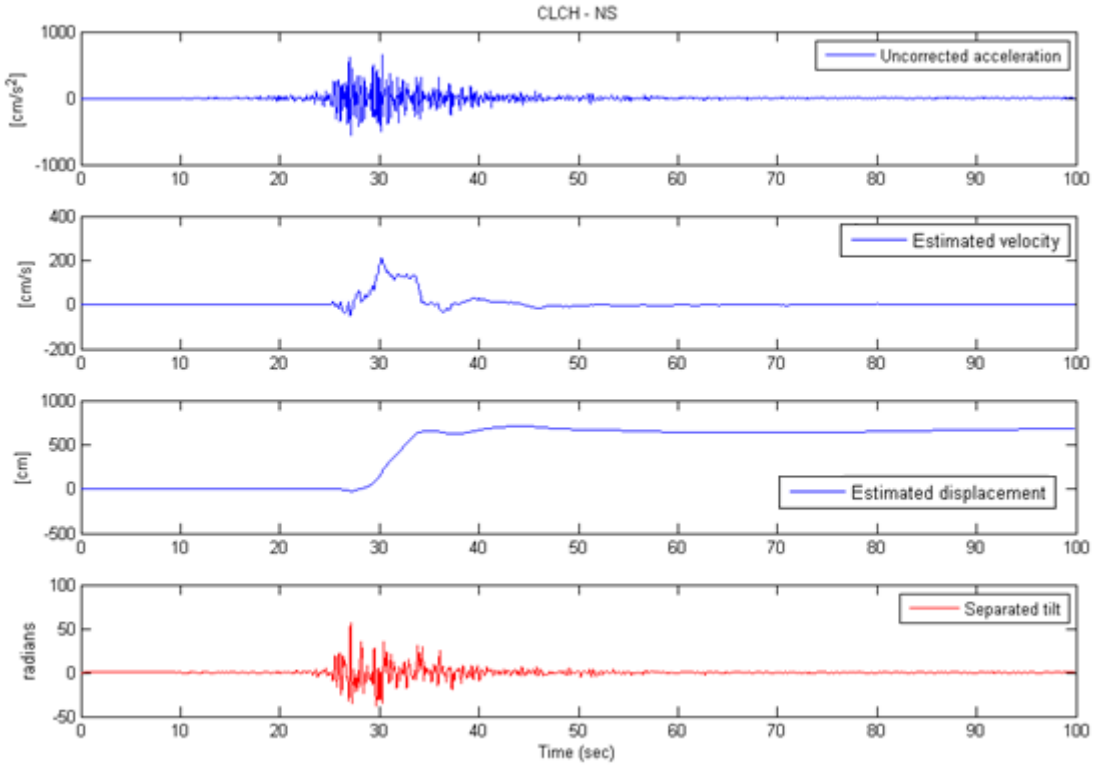


Figure 6.3.1(a): Maule earthquake (27 February 2010, Chile; ); (1) plot shows the original contaminated acceleration signals in ; (2) plot shows estimated velocity in obtained by time integration of the corrected acceleration signals; (3) plot shows the estimated displacement in obtained by the second integration of the corrected acceleration signals; (4) plot shows the separated tilt from the acceleration time histories. The estimated tilt maximum amplitude in the positive direction.

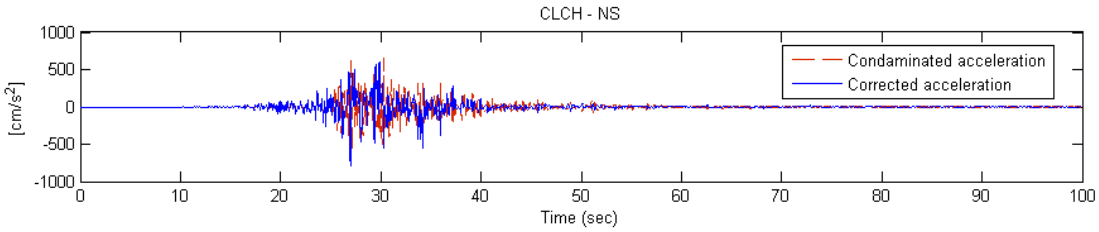


Figure 6.3.1(b): Comparison between the actual acceleration (dotted line) with corrected acceleration (dashed line) of CLCH-NS component.

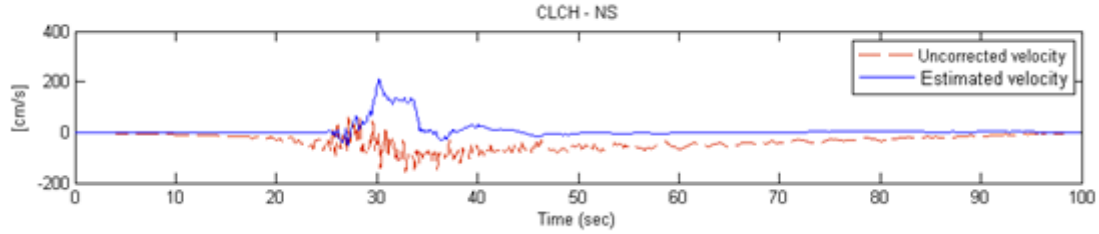


Figure 6.3.1(c): Comparison between, without baseline corrected velocity (dotted line) with baseline corrected velocity (dashed line) of CLCH-NS component.

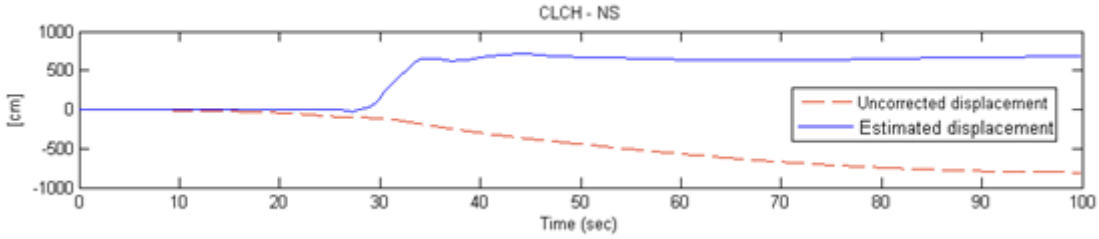


Figure 6.3.1(d): Comparison between uncorrected displacement (dotted line) with baseline corrected displacement (dashed line) of CLCH-NS component.

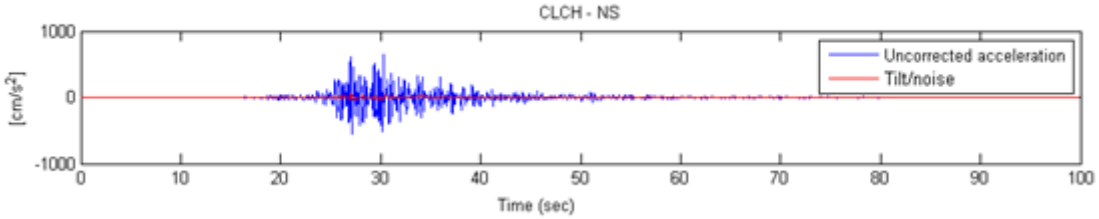


Figure 6.3.1(e): Raw acceleration data with superimposed deduced tilt component of the CLCH-NS component.

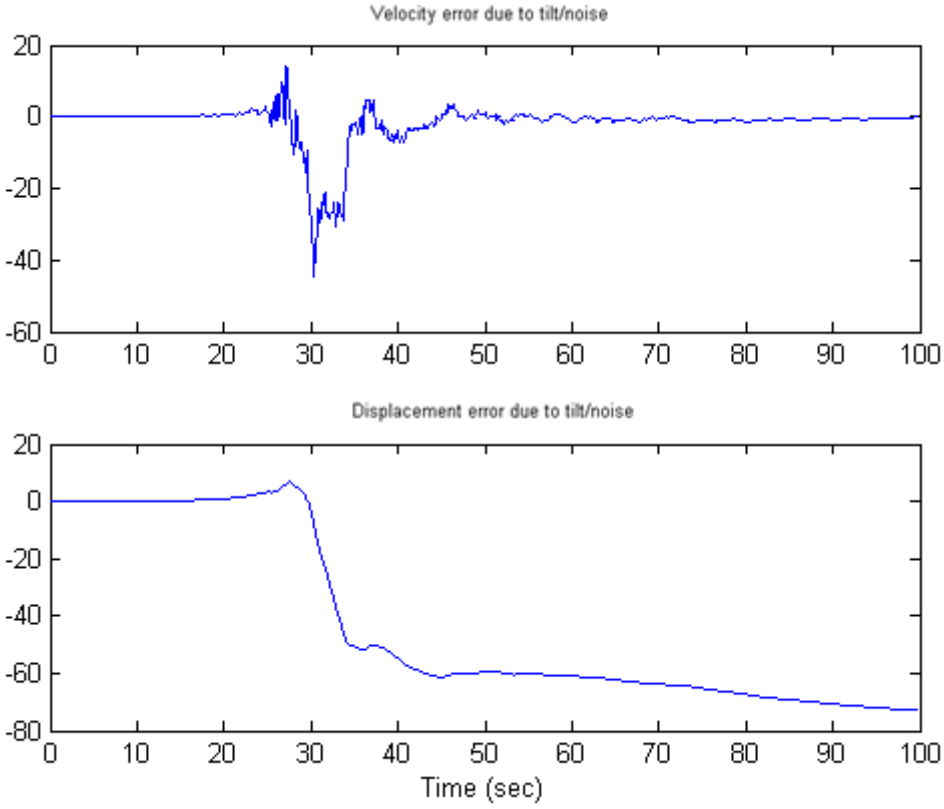


Figure 6.3.1(f): (1) Separated tilt velocity of the CLCH-NS component; (2) tilt displacement of the CLCH-NS component.

### 6.3.2 CLCH-EW horizontal component

This section shows the results of the horizontal EW component of station CLCH of the Chile earthquake data, comparison of actual data with baseline corrected output of estimated velocity, estimated displacement, separated tilt, tilt velocity and displacement.

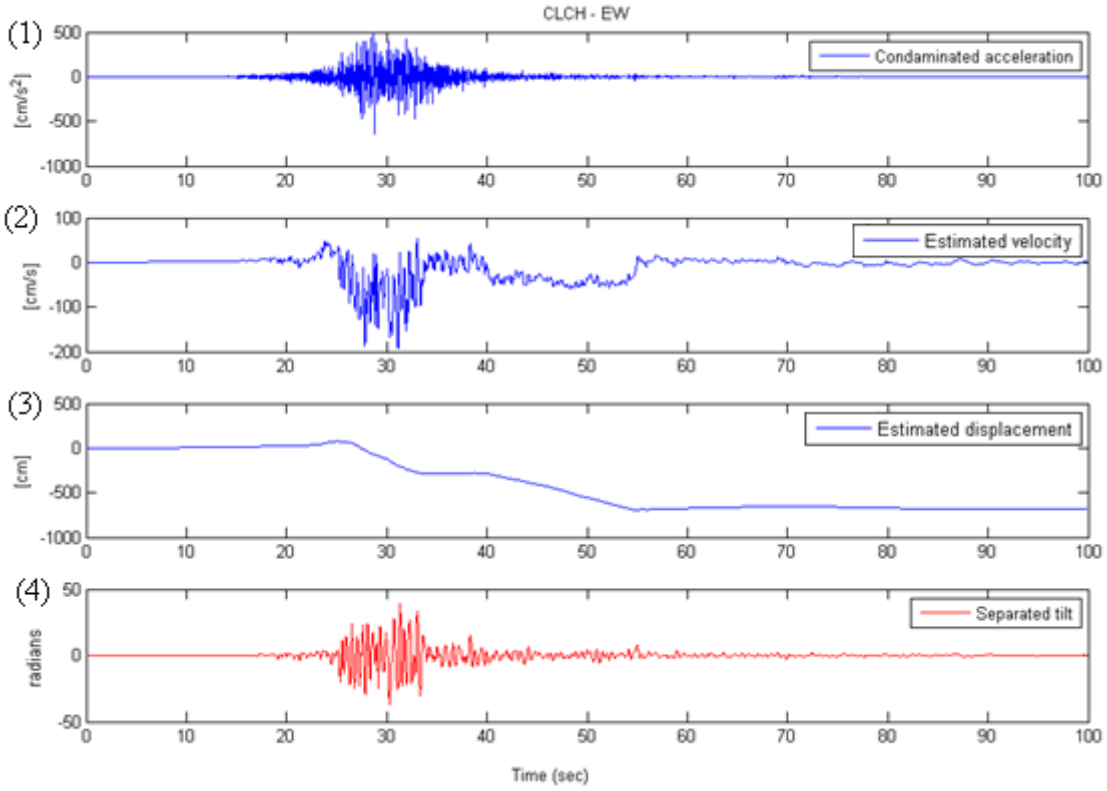


Figure 6.3.2 (a): Maule earthquake (27 February 2010, Chile; ); (1) plot shows the original contaminated acceleration signals in ; (2) plot shows estimated velocity in obtained by time integration of the corrected acceleration signals; (3) plot shows the estimated displacement in obtained by the second integration of the corrected acceleration signals; (4) plot shows the separated tilt from the acceleration time histories. The estimated tilt maximum amplitude in the negative direction.

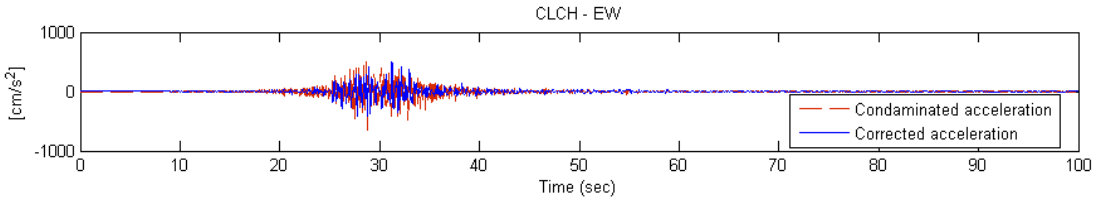


Figure 6.3.2 (b): Comparison between the actual acceleration (dotted line) with corrected acceleration (dashed line) of CLCH-EW component.

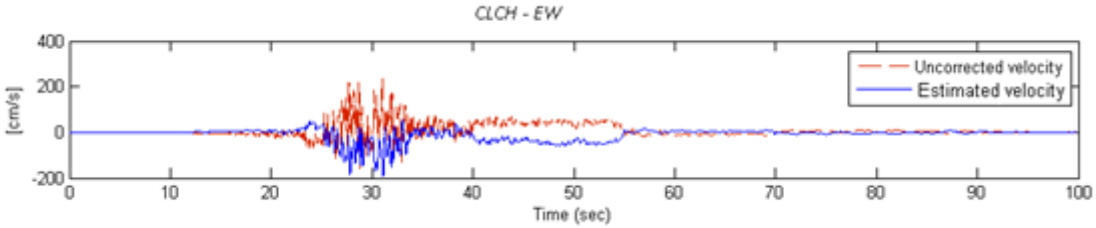


Figure 6.3.2 (c): Comparison between, without baseline corrected velocity (dotted line) with baseline corrected velocity (dashed line) of CLCH-EW component.

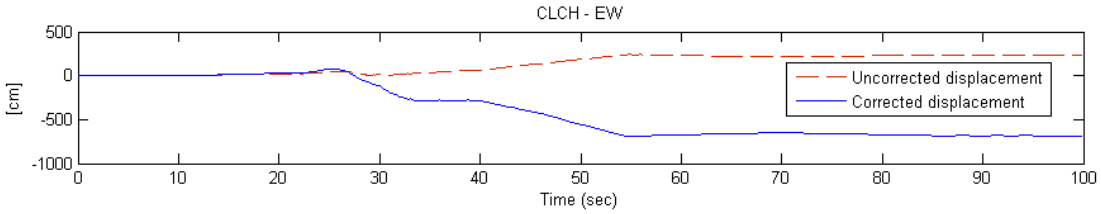


Figure 6.3.2 (d): Comparison between uncorrected displacement (dotted line) with baseline corrected displacement (dashed line) of CLCH-EW component.

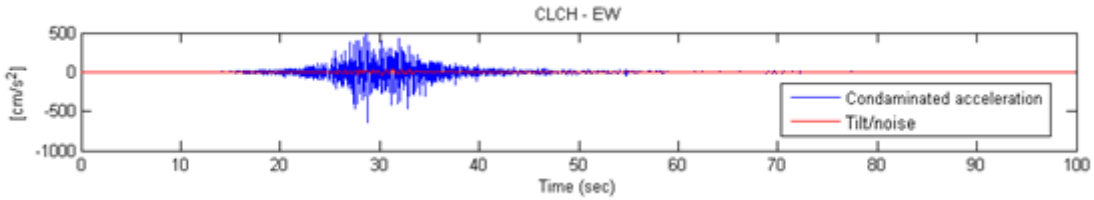


Figure 6.3.2 (e): Raw acceleration data with superimposed deduced tilt component of the CLCH-EW component.

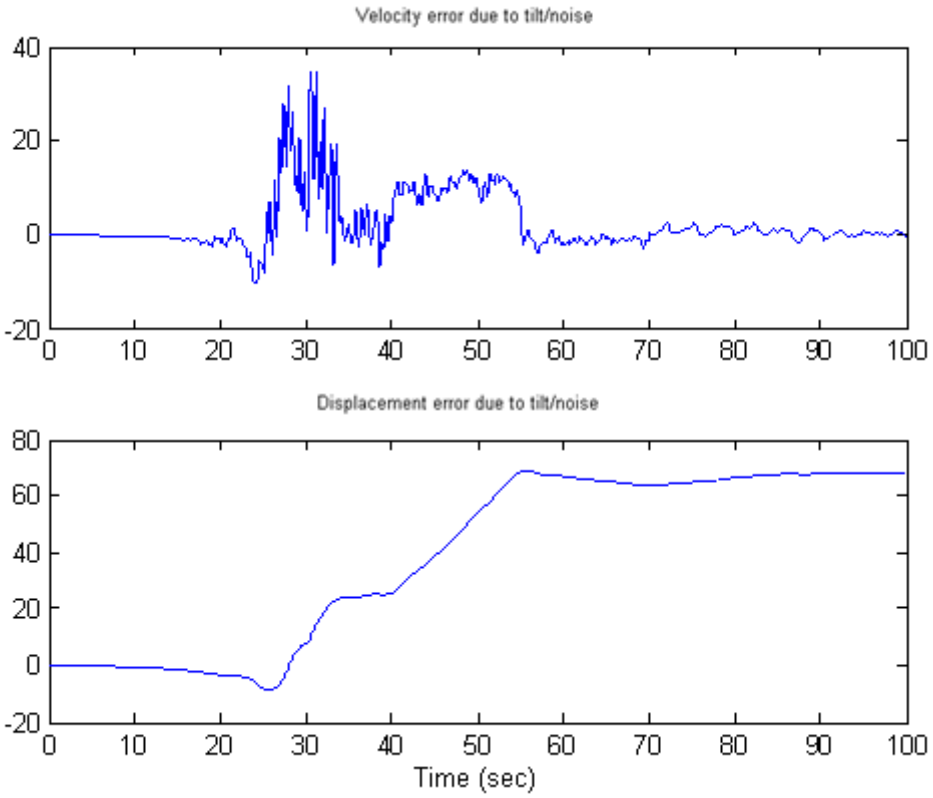


Figure 6.3.2 (f): (1) Separated tilt velocity of the CLCH-EW component; (2) tilt displacement of the CLCH-EW component.

### 6.3.3 CLCH-V vertical component

This section shows the results of the vertical V component of station CLCH of the Chile earthquake data, comparison of actual data with baseline corrected output of estimated velocity, estimated displacement, separated tilt, tilt velocity and displacement.

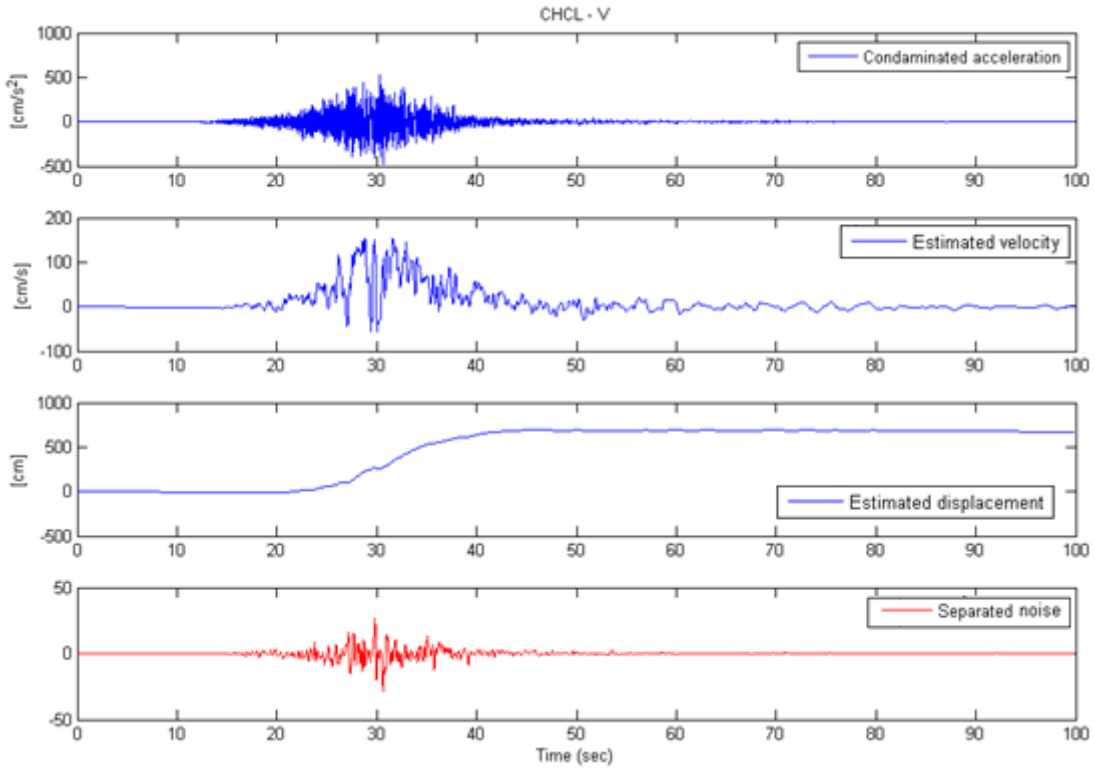


Figure 6.3.3 (a): Maule earthquake (27 February 2010, Chile; ); (1) plot shows the original contaminated acceleration signals in ; (2) plot shows estimated velocity in obtained by time integration of the corrected acceleration signals; (3) plot shows the estimated displacement in obtained by the second integration of the corrected acceleration signals; (4) plot shows the separated noise from the acceleration time histories.

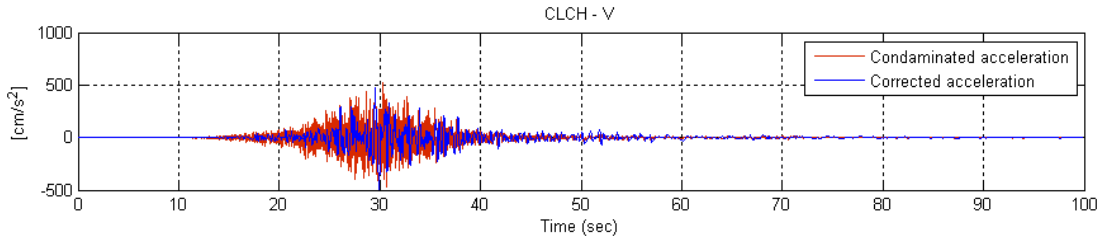


Figure 6.3.3 (b): Comparison between the actual acceleration (dotted line) with corrected acceleration (dashed line) of CLCH-V component.

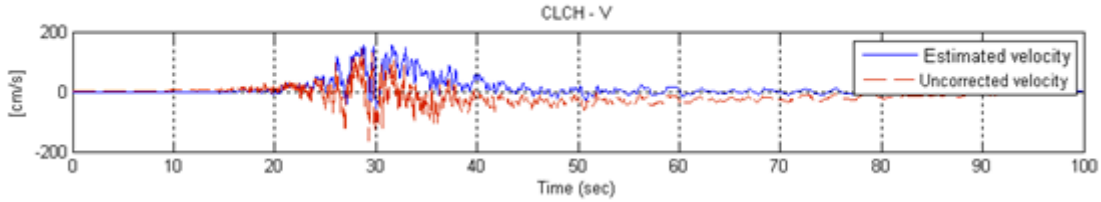


Figure 6.3.3 (c): Comparison between, without baseline corrected velocity (dotted line) with baseline corrected velocity (dashed line) of CLCH-V component.

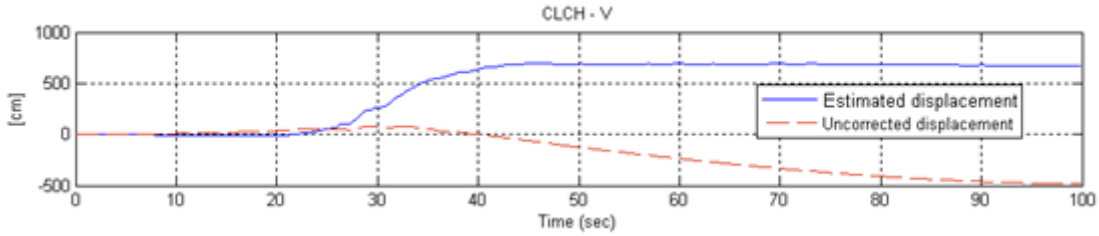


Figure 6.3.3 (d): Comparison between uncorrected displacement (dotted line) with baseline corrected displacement (dashed line) of CLCH-V component.

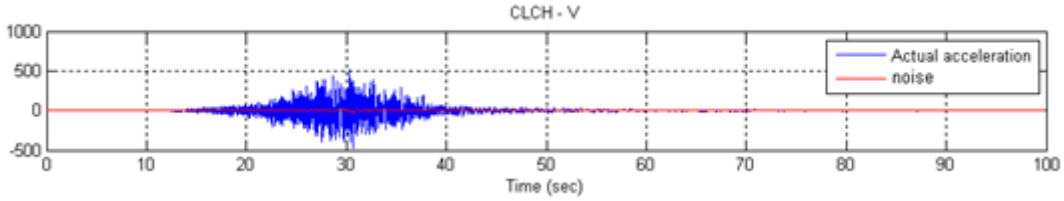


Figure 6.3.3 (e): Raw acceleration data with superimposed separated noise of the CLCH-V component.

## 6.4 Kocaeli earthquake, Turkey

### 6.4.1 Data used

The third data set of the Kocaeli earthquake, Turkey (Akkar and Gülkan 1999) was used with a magnitude of . The header file contains the information about the type of instrument SMA-1 and station latitude – (40.7000), station longitude – (29.9100), record length and the sampling rate. The representations of three components are U_D for the V-vertical component, N-S for the NS-horizontal component and E-W for the EW-horizontal component.

The raw seismic data was recorded using the station 5401 accelerometric of the Sakarya Province of the TKYHP network (*Turkey National Strong Ground Motion Program* (TKYHP, 2009)).

```
STRONG GROUND MOTION RECORDS OF TURKIYE
PLACE                    : SAKARYA MERKEZ BAYINDIRLIK VE ISKAN MUDURLUGU
EARTHQUAKE DATE          : 17/08/1999 00:01:39.07 (GMT)
EPICENTER COORDINATES    : 40.70000N-29.91000E
EARTHQUAKE DEPTH (km)    : 15.9
EARTHQUAKE MAGNITUDE     : 7.4Md
STATION ID               : 5401
STATION COORDINATES      : 40.73707N-30.38005E
STATION ALTITUDE (m)     : 46
RECORDER TYPE            : GSR-16
RECORDER SERIAL NO       : 246
RECORD TIME              : 17/08/1999 00:01:51 (GMT)
NUMBER OF DATA           : 38881
SAMPLING INTERVAL (sec)  : 0.01000000
RAW PGA VALUES (gal)     : (N-S) 0.213620 (E-W) 407.043750 (U-D) 259.002870
Copyright EARTHQUAKE RESEARCH DEPARTMENT
GENERAL DIRECTORATE OF DISASTER AFFAIRS
       N-S          E-W          U-D
    -0.061040     0.061040     0.000000
    -0.030520     0.000000     0.000000
    -0.030520     0.030520     0.000000
    -0.030520    -0.030520    -0.030520
    -0.030520     0.000000    -0.030520
    -0.030520     0.000000     0.030520
    -0.030520     0.030520     0.000000
     0.030520     0.030520     0.030520
     0.030520     0.000000     0.030520
     0.000000     0.030520     0.030520
     0.000000     0.000000     0.000000
     0.000000    -0.030520     0.030520
     0.000000     0.000000     0.030520
    -0.030520     0.030520     0.030520
    -0.030520     0.000000     0.000000
     0.000000     0.000000     0.000000
     0.000000     0.000000     0.000000
    -0.030520     0.000000     0.000000
     0.000000     0.000000     0.000000
    -0.030520     0.000000     0.000000
     0.000000     0.030520     0.000000
     0.000000     0.030520    -0.030520
```

Header file: Station ID 5401, Kocaeli (1999) earthquake data.

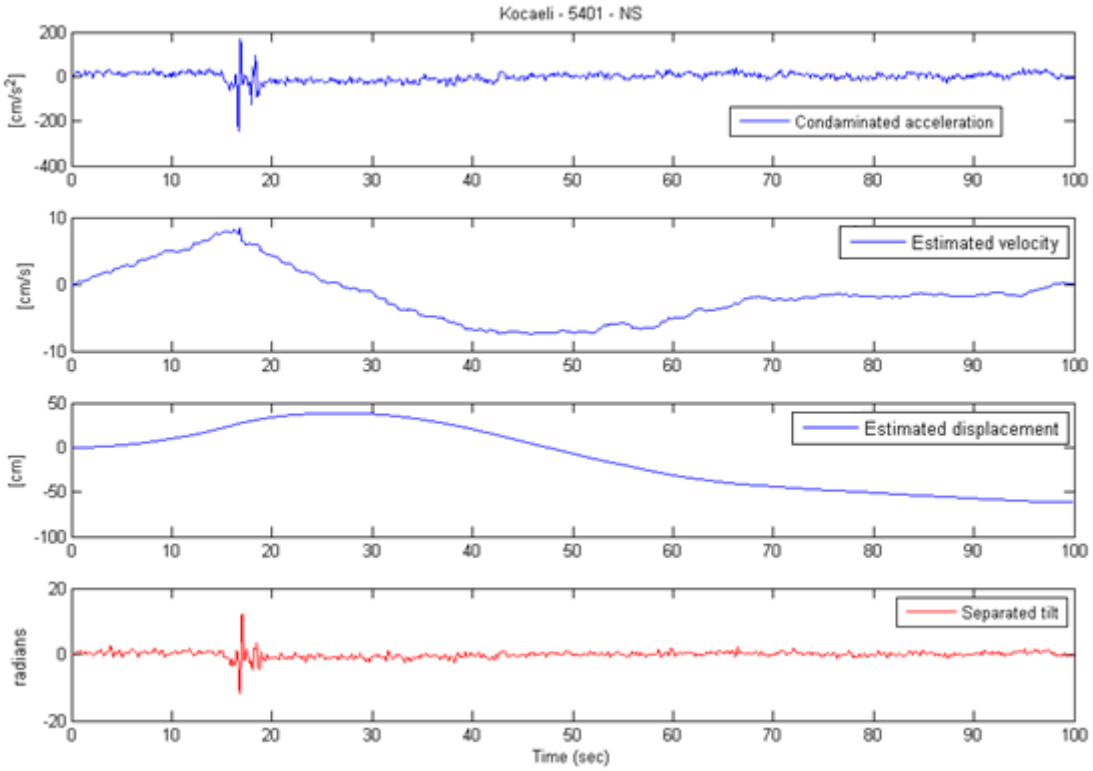


Figure 6.4.1 (a): Kocaeli earthquake (17 August 1999, Turkey; ); (1) plot shows the original contaminated acceleration signals in ; (2) plot shows estimated velocity in obtained by time integration of the corrected acceleration signals; (3) plot shows the estimated displacement in obtained by the second integration of the corrected acceleration signals; (4) plot shows the separated tilt from the acceleration time histories. The estimated tilt maximum amplitude in the negative direction.

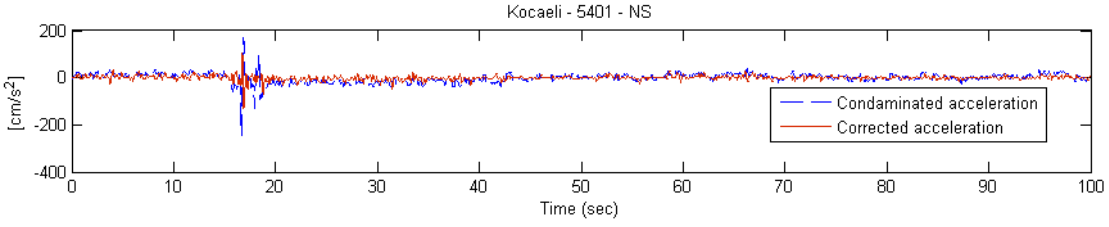


Figure 6.4.1 (b): Comparison between the actual acceleration (dotted line) with corrected acceleration (dashed line) of station 5401 NS component.

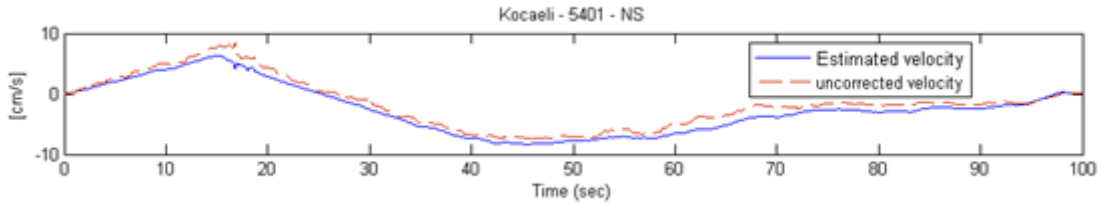


Figure 6.4.1 (c): Comparison between, without baseline corrected velocity (dotted line) with baseline corrected velocity (dashed line) of station 5401 NS component.

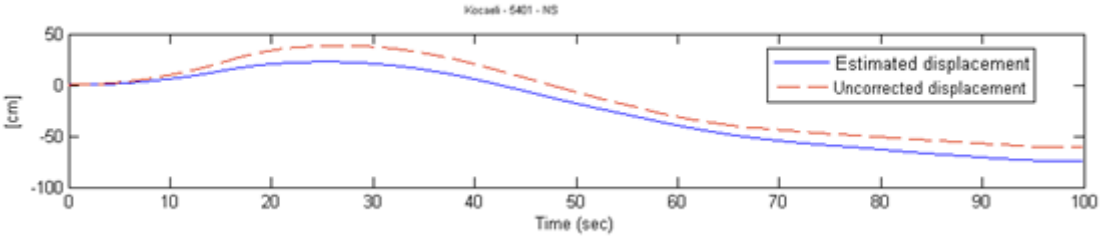


Figure 6.4.1 (d): Comparison between uncorrected displacement (dotted line) with baseline corrected displacement (dashed line) of station 5401 NS component.

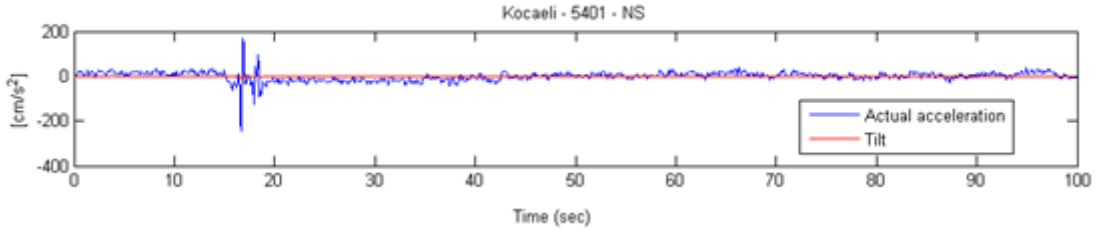


Figure 6.4.1 (e): Raw acceleration data with superimposed deduced tilt component of the station 5401 NS component.

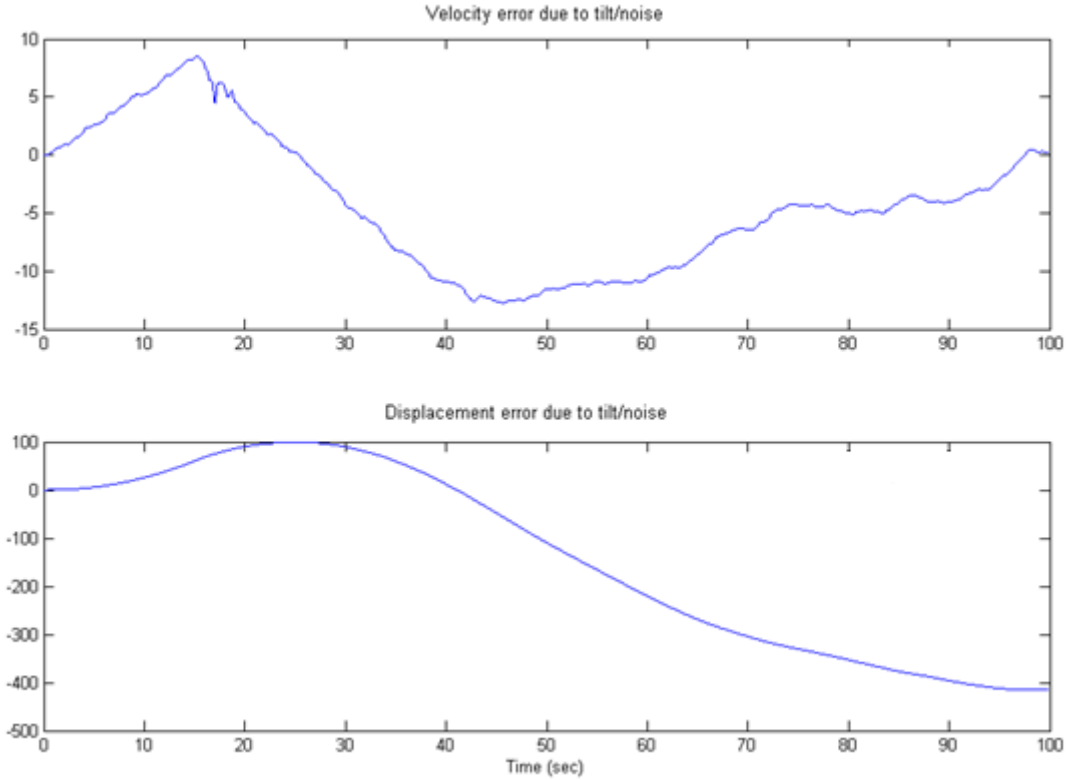


Figure 6.4.1 (f): (1) Separated tilt velocity of station 5401 NS component; (2) tilt displacement of station 5401 NS component.

### 6.4.2 Kocaeli EW horizontal component

This section shows the results of the horizontal EW component of station 5401 of the Koceali earthquake data, comparison of actual data with baseline corrected output of estimated velocity, estimated displacement, separated tilt, tilt velocity and displacement.

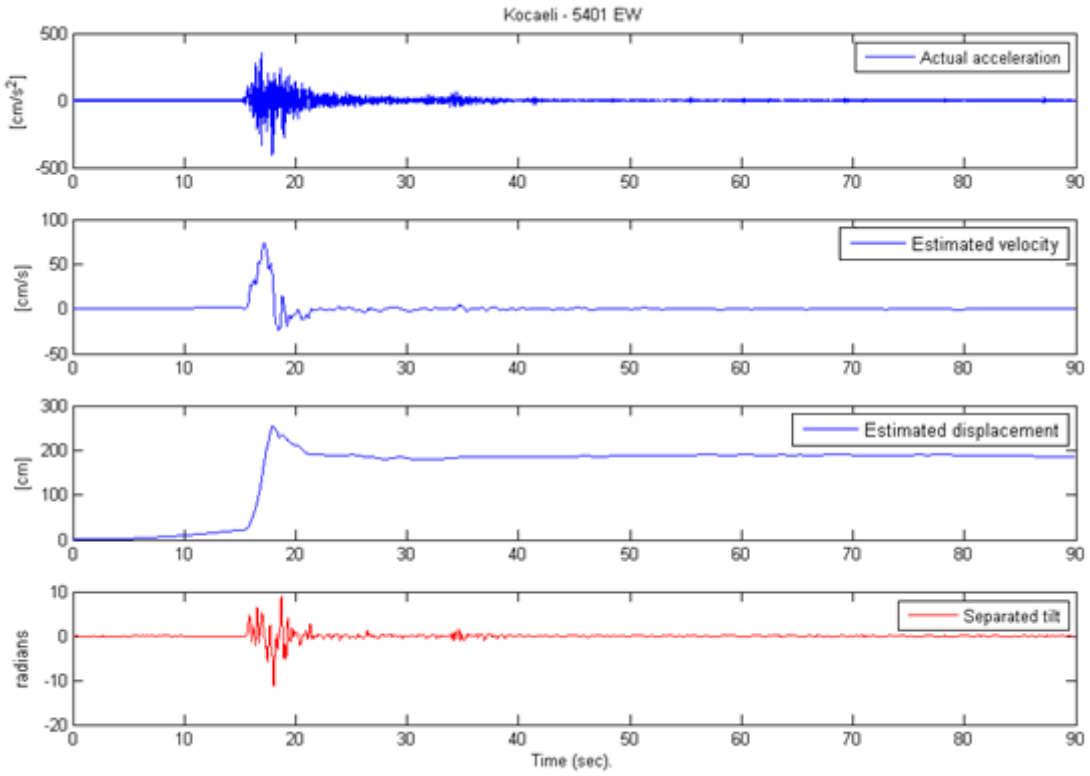


Figure 6.4.2 (a): Kocaeli earthquake (17 August 1999, Turkey; ); (1) plot shows the original contaminated acceleration signals in ; (2) plot shows estimated velocity in obtained by time integration of the corrected acceleration signals; (3) plot shows the estimated displacement in obtained by the second integration of the corrected acceleration signals; (4) plot shows the separated tilt from the acceleration time histories. The estimated tilt maximum amplitude in the positive direction.

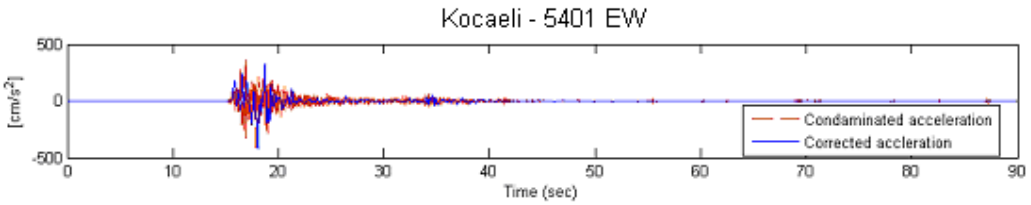


Figure 6.4.2 (b): Comparison between the actual acceleration (dotted line) with corrected acceleration (dashed line) of station 5401 EW component.

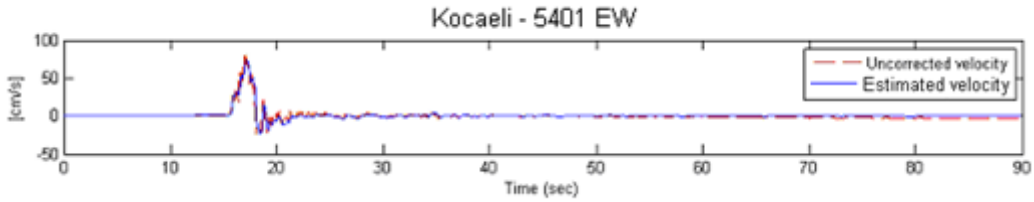


Figure 6.4.2 (c): Comparison between, without baseline corrected velocity (dotted line) with baseline corrected velocity (dashed line) of station 5401 EW component.

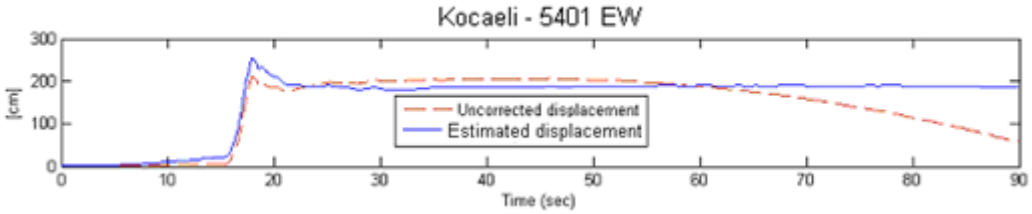


Figure 6.4.2 (d): Comparison between uncorrected displacement (dotted line) with baseline corrected displacement (dashed line) of station 5401 EW component.

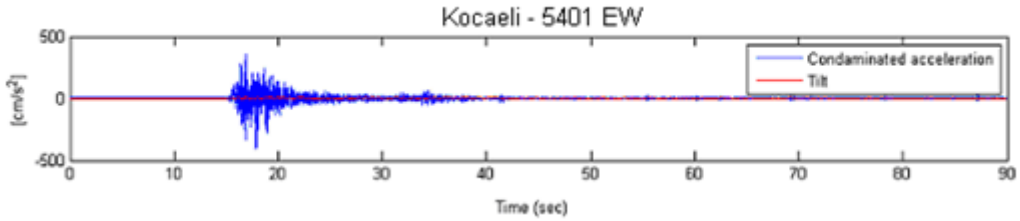


Figure 6.4.2 (e): Raw acceleration data with superimposed deduced tilt component of the station 5401 EW component.

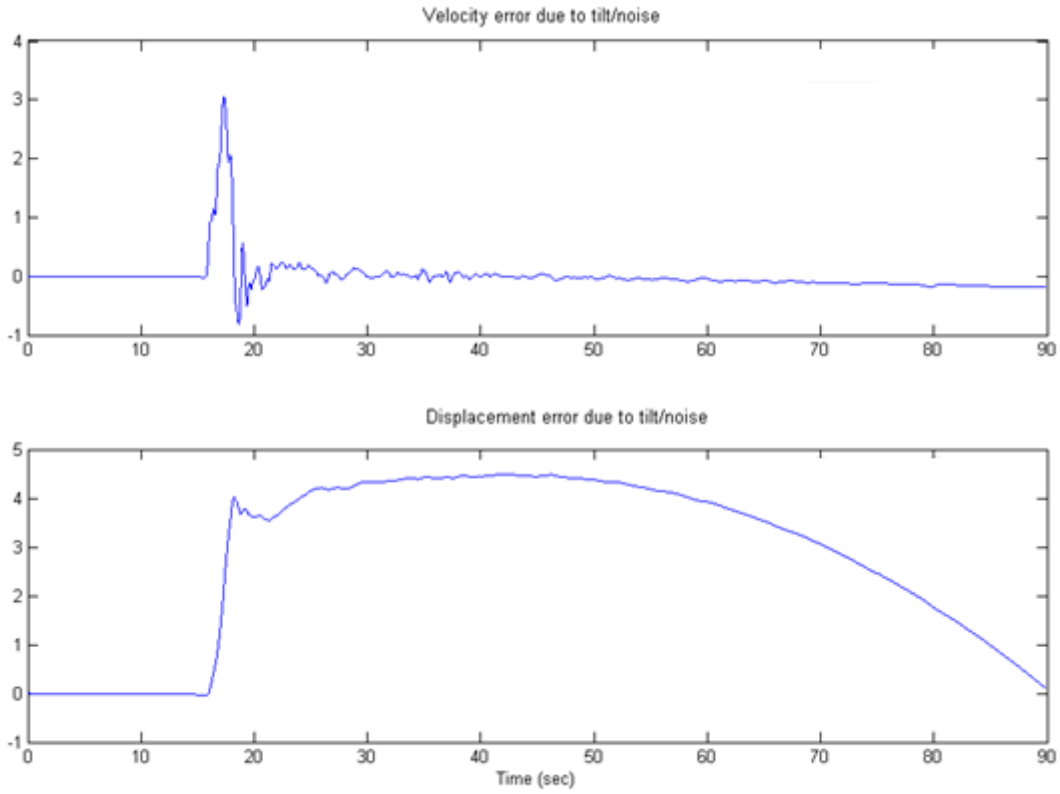


Figure 6.4.2 (f): (1) Separated tilt velocity of station 5401 EW component; (2) tilt displacement of station 5401 EW component.

### 6.4.3 Koceali 5401, Vertical component

This section shows the results of the vertical V component of station 5401 of the Koceali earthquake data, comparison of actual data with baseline corrected output of estimated velocity, estimated displacement, separated tilt, tilt velocity and displacement.

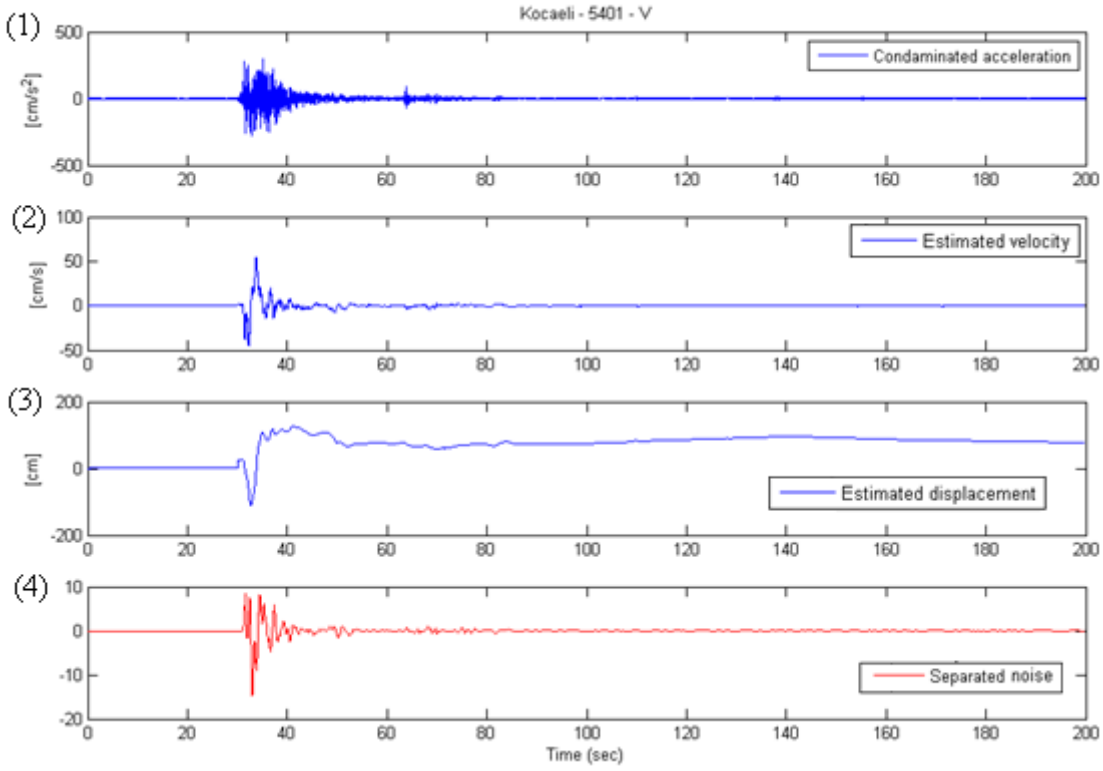


Figure 6.4.3 (a): Kocaeli earthquake (17 August 1999, Turkey; ); (1) plot shows the original contaminated acceleration signals in ; (2) plot shows estimated velocity in obtained by time integration of the corrected acceleration signals; (3) plot shows the estimated displacement in obtained by the second integration of the corrected acceleration signals; (4) plot shows the separated tilt from the acceleration time histories.

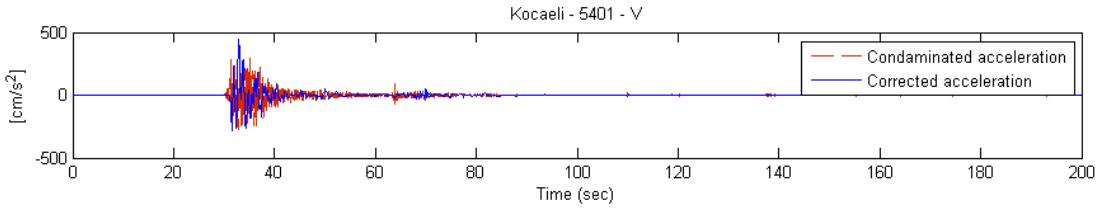


Figure 6.4.3 (b): Comparison between the actual acceleration (dotted line) with corrected acceleration (dashed line) of station 5401 V component.

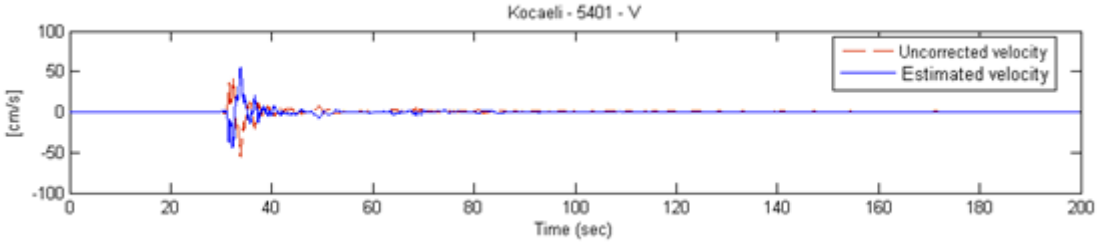


Figure 6.4.3 (c): Comparison between, without baseline corrected velocity (dotted line) with baseline corrected velocity (dashed line) of station 5401 V component.

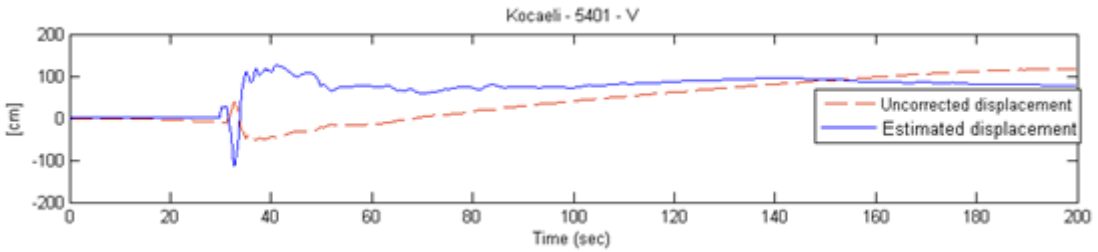


Figure 6.4.3 (d): Comparison between uncorrected displacement (dotted line) with baseline corrected displacement (dashed line) of station 5401 V component.

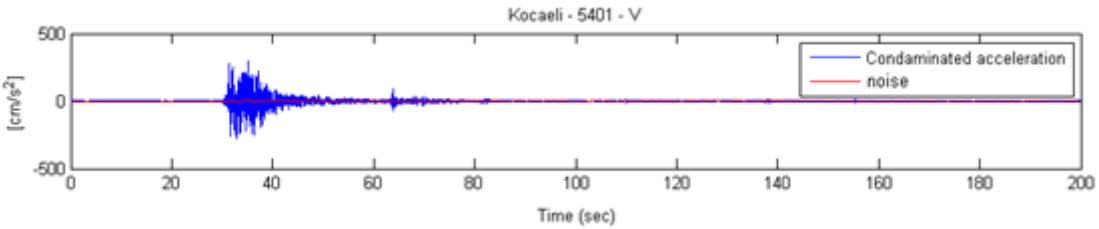


Figure 6.4.3 (e): Raw acceleration data with superimposed separated noise of the station 5401 V component.

## 6.5 Christchurch earthquake, New Zealand

### 6.5.1 Data used

The fourth data set of the Christchurch earthquake, New Zealand was used with a magnitude of . The header file contains the information about the type of instrument CUSP_331 and station latitude – ( ), station longitude – ( ). The representations of three components are UP vertical for the negative vertical component, NW horizontal for the negative component and SW horizontal for the negative component.

The raw seismic data was recorded using the station GDLC accelerometric of the Christchurch Province of the GEONET network (*GNS Science* (GNS, 2011)).

```
Corrected accelerogram 20110221_235142_CCCC GNS Science
Site CCCC      43 32 23S  172 38 50E     CUSP file:  2011.052.2351.33.CCCC.00331
Instrument CUSP_331
Resolution: 16-bit
Sampling Rate: 200 Hz
Accelerogram 20110221_235142
10 km south-east of Christchurch
2011 February 22    23:51:42 UT
Epicentre  43 34 53S 172 42 07E  Bearing S44E  Dist    6km  Depth   5Rkm Ml 6.30
Number of points  20886    Duration  110.70 sec
Sensitivity and cross-axis corrected data at 0.020 sec intervals
Data Sequence: U(+)  N(+)  S(+)

0.550865218       0.000000          0.00000
-0.119753308      0.000000          0.00000
0.167654631       0.000000          0.00000
0.059876654       0.000000          0.00000
0.023950662       0.000000          0.00000
0.580803545       0.000000          0.00000
-0.005987665      0.000000          0.00000
-0.041913658      0.000000          0.00000
0.80833483        0.000000          0.00000
0.610741872       0.000000          0.00000
0.377222921       0.000000          0.00000
-0.023950662      0.000000          0.00000
-0.317346267      0.000000          0.00000
0.06586432        0.000000          0.00000
-0.173642297      0.000000          0.00000
-0.137716304      0.000000          0.00000
0.347284594       0.000000          0.00000
-0.071851985      0.000000          0.00000
-0.029938327      0.000000          0.00000
0.389198252       0.000000          0.00000
-0.053888989      0.29938327        -0.22154362
0.28740794        0.305370936       -0.28740794
0.317346267       0.886174481       -0.455062571
-0.676606191      0                 -0.14370397
0.017962996       -0.66463086       0.347284594
0.676606191       -0.155679301      -0.245494282
-0.089814981      0.197592959       0.029938327
```

Header file: Station ID GDLC, Christchurch (2011) earthquake, New Zealand.

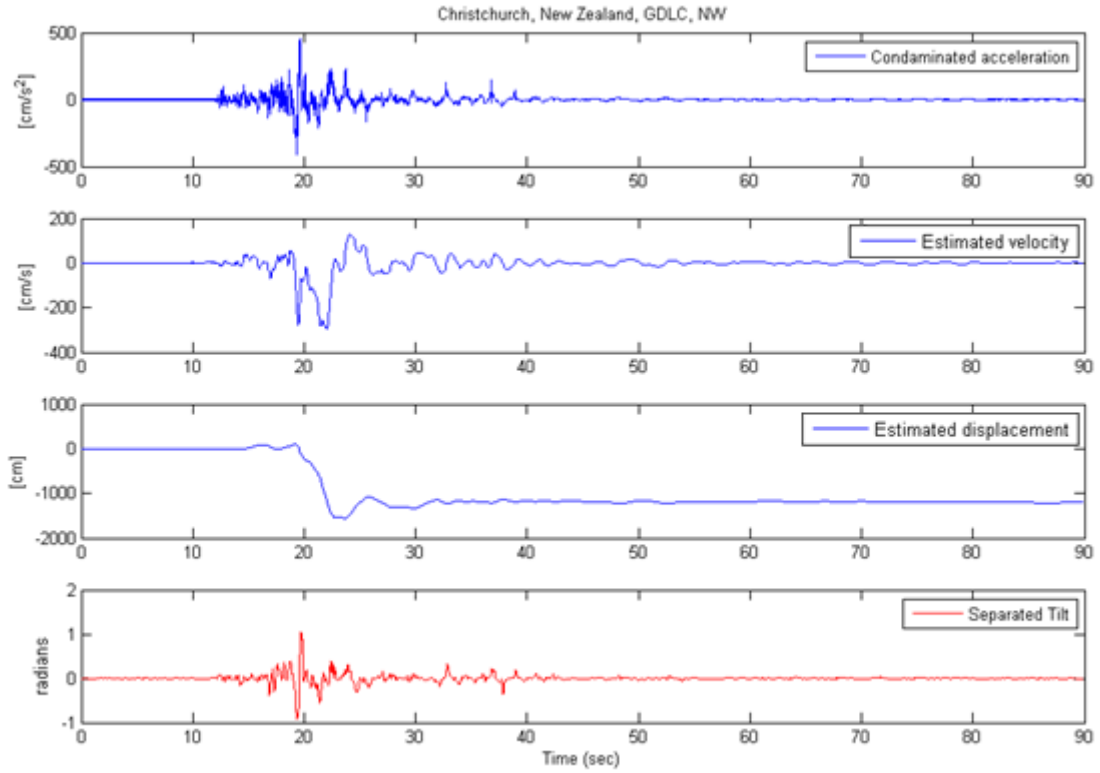


Figure 6.5.1 (a): Christchurch earthquake (22 February 2011, New Zealand; ); (1) plot shows the original contaminated acceleration signals in ; (2) plot shows estimated velocity in obtained by time integration of the corrected acceleration signals; (3) plot shows the estimated displacement in obtained by the second integration of the corrected acceleration signals; (4) plot shows the separated tilt from the acceleration time histories. The estimated tilt maximum amplitude in the negative direction.

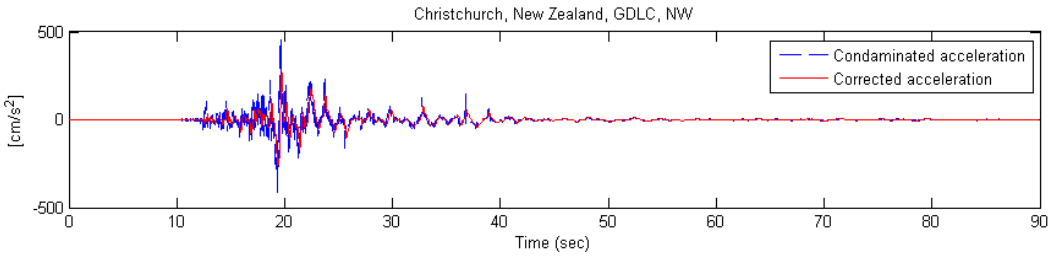


Figure 6.5.1 (b): Comparison between the actual acceleration (dotted line) with corrected acceleration (dashed line) of GDLC-NW component.

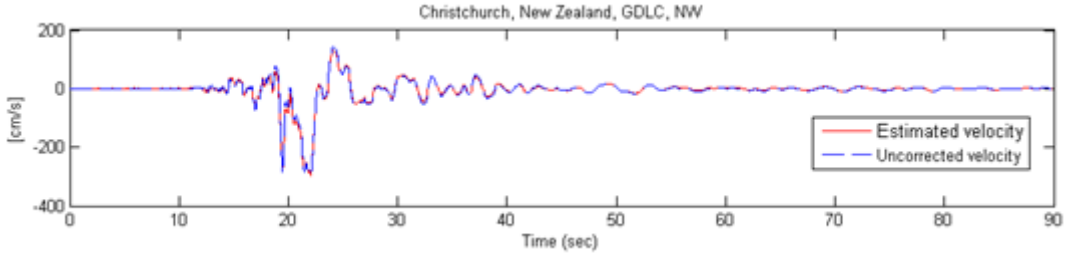


Figure 6.5.1 (c): Comparison between, without baseline corrected velocity (dotted line) with baseline corrected velocity (dashed line) of GDLC-NW component.

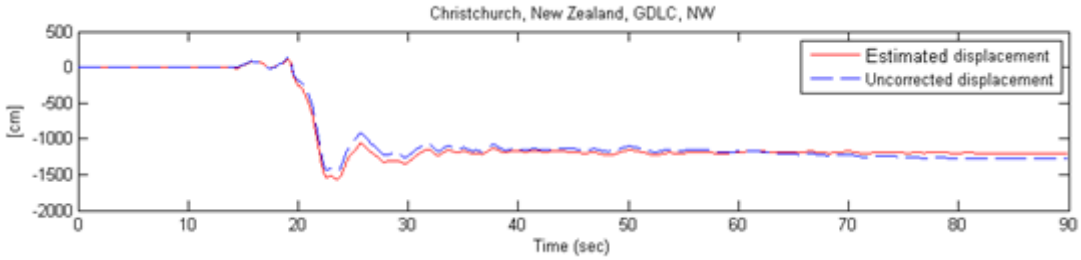


Figure 6.5.1 (d): Comparison between uncorrected displacement (dotted line) with baseline corrected displacement (dashed line) of GDLC-NW component.

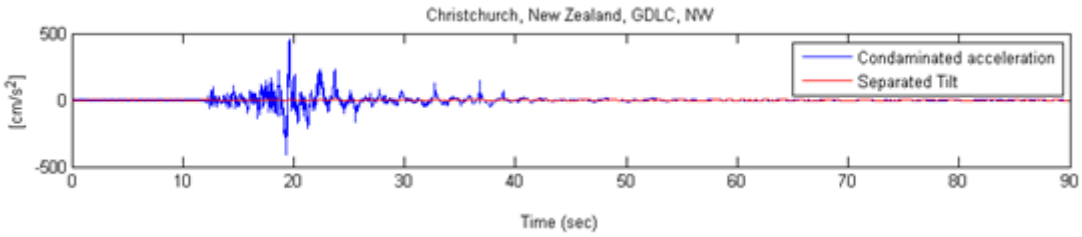


Figure 6.5.1 (e): Raw acceleration data with superimposed deduced tilt component of the GDLC-NW component.

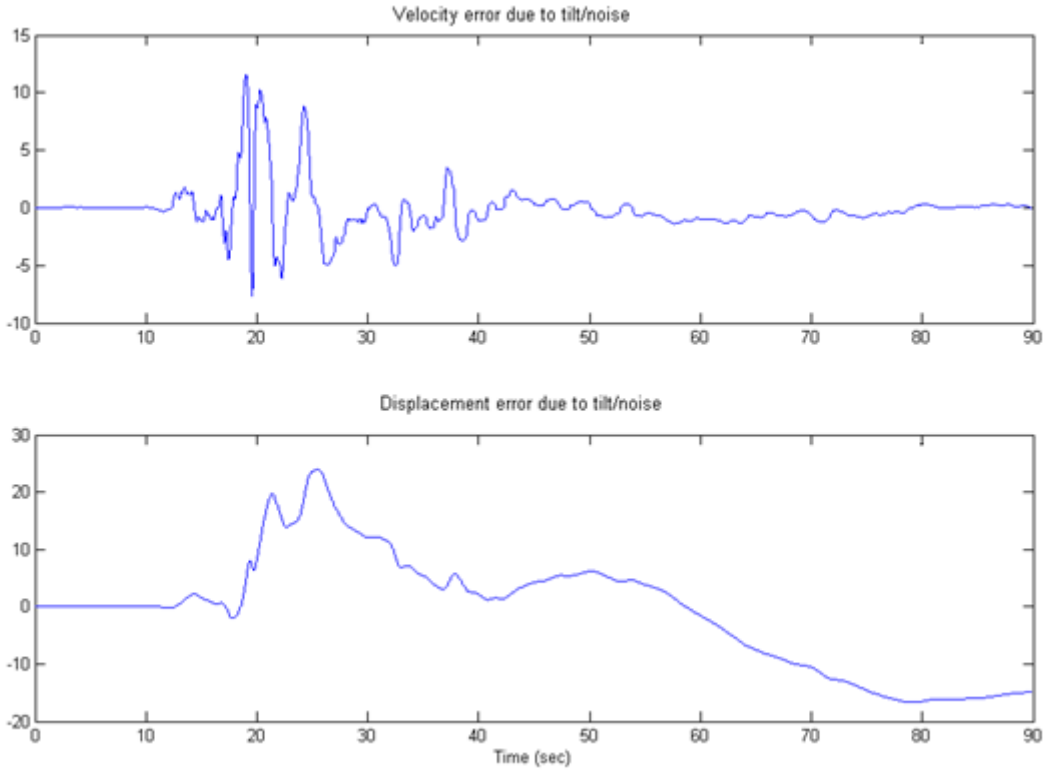


Figure 6.5.1 (f): (1) Separated tilt velocity of the GDLC-NW component; (2) tilt displacement of the GDLC-NW component.

### 6.5.2 GDLC – SW horizontal component

This section shows the results of the SW component of station GDLC of the Christchurch earthquake data, comparison of actual data with baseline corrected output of estimated velocity, estimated displacement, separated tilt, tilt velocity and displacement.

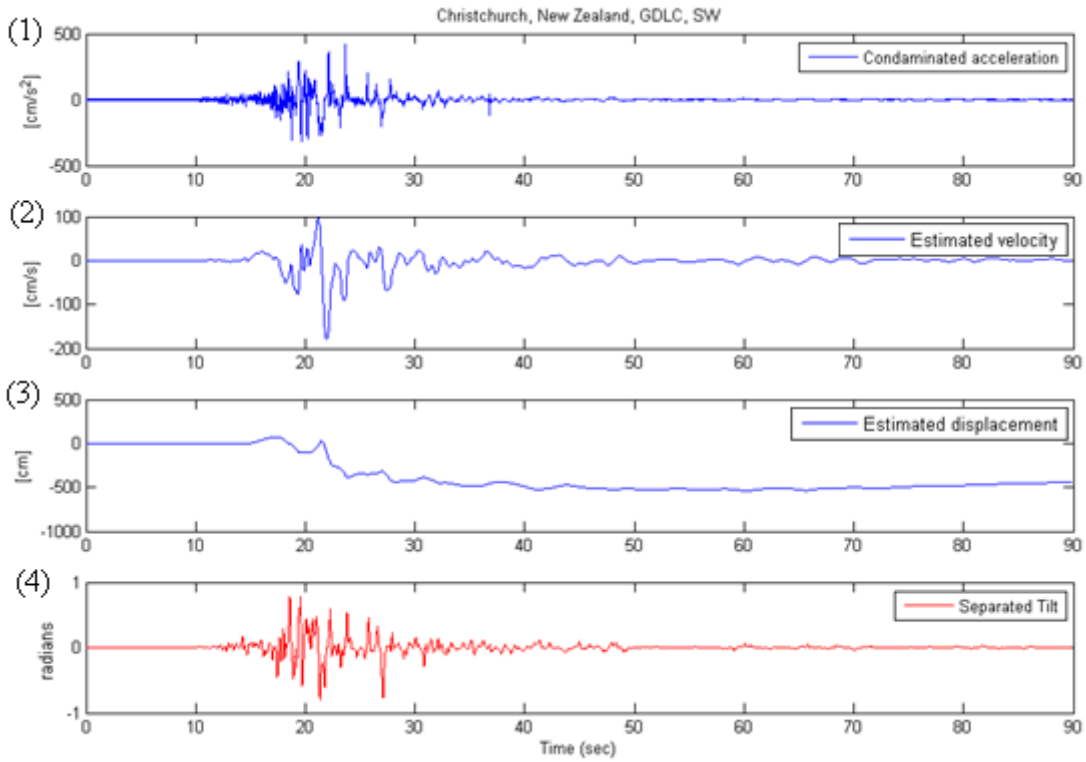


Figure 6.5.2 (a): Christchurch earthquake (22 February 2011, New Zealand; ); (1) plot shows the original contaminated acceleration signals in ; (2) plot shows the estimated velocity in obtained by time integration of the corrected acceleration signals; (3) plot shows estimated displacement in obtained by the second integration of the corrected acceleration signals; (4) plot shows the separated tilt from the acceleration time histories. The estimated tilt maximum amplitude in the negative direction.

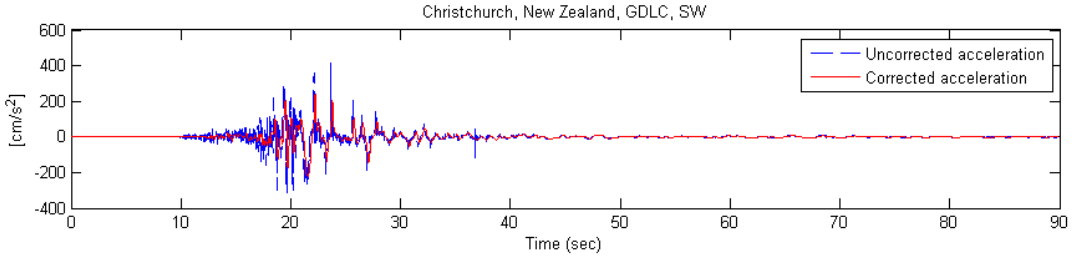


Figure 6.5.2 (b): Comparison between the actual acceleration (dotted line) with corrected acceleration (dashed line) of GDLC-SW component.

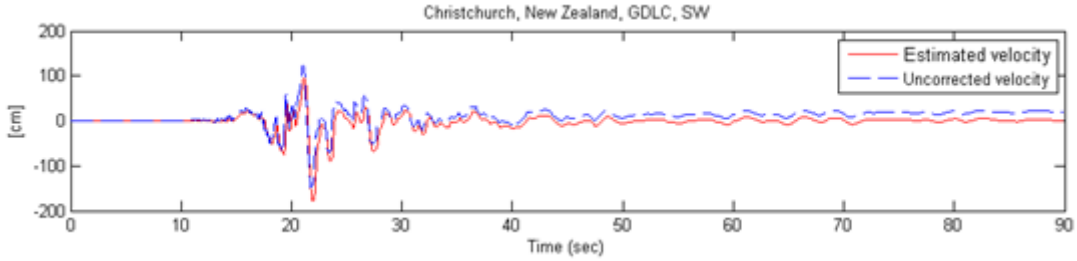


Figure 6.5.2 (c): Comparison between, without baseline corrected velocity (dotted line) with baseline corrected velocity (dashed line) of GDLC-SW component.

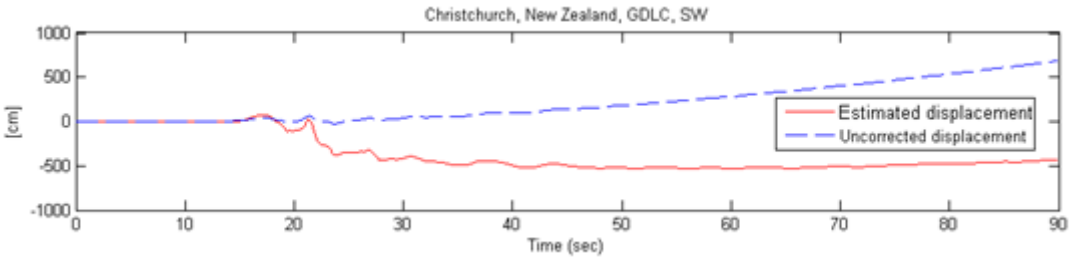


Figure 6.5.2 (d): Comparison between uncorrected displacement (dotted line) with baseline corrected displacement (dashed line) of GDLC-SW component.

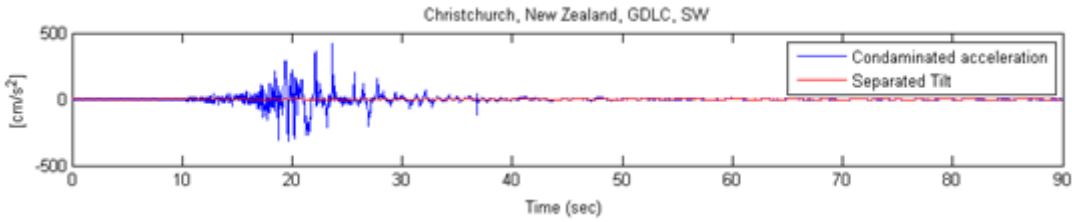


Figure 6.5.2 (e): Raw acceleration data with superimposed deduced tilt component of the GDLC-SW component.

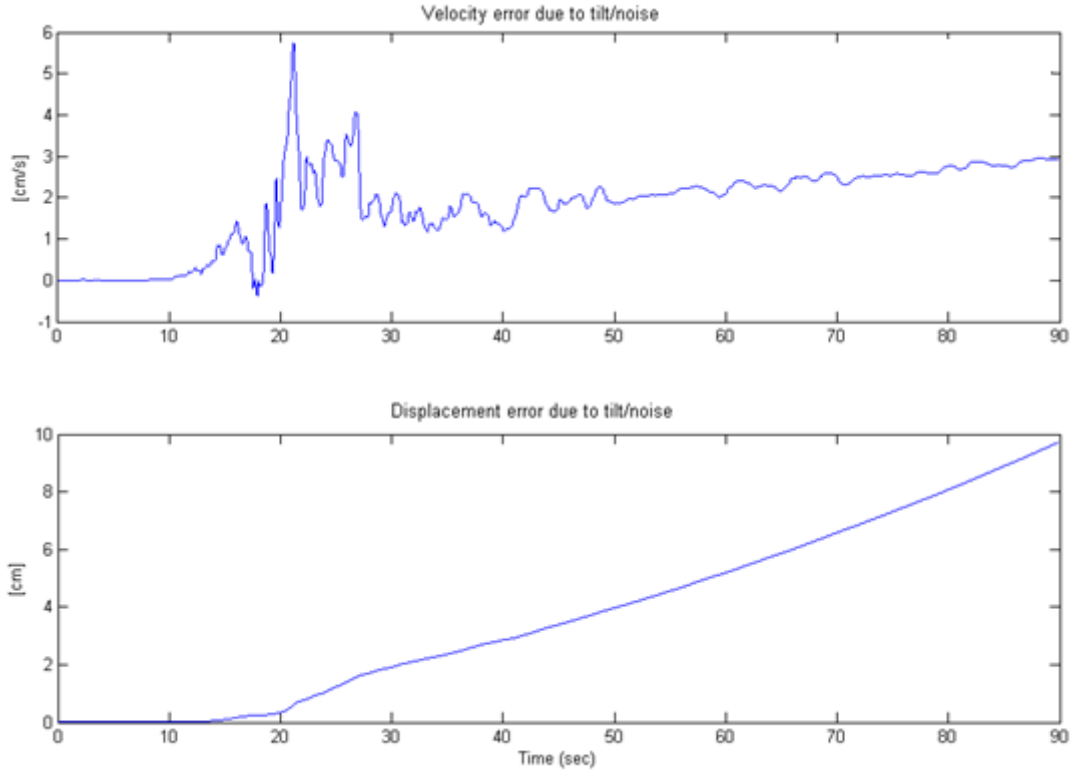


Figure 6.5.2 (f): (1) Separated tilt velocity of the GDLC-NW component; (2) tilt displacement of the GDLC-NW component.

### 6.5.3 GDLC – UP vertical component

This section shows the results of the vertical UP component of station GDLC of the Christchurch earthquake data, comparison of actual data with baseline corrected output of estimated velocity, estimated displacement, separated tilt, tilt velocity and displacement.

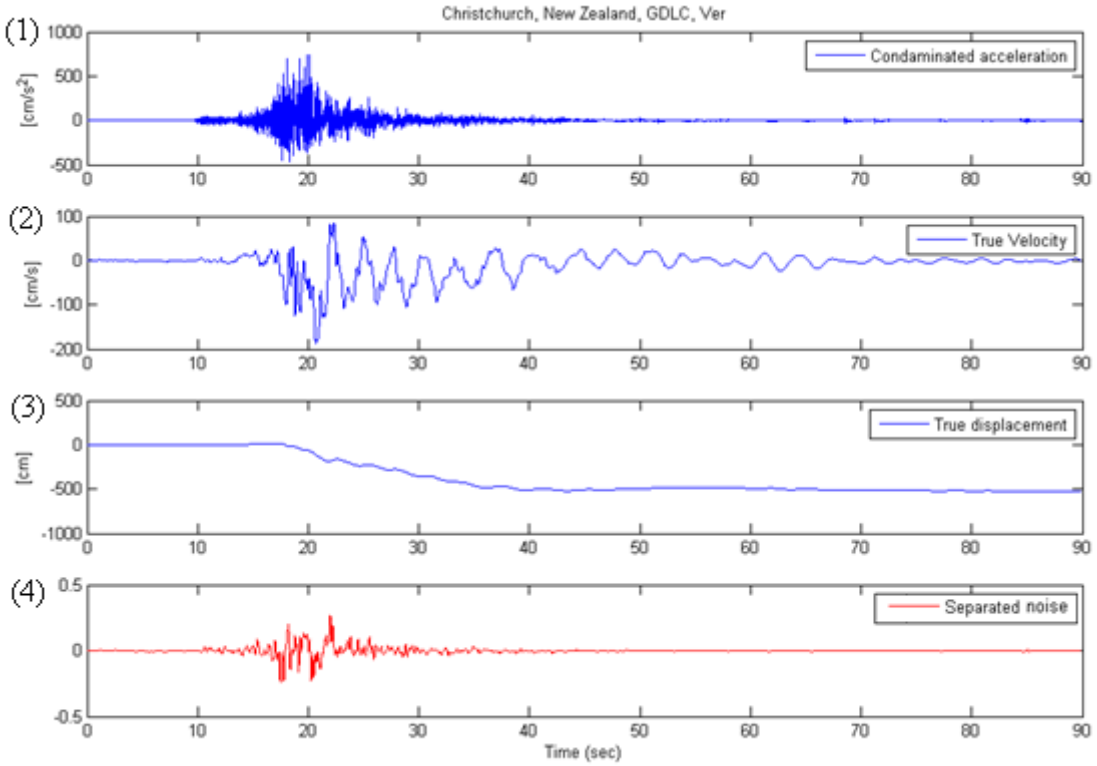


Figure 6.5.3 (a): Christchurch earthquake (22 February 2011, New Zealand; ); (1) plot shows the original contaminated acceleration signals in ; (2) plot shows the estimated velocity in obtained by time integration of the corrected acceleration signals; (3) plot shows the estimated displacement in obtained by the second integration of the corrected acceleration signals; (4) plot shows the separated tilt from the acceleration time histories. The estimated tilt maximum amplitude in the negative direction.

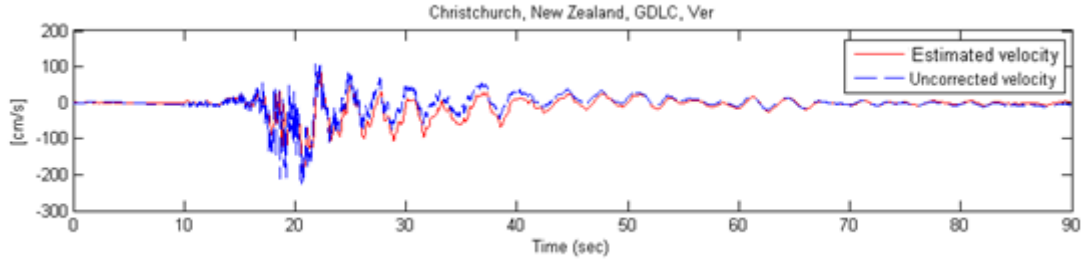


Figure 6.5.3 (b): Comparison between the actual acceleration (dotted line) with corrected acceleration (dashed line) of GDLC-V component.

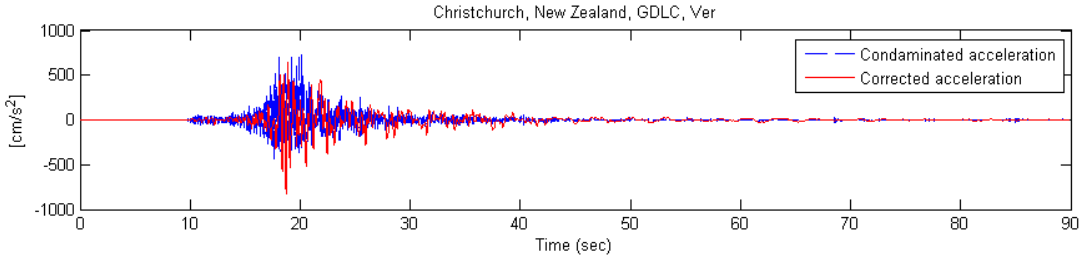


Figure 6.5.3 (c): Comparison between, without baseline corrected velocity (dotted line) with baseline corrected velocity (dashed line) of GDLC-V component.

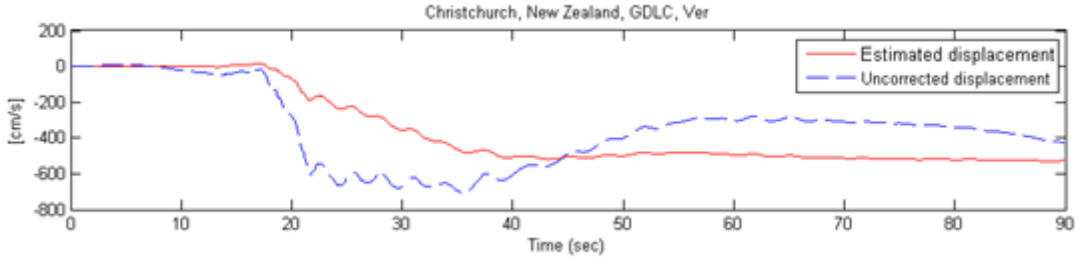


Figure 6.5.3 (d): Comparison between uncorrected displacement (dotted line) with baseline corrected displacement (dashed line) of GDLC-V component.

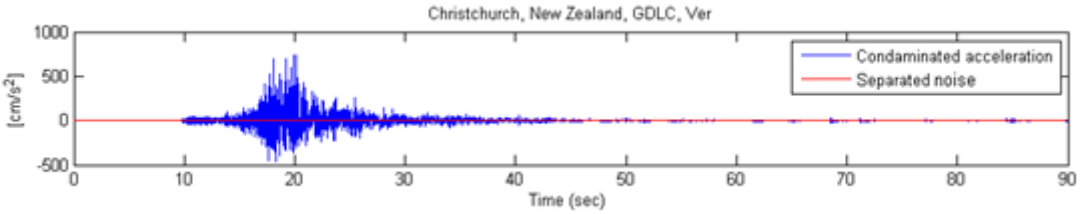


Figure 6.5.3 (e): Raw acceleration data with superimposed separated noise of the GDLC-V component.

In this chapter the results of station data of three components (two horizontal and one vertical) from earthquakes in four countries (Taiwan, Chile, Turkey and New Zealand) are shown. Additional station results are shown in the Appendix 1.

Chi-Chi (1999) earthquake, Taiwan

Stations ID are: TCU039, TCU046, TCU052, TCU059, TCU067, TCU071, TCU072, TCU074, TCU075, TCU078, TCU079, TCU084, TCU089, TCU101, TCU123, TCU128, TCU129, and TCU141.

Maule (2010) earthquake, Chile

Stations ID are: ROC1, and ANTU.

Kocaeli (1999) earthquake, Turkey

Stations ID are: 0104, 0301, 0901, 1001, 1404, 1604, 1612, 1701, 2002, 3401, 3403, 3502, 3701, 4101, 4106, 4302, 4501, 5902, 5903, 6001, 6401, and 8101

## 6.6 Summary and conclusions

This chapter has shown how source separation techniques can be applied to data analysis in real-world seismology engineering situations.

Evidence has shown that the assumption to obtain the tilt component estimation needs to be verified using the TS-ICA model, although there are some small effects due to noise that still remain and will require to be investigated further.

# Chapter 7

**Results and Comparisons**

## 7.1 Introduction

In this chapter, more useful applications occur when the TS-ICA model is used in more complex situations. An interesting result occurs when trying to separate the tilt component from the raw earthquake recorded data for three components (one vertical and two horizontal). These results were analysed and final values compared with the available estimated ground displacement results from the published papers.

The major concerns are to find the estimate of true displacement by removing the tilt and noise from the acceleration records, which are inherent in the data. The tilt curves are made up of closely located points that are highly correlated; understanding the links between individual measurements over time; the determination estimate of true displacement and the separation tilt data is possible.

Another limitation which needs to be examined is the scalability of the algorithm (number of iteration taken to attain convergence). When dealing with a randomised mixing matrix to check the adaptive estimator compared to higher order statistics, certain drawbacks must be addressed before this can be further developed. Adaptive whitening estimators must be designed in order to keep the sources within a mean of zero and a variance of one. The mixing matrix must also be chosen correctly to ensure that convergence of the signal for non-Gaussian distribution thereby satisfies the separation criteria.

There are also some computational issues associated with estimating values, particularly and , whereas and are calculated as per conversion of the estimated sample moments of and . Initially and values are obtained from the available table-II (Dudewicz and Karian, 1996). Further optimisation of and values was undertaken using the novel EGBD model.

Analysis of the results obtained from the chapter 6 is compared with the estimated results from the previously published papers. There are many corrected results of the Chi-Chi (1999) earthquake, Taiwan, which has made it easy to compare the data. However it has not been possible to find other references to the Maule, Chile (2010) earthquake, so this work has not been compared. Some work has been carried out on the Kocaeli (1999) earthquake, Turkey, which included only one EW component benchmarked but the other components of NS and V were ignored. This may have been because the component data was not clean, but the results of the Kocaeli (1999), Turkey have been considered in the experimental work and results have been produced.

The first set of graphical representations from the chapter 6 includes estimated velocity, displacement and separated tilt plus noise is shown in figure 6.2.1(a). Graphs are shown in figure 6.2.1(b) of the comparison between the corrected signals and uncorrected signals also of separated tilt plus noise after first integration and tilt plus noise after second integration is shown in figure 6.2.1(f). These graphs require further investigation to verify the scalability of measurements.

In order to analyse the results, the estimate of ground displacement from chapter 6 is compared with the available results from the published papers and also with the GPS measurements of the station TCU068 records shown in figure 6.2.1(a), 6.2.2(a), and 6.2.3(a) of the NS-, EW- and V components respectively, a summary of this data is provided in the table 7.1.

| TCU068 Displacement (in cm) | | | | | | | |
|---|---|---|---|---|---|---|---|
| Components | TS-ICA Method (2010) | Chanerley & Alexander (2009) | Rupakhety *et al.* (2009) | Akkar & Boore (2009) | Pillet & Virieux (2007) | Ma *et al.* (2001) | GPS Yu *et al.* (2001) |
| V | 204.7 | 300.0 | 350.5 | -- | 575.0 | 458.0 | 121.0 |
| NS | 892.0 | 555.0 | 617.7 | 589.0 | 996.0 | 874.0 | 652.0 |
| EW | -705.0 | -731.0 | -674.1 | -582.0 | -1017.0 | 720.0 | -821.0 |

V (vertical component), NS (North-South component) as Positive, and EW (East-West component) as negative

Table 7.1: Comparison table for estimated ground displacements at station TCU068 of Chi-Chi earthquake, Taiwan.

The second set of results from the station CLCH of the Maule (2010) earthquake, Chile with the estimated ground displacement measurements are given in table 7.2: measurements of the station CLCH records are shown in figure 6.3.1(a), 6.3.2(a), and 6.3.3(a) of NS-, EW- and V components respectively in chapter 6.

| CLCH Displacement (in cm). | |
|---|---|
| Components | TS-ICA Method (2010) |
| V | 620.0 |
| NS | 780.0 |
| EW | -692.0 |

V (vertical component), NS (North-South component) as Positive, and EW (East-West component) as negative

Table 7.2: Estimated ground displacements at station CLCH of Maule earthquake, Chile

The third set of results from the station 5401 of the Kocaeli (1999) earthquake, Turkey with the estimated ground displacement measurements are given in table 7.3: only 5401 EW components of estimated displacement are compared with the available results from the published papers. Estimated ground displacement measurements of the station 5401 records

are shown in figure 6.4.1(a), 6.4.2(a), and 6.4.3(a) of NS-, EW- and V components respectively in chapter 6.

| 5401 Displacement (in cm). | | |
|---|---|---|
| Components | TS-ICA Method (2010) | Erdik Method (2000) |
| V | -190 | -- |
| NS | -- | -- |
| EW | 240.0 | 210.0 |

V (vertical component), NS (North-South component) as Negative, and EW (East-West component) as Positive.

Table 7.3: Comparison of estimated ground displacements at station 5401 of Kocaeli earthquake, Turkey

The results obtained in this research provide a novel approach to the determining the estimation of displacement for a number of earthquake locations. It is considered that these results provide an improved accuracy since there is a separation of the tilt plus noise components as demonstrated in Table 7.1 and 7.3.

The fourth set of results from the station GDLC of Christchurch (2011) earthquake, New Zealand estimated ground displacement measurements are given in table 7.4. Estimated ground displacement measurements of the station GDLC records are shown in figure 6.5.1(a), 6.5.2(a), and 6.5.3(a) of NW- , SW- and V components respectively in chapter 6.

| Station ID: GDLC Displacement (in cm) | |
|---|---|
| Components | TS-ICA Method (2010) |
| UP | -63.0 |
| NW | -120.0 |
| SW | -45.4 |

UP (vertical component) as Negative, NW (North-West component) as Negative, and SW (South-West component) as Negative

Table 7.4: Comparison of estimated ground displacements at station GDLC of Christchurch earthquake, New Zealand

## 7.2 Conclusions

Further understanding may be gained by assuming that the mixing model is partially non-linear (that is, considering the noise model ) and applying both linear and non-linear separation techniques. The computational issues of the values are adjusted by applying the EGBD model in order to improve the stability and efficiency of the model. The ground displacement results obtained from the TS-ICA model using three countries Taiwan, Chile and Turkey earthquake data were compared with the available results from the published papers. Finally the estimated tilt from the ground acceleration will require further investigation to gain a better understanding of the behaviour of tilt.

# Chapter 8

## Tilt evaluation

### 8.1 Introduction

In this chapter, the computation to extract the tilt plus noise from the raw seismic recordings is discussed, and the tilt angles are compared with the method proposed by the French seismologist Robert Pillet (2007) to obtain tilt angles. A graphical representation of a horizontal component of TCU068-NS is shown with the comparison of the corrected velocity signal with the tilt angle removed.

One component (NS) of the TCU068 station data is considered as an example to show the computation of separated tilt, from the figure 8.1. The first trace plotted is the velocity signal in obtained by time integration of the original acceleration in of the equation. The second trace is velocity in obtained by time integration of the corrected acceleration signal in obtained by using the model TS-ICA from the equation (8.1). The last trace is velocity in obtained by time integration of the acceleration signal in which is subtracted tilt from the original acceleration signal in using equation (8.2).

(8.1)

(8.2)

where,

is the estimated tilt

is the corrected ground acceleration signal using TS-ICA model

is the new corrected ground acceleration signal

is the raw ground acceleration signal

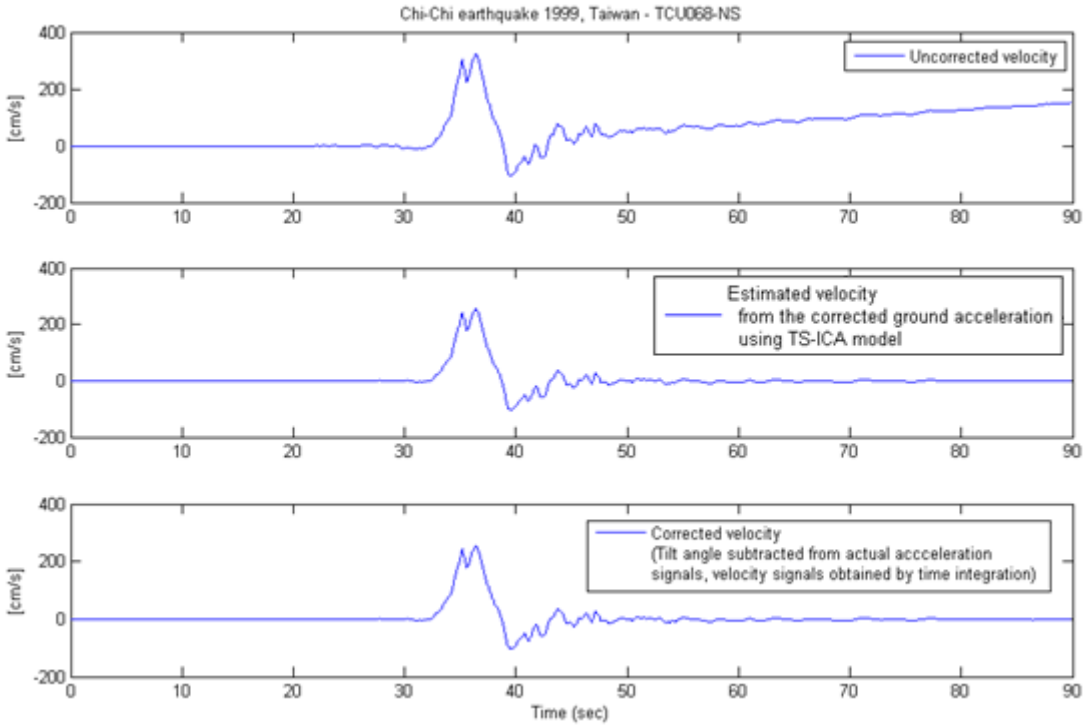


Figure 8.1: The three traces of velocity in signals are obtained by time integration.

From figure 8.2, two signals in were obtained from the equations ( ) which are superimposed to show the difference of each signal that includes the uncorrected velocity signal (blue curve) and corrected velocity (orange curve).

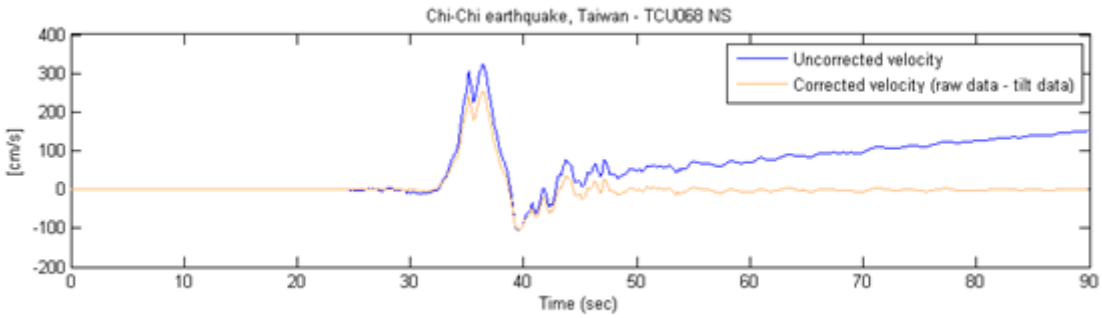


Figure 8.2: Superimposed of three signals velocity in of NS component of TCU068.

## 8.2 TCU068 NS tilt angle calculation

The estimated tilt angles of the TCU068 NS component after separating the tilt maximum amplitude was as shown in the last trace of figure 6.2.1(a) (4) in chapter 6. Pillet and Virieux (2007) found the value of the TCU068 NS component tilt amplitude of for the azimuth, and concluded that the initial tilt has a value of which is equal to . As a comparison of the tilt angle from the TS-ICA model had an amplitude of for the azimuth, so the initial value is which is .

From the station TCU068 the nearest GPS measurement value for the displacement was from the TS-ICA model the estimated true ground displacement was which is shown in figure 8.3.

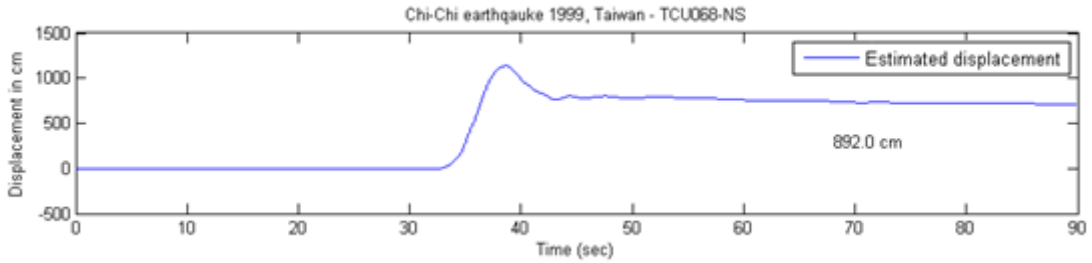


Figure 8.3: Estimated ground displacement of TCU068 NS component.

## 8.3 TCU068 EW tilt angle calculation

The estimated tilt angles of the TCU068 EW component after separating the tilt maximum amplitude was as shown in the last trace of figure 6.2.2(a) (4) in chapter 6. The tilt angle from the TS-ICA model had an amplitude of for the azimuth, so the initial value was which is negative.

From the station TCU068 the nearest GPS measurement value for the displacement was from the TS-ICA model and the estimated true ground displacement was which is shown in figure 8.4.

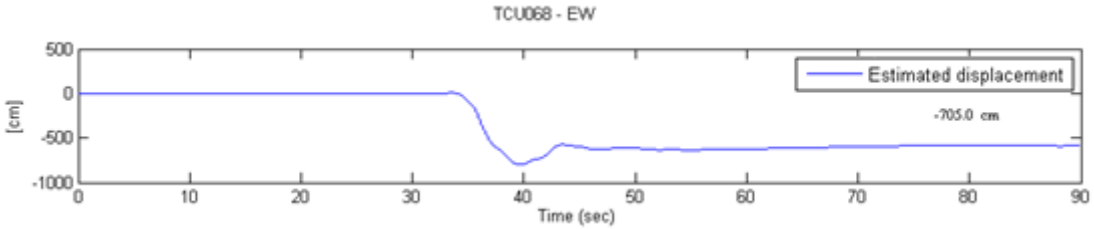


Figure 8.4: Estimated ground displacement of TCU068 EW component.

### 8.4 TCU068 V component

From the station TCU068 the nearest GPS measurement value for the displacement was from the TS-ICA model and the estimated true ground displacement was which is shown in figure 8.5.

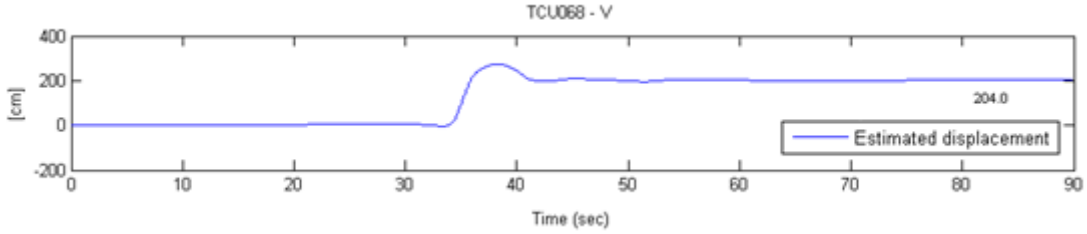


Figure 8.5: Estimated ground displacement of TCU068 V component.

### 8.5 CLCH NS tilt angle calculation

The estimated tilt angles of the CLCH NS component after separating the tilt maximum amplitude was as shown in the last trace of figure 6.3.1(a) (4) in chapter 6. The tilt angle from the TS-ICA model had an amplitude of , so the initial value was and which is .

From the TS-ICA model the estimated true ground displacement was which is shown in figure 8.6.

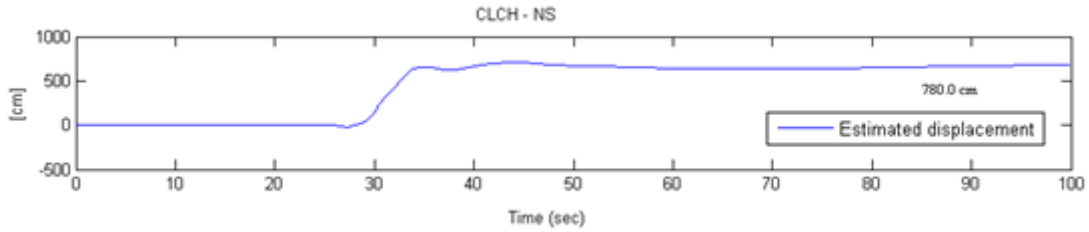


Figure 8.6: Estimated ground displacement of CLCH NS component.

### 8.6 CLCH EW tilt angle calculation

The estimated tilt angles of the CLCH EW component after separating the tilt maximum amplitude was as shown in the last trace of figure 6.3.2(a) (4) in chapter 6. The tilt angle from the TS-ICA model had an amplitude of , so the initial value was and which is negative.

From the TS-ICA model the estimated true ground displacement was which is shown in figure 8.7.

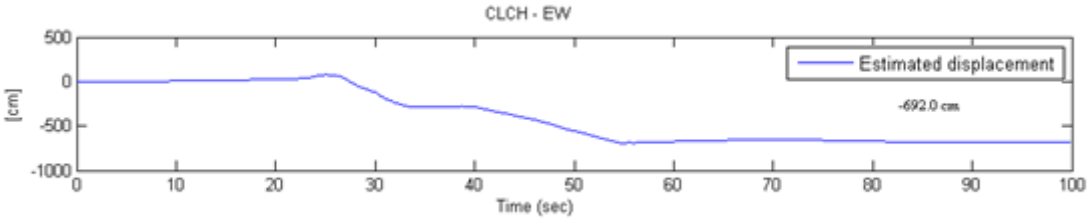


Figure 8.7: Estimated ground displacement of CLCH EW component.

### 8.7 CLCH V component

From the TS-ICA model the estimated true ground displacement was which is shown in figure 8.8.

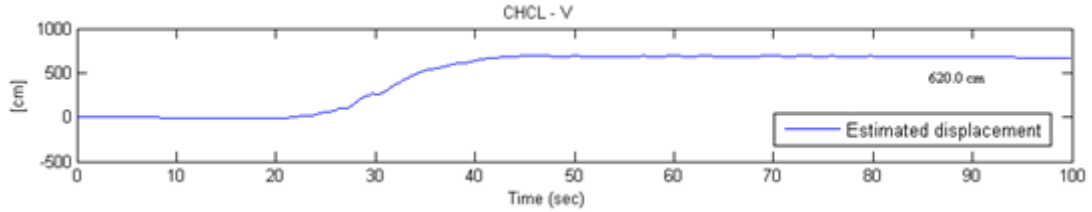


Figure 8.8: Estimated ground displacement of CLCH V component.

## 8.8 KOCAELI 5401 NS tilt angle calculation

The estimated tilt angles of the Kocaeli 5401 NS component after separating the tilt maximum amplitude was as shown in the last trace of figure 6.4.1(a) (4) in chapter 6. The tilt angle from the TS-ICA model had an amplitude of , so the initial value was and which is negative.

From the TS-ICA model the estimated true ground displacement is shown in figure 8.9.

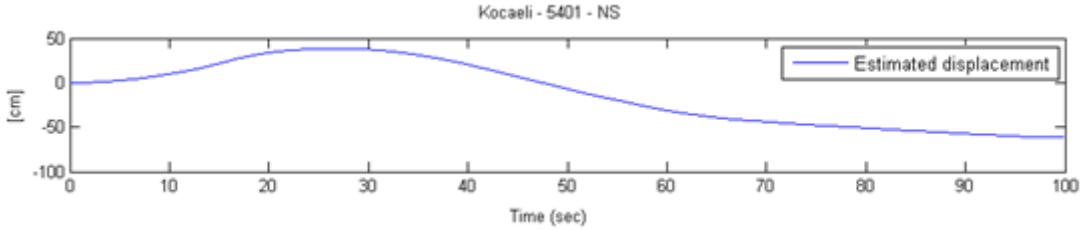


Figure 8.9: Estimated ground displacement of 5401 NS component.

## 8.9 KOCAELI 5401 EW tilt angle calculation

The estimated tilt angles of the Kocaeli 5401 EW component after separating the tilt maximum amplitude was as shown in the last trace of figure 6.4.2(a) (4) in chapter 6. The tilt angle from the TS-ICA model had an amplitude of , so the initial value was and which is .

From the TS-ICA model the estimated true ground displacement was which is shown in figure 8.10.

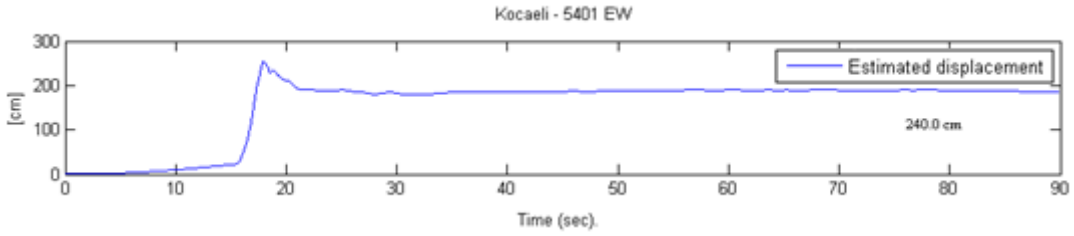


Figure 8.10: Estimated ground displacement of 5401 EW component.

### 8.10 KOCAELI 5401 V component

From the TS-ICA model the estimated true ground displacement was which is shown in figure 8.11.

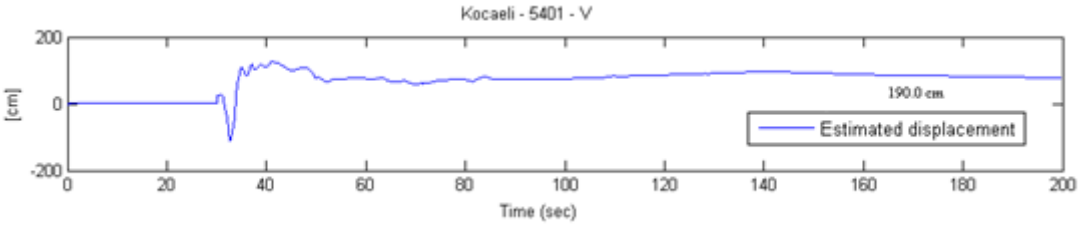


Figure 8.11: Estimated ground displacement of 5401 EW component.

### 8.11 CHRISTCHURCH GDLC NW tilt angle calculation

The estimated tilt angles of the GDLC NW component after separating the tilt maximum amplitude was as shown in the last trace of figure 6.5.1(a) (4) in chapter 6. The tilt angle from the TS-ICA model had an amplitude of , so the initial value was and which is negative.

From the TS-ICA model the estimated true ground displacement was which is shown in figure 8.12.

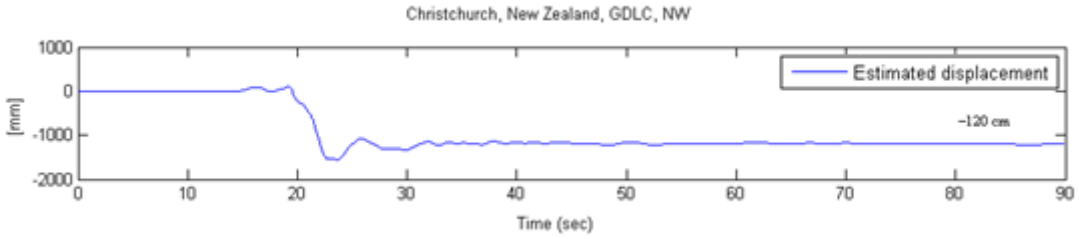


Figure 8.12: Estimated ground displacement of GDLC NW component.

## 8.12 CHRISTCHURCH GDLC SW tilt angle calculation

The estimated tilt angles of the GDLC SW component after separating the tilt maximum amplitude was as shown in the last trace of figure 6.5.2(a) (4) in chapter 6. The tilt angle from the TS-ICA model had an amplitude of , so the initial value was and which is negative.

From the TS-ICA model the estimated true ground displacement was which is shown in figure 8.13.

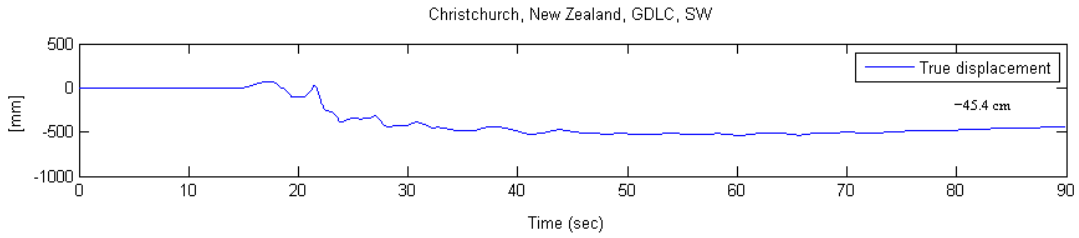


Figure 8.13: Estimated ground displacement of GDLC SW component.

## 8.13 CHRISTCHURCH GDLC UP vertical component

From the TS-ICA model obtained and the estimated true ground displacement was which is shown in figure 8.14.

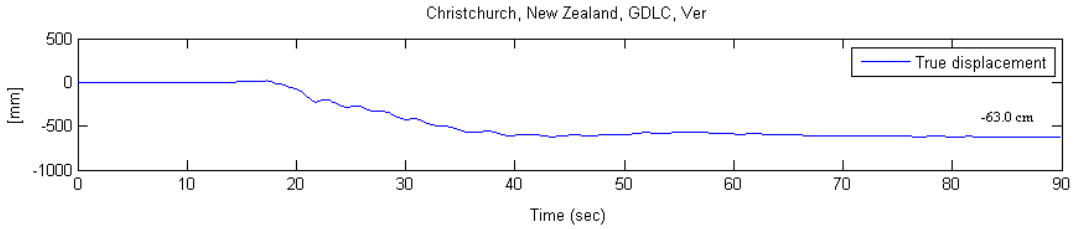


Figure 8.14: Estimated ground displacement of GDLC V component.

| Tilt ($\psi_{tilt}$) angle calculation | | |
|---|---|---|
| Station ID: | Tilt ($\psi_{tilt}$) angle in radians | Tilt ($\psi_{tilt}$) angle in degrees |
| Chi-Chi, TCU068 NS | $1.31 \text{ X } 10^{-2}\ rad$ | $0.75^0$ |
| Chi-Chi, TCU068 EW | $-1.33 \text{ X } 10^{-2}\ rad$ | $0.76^0$ negative |
| Maule, CLCH NS | $10.2 \text{ X } 10^{-2}\ rad$ | $22.4^0$ |
| Maule, CLCH EW | $-10.2 \text{ X } 10^{-2}\ rad$ | $22.4^0$ negative |
| Kocaeli, 5401 NS | $-3.55 \text{ X } 10^{-2}\ rad$ | $20.3^0$ negative |
| Kocaeli, 5401 EW | $2.0 \text{ X } 10^{-2}\ rad$ | $11.4^0$ |
| Christchurch, GDLC NW | $-0.20 \text{ X } 10^{-2}\ rad$ | $1.14^0$ negative |
| Christchurch, GDLC SW | $-0.16 \text{ X } 10^{-2}\ rad$ | $0.91^0$ negative |

Table 8.1: Summary of calculated tilt angle

## 8.14 Conclusions

There is no proof that the mixing model is linear or even stationary and the parameters of the latent variables are similarly obscured. Consequently, any results obtained using simple source separation must be viewed as quantitative educated guesses at best. Ideally, the application of such a technique should be carried out with as much a priori expert knowledge of the system as possible in terms of quantitative analysis although other analytical methods can be used to evaluate the recovered ground displacement and tilt.

# Chapter 9

## Conclusions and Further Work

The performance of the proposed TS-ICA source separation model have been identified and discussed. This has led to exploit the learning algorithm as observed by Karian *et al,* (1996) and later by Eriksson *et al,* (2000) through his Generalised Beta Distribution which provides a platform to consider the development of other adaptive algorithms. The extension of this research work will be an examination of the convergence properties of the novel EGBD method and consideration to simplify the TS-ICA algorithm in order to speed up the process of convergence.

The analysis has shown that the acceleration jump is due to tilt plus noise inherent within the acceleration time histories. By removing the tilt plus noise from the acceleration time histories, the drift in the baseline has been corrected. So the proposed TS-ICA model can be recommended to the analysis of seismic data in separating tilt plus noise. The MATLAB code developed in this research is specific only for removing the tilt plus noise components from the ground acceleration time histories as presented in section 3.2.1. The numerical simulation setup to extract tilt plus noise and correct baseline offset for earthquake recordings of higher magnitude have been provided in Chapter 6. The results have demonstrated that double integration is possible using the TS-ICA model in processing of the main-shock raw recordings from four countries Chi–Chi (1999) earthquake Taiwan, Maule (2010) earthquake Chile, Kocaeli (1999) earthquake Turkey and Christchurch (2011) earthquake New Zealand from the four stations TCU068, CLCH, 5401 and GDLC respectively. The TS-ICA model has enabled the ease of integration due to separation of the tilt/noise time histories from the raw data of the acceleration time histories and provides better estimates of true ground velocity and displacement.

Further work with the EGBD method was to verify the stable model by analysing the learning rate. The learning rate depends on the updates of and values which were calculated using the novel EGBD method. It is important for modelling these parameters to their

equilibrium values and this EGBD method needs to be examined further to specify the scalability of the TS-ICA algorithm.

The question of the tilt plus noise time history needs further investigation. The TS-ICA algorithm does separate a tilt plus noise time history from the main acceleration obtained from seismic records and the tilt angle was calculated for four stations TCU068, CLCH, 5401, GDLC, which was shown in Table 8.1. It is difficult to define how much of the separated time history is contained in the tilt and how much is contained in the noise. Undoubtedly the tilt plus noise is separated out from the main acceleration time history, otherwise double-integration would not be possible. It is likely that the TS-ICA algorithm has separated the tilt and noise together into one time history. Further work will involve either pre-processing the acceleration time history in order to remove the noise, but retain the tilt. The more likely scenario would be to post-process the residual and separated time histories in order to extract the tilt/rotation from it.

# Chapter 10

## 10.1 References and Bibliography:

**Achard, S. and Jutten, C. (2005).** "Identifiability of post nonlinear mixtures," IEEE Signal Processing Letters, vol. 12, no.5, pp 423-426.

**Aki, K. and Richards, P. G. (1980).** *Quantitative Seismology*. W.H.Freeman and Company.

**Aki, K. and Richards, P. G. (2002).** *Quantitative Seismology*. University Science Books, 2nd edition. ISBN: 0935702962

**Aki, K. and Lee, W. H. K. (2003).** Glossary of Interest to Earthquake and Engineering Seismologists, in International handbook of Earthquake and Engineering Seismology, Part B, W.H.K. Lee, H. Kanamori, P.C. Jennings, and C. Kisslinger (Editors), Academic Press, Amsterdam, pp 1793-1856

**Akkar, S., and Gülkan, P. (1999).** Effect of record processing schemes on damage potential of near-field earthquakes, in Structural Dynamics-EURODYN '99, Ed. L. Fryba and J. Naprstek, Balkema, vol. 2, pp. 1101-1106.

**Akkar, S. and Bommer, J. J. (2007).** Prediction of elastic displacement response spectra in Europe and the Middle East. Earthq. Eng. Struct. Dyn. 36, 1275-1301

**Akkar, S. and Boore, D. M. (2009).** On Baseline Corrections and uncertainty in Response Spectra for Baseline Variations Commomly Encountered in Digital Accelerograph Records. Bulletin of the Seismological of America, vol.99, No.3, pp. 1671-1690.

**Alexander, N. A., Chanerley, A. A. and Goorvadoo, N. (2001).** A Review of Procedures used for the Correction of Seismic data. *Proceeding of the Eighth International Conference on Civil and Structural Engineering Computing*. Scotland: Civil-Comp Press, Paper 39

**Al-Homoud, A. S. and Whitman, R. V. (1995).** Comparison between of predications and results from dynamic centrifuge tests on tilting gravity walls. Soil Dynamics and Earthquake Engineering, 14, pp 259-268.

**Almedia, L. B. (2000).** "Linear and nonlinear ICA based on mutual information," in Proc. Symp. 2000 Adaptive Systems for signal Processing, Communications, and Control, Lake Louise. 2000. [Online]. Available: http://www.lx.it.pt/~lbalmedia/papers/AlmeidiaASSPCC00.ps.zip.

**Almeida, L. B.(2002).** "MISEP – an ICA method for linear and nonlinear mixtures, based on mutual information", in Proc. 2002 Int. Joint Conf. on Neural Networks, Honolulu, Hawaii, Available: http://www.lx.it.pt/~lbalmeida/ica/mitoolbox.html, Last accessed 09 November 2008.

**Almedia, L. B. (2006).** Nonlinear Source Separation, Synthesis Lectures on Signal Processing, Morgan & Claypool, First edition, ISBN-10: 1598290304.

**Amari, S. and Cichocki, A. (1998).** "Adaptive blind signal processing" *Proc of the IEEE*, 86(10):2026-2048

**Ambraseys, N., Smith, P., Berardi, R., Rinaldis, D., Cotton, F., and Thierry, B. C. (2000).** "Disseminated of European Strong-Motion Data. CD-ROM Collection." European Council, Environment and Climate Research Programme

**Bartlett, M. S. (1948).** Smoothing Periodograms from Time Series with Continuous Spectra, *Nature* (London), vol. 161, pp 686-687.

**Bartlett, M. S. (1950).** "Periodogram Analysis and Continuous Spectra", University of Manchester, vol 37, Parts 1 and 2, pp 1-16.

**Battaglia, J., Aki, K. and Montagner, J.-P. (2000).** Tilt signals derived from a geoscope VBB station on the Piton de la Fournaise volcano, Geophys. Res.lett., 27, 605-608.

**Bell, A. J., and Sejnowski, T. J. (1995).** "The Maximum Entropy method for Blind Source Separation", Computational Neurobiology, La Jolla, CA 92037, USA.

**Bermejo, S., (2007).** "Finite sample effects of the fast ICA algorithm", Neurocomputing, vol 71, pp 392–399.

**BGS (2010)**. Natural Environment Research Council, "http://www.earthquakes.bgs.ac.uk/earthquakes/education/eq_booklet/eq_booklet_how_we_measure.htm". Last accessed 21 May 2010

**Bonaccorso, A. (1998).** Evidence of a dyke-sheet intrusion at Stromboli volcano inferred through continuous tilt, Geophys. Res.Lett., 25, 4225-4228.

**Boore, D. M., Joyner, B. W. and Fumal, T. E. (1993).** Estimation of response spectra and peak acceleration from Western North American earthquakes: an interim report. U.S. Geological Survey, Open-File Report 93-509. pp 01-72.

**Boore D. M., Stephens, C. D. and Joyner, W. B. (2001).** Comments on baseline correction of digital strong-motion data: Examples from the 1999 Hector Mine, California, earthquake. Bull. Seism. Soc. Am. In press

**Boore D. M. (2001).** Effect of baseline corrections on displacements and response spectra for several recordings of the 1999 Chi-Chi, Taiwan, earthquake. Bull. Seism. Soc. Am., vol. 91, no. 5, pp. 1199-1211.

**Boore D. M. (2003).** Analog-to-digital conversion as a source of drifts in displacements derived from digital recordings of ground acceleration, Bull. Seism. Soc. Am., vol. 93, pp. 2017-2024.

**Boore, D. M. and Bommer, J. J. (2005).** Processing of Strong-Motion Accelerogram: Needs, options and consequences, Soil Dynamics and Earthquake Engineering, vol 25, pp 93-115

**Boore, D. M. and Bommer, J. J. (2008).** Ground Motion Predicition Equations for the Average Horizontal Component of PGA, PGV, and 5% Damped PSA at Spectral Periods between 0.01 s and 10.0 s, Earthq. Spectra, 24, 99-138.

**Boroschek, R. and Legrand, D. (2006).** Tilt motion effects on the double-time integration of linear accelerometers: an experimental approach, Bull. Seism. Soc. Am., 96(6), pp 2072–2089.

**Bouchon, M. and Aki, K. (1982).** Strain, Tilt, and Rotation associated with strong ground motion in the vicinity of earthquake faults, Bull. Seism. Soc. Vol. 72, pp. 1717-1738

**Bradner, H. and Reichle, M. (1973).** Some methods for determining acceleration and tilt by use of pendulums and accelerometers, Bull. Seism. Soc. Vol. 63, pp. 1-7.

**Cardoso, J., and Laheld, B.(1996).** "Equivariant adaptive source scparation", IEEE Transactions on Signal Processing, vol. 44. no. 12, pp 3017-3030

**Cardoso, J. F. (1998).** Blind signal separation: Statistical principles. Proceedings of the IEEE, vol. 86, no. 10: pp 2009-2025

**CBW, (2010).** Central Whether Bureau, Geophysical Database Management System, Taiwan, Data sets Available: http://www.cwb.gov.tw/V6e/index.htm, Last accessed 14 January 2010.

**Chanerley, A. A. and Alexander, N. A. (2003).** A New Approach to Seismic Correction using Recursive Least Squares and Wavelet De-Noising. *Proceeding of the Ninth International Conference on Civil and Structural Engineering Computing*. Scotland: Civil-Comp Press, Paper 107

**Chanerley, A. A. and Alexander, N. A. (2005).** Using the Method of Total Least Squares for Seismic Correction. In: *Proceeding of the Tenth International Conference on Civil, Structural and Environmental Engineering Computing*, B.H.V. Topping (Editor), Civil-Comp Press, Stirling, Scotland, Paper 217.

**Chanerley, A. A. and Alexander, N. A. (2009).** Obtaining estimates of the low-frequency 'fling', instrument tilts and displacement timeseries using wavelet decomposition, Bull Earthquake Eng, DOI 10.1007/s10518-009-9150-5, pp 1-25.

**Cheng, H., Winterflood, J., Ju, L. and Blair, D. G. (2001).** Tilt sensor and servo control system for gravitational wave detection, Classical and Quantum Gravity, pp 1-6.

**Chong, E. and Zak, S. (2001).** *"An introduction to Optimisation"*, Wiley, pp 187-212

**Chouet, B., Saccorotti, G., Dawson, P., Martini, M., Scarpa, R., Luca, G.D., Milana, G. and Cattaneo, M. (1999).** Broadband measurements of the sources of explosions at Stromboli volcano, Italy, Geophys. Res.Lett., 26, 1937-1940.

**Cochard, A., Igel, H., Schuberth, B., Suryanto, W., Velikoseltsev, A., Schreiber, U., Wassermann, J., Scherbaum, F., and Vollmer, D. (2006).** Rotational Motions in Seismology: Theory, Observation, Simulation. BMBF-Geotechnologien.

**Comon, P. (1994).** "Independent Component Analysis, a New Concept?" *SignalProcessing*, vol 36: pp 287-314

**Cooley, J. W., Lewis, P. A. W. and Welch, P. D. (1969).** The Fast Fourier Transform and its Applications, 'IEEE Transactions on Education', vol. 12, no. 1, pp 27-34.

**DGF, (2002).** Universidad de Chile – Depto. De. Geofisica, Servicio Sismologico, Blanco Encalada 2002 - Casilla 2777 Santiago Chile, Data Available: http://ssn.dgf.uchile.cl/seismo.html Last accessed 27 Feburary 2010.

**Donoho, D. L. (1992).** "De-noising by soft thresholding." IEEE Transactions on Information Theory, Stanford University, California. 41(3):613-627

**Dudewicz, E. J., Ramberg, J. S., and Tadikamalla, P. R. (1974).** A distributions for data fitting and simulations. Annual Technical Conference Transactions of the American Society for Quality Control, vol. 28, pp 407-418

**Dudewicz, E. J. (1976).** *Introduction to Statistics and Probability.* New York: Holt, Rinehert and Winston.

**Dudewicz, E. J., Johnson, M. E., and Ramberg, J. S. (1976).** Fitting distributions to data with moments: sampling variability effects. Annual Technical Conference Transactions of the American Society for Quality Control, vol. 30, pp 337-344

**Dudewicz, E. J. and Karian, Z. A. (1996).** "The Extended Generalized Lambda Distribution System for Fitting Distributions to Data with Moments II: Tables," American Journal of Mathematical and Management Sciences, Special Volume on Advances in Modern Simulation, 16(3 & 4), 271–332.

**Erdik, M. (2000).** REPORT ON 1999 KOCAELI AND DÜZCE (TURKEY) EARTHQUAKES, Bogazici University, Dept. of Earthquake Engineering, 81220 Cengelkoy, Istanbul, Turkey [online] Available: http://www.iiasa.ac.at/Research/RMS/july2000/Papers/erdik.pdf. Last accessed 06 April 2010.

**Eriksson, J., Karvanen, J., and Koivunen, V. (2000).** "Source Distribution Adaptive Maximum Likelihood Estimation of ICA Model" In: Proceeding of the Second International Workshop on Independent Component Analysis. Finland, pp. 227 – 232.

**ESD. (2002).** "*The European Strong Motion Database*", *Documentation*. [online] Available: http://www.isesd.hi.is/. Last accessed 06 August 2009.

**Evans, J. R., and the Members of the International Working Group on Rotational Seismology. (2009).** Tutorial: Suggested notation conventions for rotational seismology, Bull. Seis. Soc. Am., 99, special issue on rotational seismology

**Girolami, M. (1997).** Self-organizing artificial neural networks for signal separation. Unpublished Ph.D. dissertation, Paisley University, Scotland.

**GNS. (2011).** "*Seismological Observatory, Geophysics Division, Institute of Geological and Nuclear Sciences* ", *Dataset*. Available: http://www.gns.cri.nz/index.php/Home/Products/Databases/Strong-Motion-Database. Last accessed 09 March 2011.

**Graizer V. M. (1979).** Determination of the true ground displacement by using strong motion records. Izvestiya Academy of Sciences, USSR, Physics of the Solid Earth, vol. 15, no. 12, pp. 875-885

**Graizer V. M. (1989).** Bearing on the problem of inertial seismometry. Izvestya USSR Acad Sci Phys Solid Earth 25(1): 26-9

**Graizer V. M. (2006a).** Tilts in Strong Ground Motion. Bull. Seism. Soc. Am., vol. 96, no. 6, pp. 2090-2102.

**Graizer, V. M. (2006b).** Equation of pendulum motion including rotations and its implications to the strong-ground motion, in *Earthquake Source Asymmetry, Structural Media and Rotation Effects* R.Teisseyre, M.Takeo, and E.Majewski (Editors), Springer-Verlag, New York, pp. 471-485.

**Hart, G.C., Dijulio, M., and Lew, M. (1975).** Torsional Response of High-rise Buildings, J.Struct. Div., ASCE 101, 397-414.

**Hayes, M. H. (1996).** "Statistical Digital Signal Processing and Modeling", *Wiley*, pp 493-552

**Haykin, S. (1999).** "Neural Networks a Comprehensive Foundation." Prentice Hall, Second edition, pp 544-547

**Hidayat, D., Voight, D., Langston, C., Ratdomopurbo, A. and Ebeling, C. (2000).** Broadband seismic experiment at Merapi Volcano, Java, Indonesia: very-long period pulses embedded in multiphase earthquake, *J. volcano. Geotherm. Res.*, vol. 100, pp 215-231

**Hyvarinen, A., and Oja, E. (1997).** "A Fast Fixed Point Algorithm for ICA", Neural Computing 1997 – 1483-1492.

**Hyvarinen, A. (1999).** "Fast and Robust Fixed-Point algorithms for ICA", *IEEE Transactions in Neural networks*, 10(3): 626-634

**Hyvarinen, A. (1999a).** "The fixed point algorithm and maximum likelihood estimation for ICA", *Neural Processing Letters*, 10(1): 1-5

**Hyvarinen, A., Karhunen, J., and Oja, E. (2000).** "Independent Component Analysis." John Wiley and sons. Second edition, pp 01-11

**Igel, H., Schreiber, U., Flaws, A., Schuberth, B., Velikoseltsev, A., and Cochard, A. (2003).** "Rotational motions induced by the M8.1 Tokachi-oki earthquake" Vol 32, American Geophysical Union, Sep 25.

**Igel, H., Cochard, A., Wassermann, J., Flaws, A., Schreiber, U., Velikoseltsev, A., and Pham, N. D. (2007).** Broadband Observations of Earthquake Induced Rotational Ground Motions, Geophys.J.Int. 168, 182-196, doi 10.11111/j.1365-246X.2006.03146x.

**Ilin, A., Valpola, H., and Oja, E.(2004).** Nonlinear dynamical factor analysis for state change detection. IEEE Transaction on Neural Networks, 15(3): pp 559–575

**Iwan W. D., Moser, M. A. and Peng, C. -Y. (1985).** Some observations on strong-motion earthquake measurements using a digital accelerograph. Bull. Seism. Soc. Am., vol. 75, no. 5, pp. 1225-1246.

**Jung, T., Humphries, C., Lee, T., Makeig, S., Mckeown, M. J., Iragui, V and Sejnowski, T. J. (1998).** Removing electroencephalographic artefacts: comparison between ICA and PCA, Neural Networks for Signal Processing VIII.

**Karhunen, J., Wang, L., and Vigario, R.(1995).** "Nonlinear PCA type approaches for source separation and independent component analysis," Proceedings of the '95 IEEE International Conference on Neural Networks, Perth, Australia, pp 995-1000

**Karhunen, J. and Koivunen, V. (2002).** "Blind separation method based on Pearson system and its extensions." Signal Processing Laboratory, Helsinki University of Tech, Finland. 82(2002) 663-673

**Karian, Z. A., Dudewicz, E. J. (1991).** *Modern Statistical, Systems, and GPSS Simulations*, Computer Science Press, New York.

**Karian, Z. A., Dudewicz, E. J. and McDonald, P. (1996).** "The Extended Generalised Lambda Distribution System for Fitting Distributions to Data: History, Completion of Theory, Tables, Applications, the `Final Word' on Moment Fits", *Communications in Statistics: Simulation and Computation*, Vol. 25, No. 3, pp. 611—642

**Kenett, B. L. N. (2002).** The Seismic Wavefield, Volume II: interpretation of seismograms on regional and global scales. Cambridge, ISBN 0521006651

**Kennett, B. L. N. (2000).** Stacking Three Component Seismograms, Geophys.J.Int. 141, pp 263-269

**Kinoshita, S. (2008).** Tilt Measurments Using Broadband Velocity Seismograph. Bulletin of the Seismological of America, vol.98, No.4, pp. 1887-1897.

**Kinoshita, S., Ishikawa, H., and Satoh, T. (2009).** Tilt Motions Recorded at Two Wise Sites for the 2003 Tokachi-Oki Earthquake (*m* 8.3). Bulletin of the Seismological of America, vol.99, No.2B, pp. 1251-1260.

**Lee, T. W., Girolami, M., Bell, A. J., and Sejnowski, T. J. (1999).** A unifying frame work for independent component analysis. Computers and Mathematics with Applications, In Press.

**Lee, W. H. K, Kanamori., H, Jennings., P. C. and Kisslinger, C. (2002a).** International handbook of earthquake and engineering seismology, Part A, Academic Press, Amsterdam. ISBN: 0124406521

**Lee, W. H. K. (2003).** International Handbook of Earthquake and Engineering Seismology, International geophysics series; vol 81B, Academic Press, Amsterdam

**Lee, W. H. K., Çelebi, M., Todorovska, M.I. and Igel, H. (2009).** Introduction to the Special Issue on Rotational Seismology and Engineering Applications, Bull. Seism. Soc. Am., vol. 99, no. 2B, pp. 945-957.

**Lee, W. H. K., Igel, H., and Trifunac, M.D. (2009).** Recent Advances in Rotational Seismology. Seismological Research Letters, vol.80, No.3, pp. 479-490.

**Li, H., Sun, L., and Wang, S. (2001).** Improved approach for obtaining rotational components of seismic motion, Transactions, SmiRT 16, pp 1-8.

**Lindgren, B. W. (1976).** "Statistical Theory", 3rd Edition, Mac Millan Publishing Co. Inc, 1976, ISBN 0-02-3708301

**Lippmann, G. (1890).** Sur la theorie et le mode d'emploi des appareils seismographiques, C. r. hebd. Séanc. Acad. Sci., Paris, vol. 110, pp 440-444.

**Lomnitz, C. and Castaños, H. (2006).** Earthquake Hazard in the valley of Mexico: Entropy, Structure, Complexity; In Earthquake Source Asymmetry, Structural Media and Rotation Effects, R. Teisseyre, M. Takeo and E. Majewski (editors), Springer-Verlag, New York. Pp 347-364

**Ma, K. F., Mori, J., Lee, S. J. and Yu, S. B. (2001).** Spatial and Temporal Distribution of slip for the 1999 Chi-Chi, Taiwan, earthquake, Bulletin of the Seismological of America, vol.91, pp. 1069-.1087

**MacKay, D. J. C. (1996).** "Maximum likelihood and covariant algorithms for independent component analysis", Draft 3.1, Available: http://wol.ra.phy.cam.ac.uk/mackay/ Last accessed 09 September 2009.

**Marcel, J., Heinz, M. and Russell, H. L. (2000).** Overdetermined Blind Source Separation: Using more sensors than source signals in noisy mixtures. In: Proceeding of the Second International Workshop on Independent Component Analysis. Finland: June 19 – 22.

**Mendis, D. R. (2007).** The Re-evaluation of Earthquake Actions for Displacement based Seismic Design, PhD Thesis, Imperial College London, U.K.

**Mutihac, R., and Marc Hulle, V. M. (2003).** "A Comparative Survey on Adaptive Neural Network Algorithms for Independent Component Analysis." Katholieke Universiteit Leuven, Labo voor Neuro- en Psychofysiologie, Campus Ghastuisberg, B-3000 Leuven, Belgium.

**Nigbor, R. L. (1994).** "Six-Degree-of-Freedom Ground Motion Measurement" Vol 84, No 5, Seismological Society of America, October 1994, pp. 1665-1669.

**Nikias, C., and Mendel, J.(1993).** "Signal processing with higherorder spectra", Signal Processing Magazine, pp. 10-37

**Pham, D. T. and Garat, P. (1997).** "Blind Source Separation of mixtures of independent sources through a quasi-maximum likelihood approach", *IEEE Trans. Signal Processing*, 45(7): pp 1712-1725

**Pham, N. D., Igel, H., Wassermann, J., Kaser, M., de la Puente, J. and Schreiber.U. (2009a).** Observations and modelling of Rotational signals in the P coda: constraints on crustal scattering, Bulletin of the Seismological of America, vol.99, No.2B, pp. 1315-1332.

**Pham, N. D., Igel, H., Wassermann, J., Cochard, A., and Schreiber.U. (2009b).** The Effects of Tilt on Interfermetric Rotation Sensors. Bulletin of the Seismological of America, vol.99, No.2B, pp. 1352-1365.

**Pillet, R. and Virieux, J. (2007).** The Effects of Seismic Rotations on Inertial Sensors, Geophys.J.Int. 171, no.3, 1314-1323

**Plumbley, M. (1993).** "A Hebbian/anti-Hebbian network which optimizes information capacity by orthonormalizing the principal subspace", Proc. IEE Conference on Artificial Neural Networks, pp 86-90

**Poincare, P., (1888).** Les tremblements de Terre, Bailliere, Paris.

**Pritchard, M. E. (2006).** InSAR, a tool for measuring Earth's surface deformation. Available: http://www.geo.cornell.edu/eas/PeoplePlaces/Faculty/matt/vol59no7p68_69.pdf. Last accessed 06 August 2007

**Proakis, J. G. and Manolakis, D. G. (1996).** Digital Signal Processing, Upper Saddle River, New Jersey: Prentice-Hall, pp 910-913. Chapter 7 and 12. ISBN 0133737624

**Ramberg, J. S., Tadikamalla, P. R., Dudewicz, E. J. and Mykytka, E. F. (1979).** A Probability Distributions and Its Uses in Fitting Data, Technometrics, Vol. 21, No.2, pp 201-209.

**Rodgers, P. (1968).** The response of the horizontal pendulum seismometer to Rayleigh and Love waves, tilt and free oscillations of the Earth, Bull. Seism. Soc. Vol. 58, pp. 1385-1406

**Rowe, C., Aster, R., Kyle, P. and Schlue, J. (1998).** Broadband recording of Strombolian explosions and associated very-long period seismic signals on Mount Erebus volcano, Ross Island, Antarctica, *Geophys. Res, Lett.*, vol. 25, no. 13, pp 2297-2300.

**Rupakhety, R., Halldorsson, B., and Sigbjornsson, R. (2010).** Estimating coseismic deformation from near source strong motion records: methods and case studies, Bull Earthquake Eng, vol. 8, pp 787-811

**Sargeant, S. L., and Musson, R. M.W. (2009).** Short note on Rotational Earthquake Effects in the United Kingdom. Bulletin of the Seismological of America, vol.99, No.2B, pp. 1475-1479.

**Schreiber, U., Stedman, G. E., Igel, H. and Flaws, A. (2006).** Ring Laser Gyroscopes as Rotation Sensors for Seismic Wave Studies, In Earthquake Source Asymmetry, Structural Media and Rotation Effects, R. Teisseyre, M. Takeo and E. Majewski (editors), Springer-Verlag, New York. Pp 377-390

**Seismosoft (2004).** "Seismosignal – A Computer program for Signal Processing of Strong Motion Data" (online) Available from URL http://www.seismosoft.com

**Spencer, B. F. and HU, Y. X. (2000).** Earthquake engineering frontiers in the new millennium, China ISBN: 9026518528

**SS. (2010).** "INFORME TECICO ACTUALIZADO 27 MAYO 2010", *Dataset*. Available: URL: http://ssn.dgf.uchile.cl. Last accessed 09 June 2010.

**Stearns, S. D. and Vortman, L.J. (1981).** "Seismic event detection using adaptive predictors", *IEEE proc. ICASSP, ICASSP*

**Takemoto, S. and Geophys, J. (1991).** Some problems on detection of earthquake precursors by means of continuous monitoring of crustal strains and tilts: Res vol 96, NB6, P10377–10390

**Taleb, A., and Jutten, C. (1999).** Source Separation in Post Non Linear Mixtures
IEEE Trans. on Signal Processing, Vol. 47, pp. 2807-20

**Teisseyre, R., Takeo, M. and Majewski, E (2006).** Earthquake Source Asymmetry, Structural Media and Rotation Effects, Springer, ISBN: 3540313362.

**Thiyagu, R. D. and Chanerley, A. A. (2009).** Using ICA for Analysis of Seismic Events. Adv. Comp and Tech. vol. 1, pp 160-166.

**Thiyagu, R. D. and Chanerley, A. A. (2010).** Problems Associated with Instrument Tilts during Seismic Events. Adv. Comp and Tech. vol. 4, pp 119-127.

**TKYHP. (2009).** *"Turkey National Strong Ground Motion Program Database "*, *Dataset*. Available: http://angora.deprem.gov.tr/TKYHAKKen.htm. Last accessed 09 September 2009.

**Trifunac, M. (1971).** Zero baseline correction of strong-motion accelerograms. Bull. Seism. Soc. Am., vol. 61, no. 5, pp. 1201-1211.

**Trifunac, M. (1972).** A note on correction of strong-motion accelerograms for instrument response. Bull. Seism. Soc. Am., vol. 62, no. 1, pp. 401-409.

**Trifunac, M.D. and Lee, V.W. (1973)**. "Routine computer processing of strong motion accelerograms*"*, *Earthq. Eng. Research Lab. Report*. California Institute of Technology, Pasadena, California. EERL 73(03)

**Trifunac, M. D., Lee, V. and Todorovska, M. (1999).** Common problems in automatic digitization of strong motion accelerograms. Soil Dyn Earthq Eng 18: pp 519–530

**Trifunac, M. D. and Todorovska, M.I. (2001).** A note on the useable dynamic range of accelerographs recording translation, Soil Dyn. Earthq.Eng, no. 21, pp. 275-286.

**Tukey, J. W. (1960).** "A practical relationship between the common transformation of percentages of counts and of amounts." Technical Report 36, Statistical techniques research group. (Princeton University).

**UNIVERSIDAD DE CHILE (2010).** TERREMOTO CAUQUENES 27 FEBRERO 2010, Servicio Sismologico, Santiago, CHILE. ANEXO I.

**Vinther, M. (2002).** Independent Component Analysis of Evoked Potentials in EEG. Orsted, DTU.

**Wielandt, E. and Forbriger, T. (1999).** Near-field seismic displacement and tilt associated with the explosive activity of Stromboli, Annali Di Geofisica , vol. 42, no. 3, pp 407-416.

**Yu, S.B., Kuo, L.C., Hsu, Y.R., Su, H.H., Liu, C.C., Hou, C.S., Lee, J.F., Lai, T.C., Liu, C.C., and Liu, C.L. (2001).** Preseismic Deformation and Coseismic Displacements associated with the 1999 Chi-Chi Taiwan, earthquake. Bull Seism Soc. Am., vol. 91, pp. 955-1012.

**Zembaty, Z. (2009a).** Tutorial on surface rotations from wave passage effects: stochastic spectral approach, Bull. Seism. Soc. Am., vol. 99, no. 2B, pp. 1040-1049.

**Zembaty, Z. (2009b).** Rotational seismic load definition in Eurocode 8, part 6 for slender tower-shaped structures, Bull. Seism. Soc. Am., vol. 99, no. 2B, pp. 1483-1485.

# Appendix

**Appendix A:** Other results of estimated ground displacement, velocity and tilt from the different station.

**Appendix B:** MATLAB project source code.

# Appendix A

Other results of estimated ground displacement, velocity and tilt from the different station.